

Using Pyrene to Probe Interparticle Polymer Diffusion in a Latex Film

by

Remi Casier

A thesis
presented to the University of Waterloo
in fulfillment of the
thesis requirement for the degree of
Master of Science
in
Chemistry

Waterloo, Ontario, Canada, 2015

©Remi Casier 2015

AUTHOR'S DECLARATION

I hereby declare that I am the sole author of this thesis. This is a true copy of the thesis, including any required final revisions, as accepted by my examiners.

I understand that my thesis may be made electronically available to the public.

Abstract

Fluorescence has been used for many years as a powerful analytical tool to probe the formation of films from aqueous latex dispersions. Currently, the most widely used method is fluorescence resonance energy transfer (FRET), which requires the use of two different fluorescently-labelled latex dispersions. As the latex particles coalesce during film formation, the amount of FRET that occurs between the particles is used to probe the level of interparticle polymer diffusion (IPD). Although FRET provides a quantitative method to probe IPD, a simpler method might only require the preparation of a single fluorescently-labelled latex using the dye pyrene.

An isolated pyrene excited by a photon of light emits as a monomer. However, if the excited pyrene encounters a ground-state pyrene, it can form an excimer. The amount of excimer formed is directly proportional to the local pyrene concentration (C_{Py}), which may be quantified by steady-state fluorescence with the ratio of the fluorescence intensity of the excimer (I_E) over that of the monomer (I_M), namely the I_E/I_M ratio. A mixture of a non-fluorescent latex with a latex consisting of polymers randomly labelled with pyrene will initially have a high C_{Py} , generating lots of excimer and resulting in a high I_E/I_M ratio. As IPD occurs during film formation, the pyrene-labelled copolymer will diffuse into the surrounding non-fluorescent latex particles lowering C_{Py} , resulting in reduced excimer formation and a decrease in the I_E/I_M ratio. Since variations in the I_E/I_M ratio reflect the extent of IPD, the I_E/I_M ratio was monitored over time to quantitatively describe the IPD of polymer chains between latex particles during film formation.

The I_E/I_M ratio was used to calculate the fraction of mixing (f_m) between the latex particles as a function of annealing time and temperature. The colour of the films irradiated by UV light was also monitored to determine whether a discernible colour change was apparent over the annealing process. In turn, f_m was used to calculate the apparent diffusion coefficients of the pyrene-labelled copolymer. Lastly,

the diffusion coefficients were used to calculate the apparent activation energy of diffusion and the c_1 and c_2 terms in the WLF equation.

Acknowledgements

I would like to thank BASF for the opportunity to work on this project. I would also like to thank my supervisors Prof. Jean Duhamel and Prof. Mario Gauthier for their continued mentorship and support. I would like to acknowledge my committee members Prof. Alexander Penlidis and Prof. Xiaosong Wang, along with BASF representatives Dr. James Taylor and Dr. Dave Campbell for their continued support. I would like to thank all the members of Prof. Duhamel's and Prof. Gauthier's groups. Finally, I would like to thank NSERC for their funding.

Table of Contents

AUTHOR'S DECLARATION.....	ii
Abstract.....	iii
Acknowledgements.....	v
Table of Contents.....	vi
List of Figures.....	viii
List of Tables.....	xii
List of Schemes.....	xiii
Abbreviations.....	xiv
Chapter 1 Introduction.....	1
1.1 Background.....	1
1.2 Using Pyrene to Probe IPD.....	2
1.3 FRET Theory.....	4
1.4 Thesis Outline.....	8
Chapter 2 Preparation of Pyrene-Labelled Latex Particles.....	10
2.1 Overview.....	10
2.2 Materials.....	12
2.3 Instrumentation.....	13
2.4 Synthesis of Pyrene-Labelled Monomers.....	15
2.4.1 Method 1: Williamson Ether Synthesis Using Silver (I) Oxide.....	15
2.4.2 Method 2: Anionic Polymerization.....	17
2.5 Characterization of Pyrene-Labelled Monomers.....	18
2.6 Emulsion Polymerization.....	27
2.6.1 Native Latex.....	27
2.6.2 Pyrene-Labelled Latex.....	27
2.6.3 Polymer Isolation.....	28
2.7 Characterization of Latexes.....	29
2.8 Summary.....	37
Chapter 3 Film Formation.....	39
3.1 Overview.....	39
3.2 Experimental.....	42
3.3 Steady-State Fluorescence.....	44

3.3.1 Monomer Reabsorption and the I_E/I_M Ratio.....	44
3.3.2 Fraction of Mixing Between Latex Particles	46
3.3.3 Film Colour Change.....	53
3.4 Apparent Diffusion Coefficient (D).....	57
3.4.1 The Model.....	57
3.4.2 Results and Discussion.....	58
3.4.3 Further Analysis: WLF Method.....	62
3.4.4 Further Analysis: Winnik's FRET Method.....	66
3.5 Conclusions.....	70
Chapter 4 Summary and Future Work	72
Appendix A Calculated Values from Film Formation.....	76
Python Program used to Model Diffusion Coefficients.....	81
References.....	83

List of Figures

Figure 1: Reaction scheme for pyrene excimer formation (top) and resulting steady-state fluorescence spectrum (bottom). The dashed line represents the monomer emission spectrum hidden underneath the excimer spectrum. The fluorescence intensity is displayed in arbitrary units (a.u.). 3

Figure 2: Illustration of the mixing between latex particles containing polymers labelled with a donor (D) and an acceptor (A) as the particles are annealed above the MFT..... 4

Figure 3: General structure of pyrene-labelled monomers (PyLMs) with a degree of ethoxylation n 11

Figure 4: 300 MHz ^1H NMR spectrum for 1-pyrenylmethoxy-2-ethoxy-2-ethoxy-2-ethanol in deuterated dimethyl sulfoxide ($\text{DMSO-}d_6$): δ 8.0-8.4 (m, 9 H), 5.2 (s, 2 H), 4.6 (t, 1 H), and 3.4-3.8 ppm (m, 12 H). Residual solvent peaks are present at δ 3.3 ppm for water and 2.5 ppm for DMSO. 19

Figure 5: A) Steady-state fluorescence spectrum for PyEG_3OH (—) compared to that for a fluorescently degraded PyEG_2OH (•••) and B) time-resolved fluorescence decay of PyEG_3OH . The time-resolved fluorescence decay was acquired with a time-per-channel of 2.04 ns and fitted with a bi-exponential decay where $\tau_1 = 99$ ns, $a_1 = 0.08$, $\tau_2 = 285$ ns, and $a_2 = 0.9$. $\chi^2 = 1.03$, $\lambda_{ex} = 344$ nm. $[\text{PyEG}_3\text{OH}] = 2.3 \times 10^{-6}$ M. 21

Figure 6: Comparison of the 300 MHz ^1H NMR spectra obtained for (top) fluorescently pure and (bottom) fluorescently degraded PyEG_3OH in d_6 -DMSO: δ 8.0-8.4 (m, 9 H), 5.2 (s, 2 H), 4.6 (t, 1 H), and 3.4-3.8 ppm (m, 12 H). Residual solvent peaks are present at δ 3.3 ppm for water, 2.5 ppm for DMSO, and 2.09 ppm for acetone..... 22

Figure 7: 300 MHz ^1H NMR spectrum for 1-pyrenylmethoxy-2-ethoxy-2-ethoxy-2-ethoxy methacrylate in deuterated dimethyl sulfoxide ($\text{DMSO-}d_6$): δ 8.0-8.4 (m, 9 H), 5.9 (s, 1 H), 5.6 (s, 1 H), 5.2 (s, 2 H), 4.1 (t, 2 H), 3.5-3.7 (m, 10 H) and 1.8 ppm (s, 3 H). Residual solvent peaks are present at δ 3.3 ppm for water and 2.5 ppm for DMSO. 23

Figure 8: A) Steady-state fluorescence spectrum and B) time-resolved fluorescence decay for PyEG_3MA . The time-resolved fluorescence decay was acquired with a time-per-channel of 5.06 ns and fitted with a bi-exponential decay where $\tau_1 = 80$ ns, $a_1 = 0.06$, $\tau_2 = 281$ ns, and $a_2 = 0.94$; $\chi^2 = 1.06$, $\lambda_{ex} = 344$ nm, $[\text{PyEG}_3\text{OH}] = 2.3 \times 10^{-6}$ M. 24

Figure 9: 300 MHz ^1H NMR spectrum for 1-pyrenylmethoxy-PEO_{9,4}- methacrylate in deuterated dimethyl sulfoxide ($\text{DMSO-}d_6$): δ 8.0-8.4 (m, 9 H), 6.0 (s, 1 H), 5.6 (s, 1 H), 5.2 (s, 2 H), 4.2 (t, 2 H), 3.4-3.7 (m, 35 H) and 1.8 ppm (s, 3 H). A residual solvent peak is present at δ 3.3 ppm for water. The small peaks at δ 2.0, 1.4 and 1.1 ppm are impurities from the methacrylic anhydride used. 25

Figure 10: Diagram of the experimental setup used for emulsion polymerization.	28
Figure 11: GPC traces for crude Py-PBMA-latex-1 obtained with differential refractive index (DRI, —) and UV absorbance (••) detectors. The dashed lines were added to help guide the eyes.	33
Figure 12: Fluorescence intensity of the I_I peak for pyrene derivatives in the dialysate. The I_I peak was normalized to a pyrene standard in ethanol.	34
Figure 13: GPC traces for Py-PBMA-latex-1 after dialysis obtained using the DRI (—) and UV absorbance (••) detectors. The dashed lines were added to help guide the eyes.	35
Figure 14: GPC traces for crude Py-PBMA-latex-2 obtained with DRI (—) and UV absorbance (••). The dashed lines were added to help guide the eyes.	36
Figure 15: Illustration of the diffusion of pyrene-labelled polymer across the latex particle boundaries from the initial time (t_0) to time $t > t_0$ as the film is annealed above its minimum film formation temperature.	39
Figure 16: Comparison of the UV absorbance spectra (left) for the Py-PBMA-latex-1 polymer in THF at relatively low (—) and high (••) concentrations, and the steady-state fluorescence spectrum (right) for a pyrene concentration of 0.1 OD at 344 nm. $\lambda_{ex} = 344$ nm.	45
Figure 17: Steady-state spectra for Py-PBMA-latex-1 in a thick film before annealing (—) and a thin homogeneous (cast) film (••). $\lambda_{ex} = 344$ nm.	46
Figure 18: Steady-state fluorescence spectra for a film after drying at room temperature for 3 hours (—) and overnight (••). $\lambda_{ex} = 344$ nm.	47
Figure 19: Steady-state fluorescence spectra obtained for A) Film 1 containing Py-PBMA-Latex-1 annealed at 102 °C and B) expanded area corresponding to the excimer fluorescence. The curves from top to bottom are for $t_{an} = 0, 25, 110, 560$ min., and a homogeneous film ($t_{an} = \infty$). $\lambda_{ex} = 344$ nm.	48
Figure 20: Fraction of mixing of A) Film 1 (Py-PBMA-Latex-1: $M_n = 430$ kg·mol ⁻¹) and B) Film 2 (Py-PBMA-Latex-2: $M_n = 198$ kg·mol ⁻¹) annealed at 102 °C.	49
Figure 21: Fraction of mixing for Film 1, consisting of higher molecular weight copolymer. $T_{an} = 119$ (□), 112 (◆), 111 (△), 102 (●), 98 (✕),	51
Figure 22: Fraction of mixing for Film 2, consisting of lower molecular weight copolymer. $T_{an} = 119$ (□), 112 (◆), 111 (△), 102 (●), 98 (✕), 94 (■), 88 (◇), 84 (▲), and 75 (○) °C. Py-PBMA-Latex: $M_n = 198$ kg·mol ⁻¹ , $D = 1.8$; PBMA-Latex: $M_n = 190$ kg·mol ⁻¹ , $D = 1.7$	52
Figure 23: Emission colour change for Film 2 annealed at 84 °C, irradiated by UV light. From left to right $f_m = 0.00, 0.35, 0.69, 1.00$	53

- Figure 24:** Decrease in the excimer emission intensity for Film 2 over the course of film formation at 84 °C. From left to right, $f_m = 0.00, 0.35, 0.69, 1.00$ 54
- Figure 25:** Concentration of pyrene diffusing out of a particle of radius R , as a function of distance r from the particle center, for different annealing times. From top to bottom: $(Dt/r^2)^{1/2}$ equals 0.00, 0.25, 0.50, 0.75, and 1.00, corresponding to $f_m = 0.00, 0.41, 0.71, 0.86, \text{ and } 0.93$, respectively..... 58
- Figure 26:** Plot of the apparent diffusion coefficients as a function of annealing time for A) Film 1, containing high molecular weight copolymer chains (Py-PBMA-Latex: $M_n = 430 \text{ kg}\cdot\text{mol}^{-1}$, $D = 1.9$; PBMA-Latex: $M_n = 510 \text{ kg}\cdot\text{mol}^{-1}$, $D = 2.0$) and B) Film 2, containing a lower molecular weight polymer (Py-PBMA-Latex: $M_n = 198 \text{ kg}\cdot\text{mol}^{-1}$, $D = 1.8$; PBMA-Latex: $M_n = 190 \text{ kg}\cdot\text{mol}^{-1}$, $D = 1.7$). From top to bottom $T_{an} = 119, 112, 111, 102, 98, 94, 88, 84, \text{ and } 75$ °C. 60
- Figure 27:** Plot of the apparent diffusion coefficients as a function of fraction of mixing f_m for A) Film 1, containing high molecular weight polymer chains (Py-PBMA-Latex: $M_n = 430 \text{ kg}\cdot\text{mol}^{-1}$, $D = 1.9$; PBMA-Latex: $M_n = 510 \text{ kg}\cdot\text{mol}^{-1}$, $D = 2.0$) and B) Film 2, containing lower molecular weight polymers (Py-PBMA-Latex: $M_n = 198 \text{ kg}\cdot\text{mol}^{-1}$, $D = 1.8$; PBMA-Latex: $M_n = 190 \text{ kg}\cdot\text{mol}^{-1}$, $D = 1.7$). From top to bottom $T_{an} = 119, 112, 111, 102, 98, 94, 88, 84, \text{ and } 75$ °C. 61
- Figure 28:** Master curves for the reduced diffusion coefficient plotted as a function of annealing time using a reference temperature of 102 °C for A) Film 1, containing high molecular weight polymer chains (Py-PBMA-Latex: $M_n = 430 \text{ kg}\cdot\text{mol}^{-1}$, $D = 1.9$; PBMA-Latex: $M_n = 510 \text{ kg}\cdot\text{mol}^{-1}$, $D = 2.0$), and B) Film 2, containing lower molecular weight polymer (Py-PBMA-Latex: $M_n = 198 \text{ kg}\cdot\text{mol}^{-1}$, $D = 1.8$; PBMA-Latex: $M_n = 190 \text{ kg}\cdot\text{mol}^{-1}$, $D = 1.7$). $T_{an} = 119$ (□), 112 (◆), 111 (△), 102 (●), 98 (✕), 94 (■), 88 (◇), 84 (▲), and 75 (○) °C..... 63
- Figure 29:** Plot of the linearized WLF equation used to extract the c_1 and c_2 parameters for Film 1 (◇) and Film 2 (□). The slope and intercept for the dashed line equal -0.14 and -26.8 , respectively. $R^2 = 0.84$, $T_0 = 102$ °C. 64
- Figure 30:** Arrhenius behaviour of the apparent activation energy of diffusion for Film 1 (◇, $E_a = 105 \pm 2 \text{ kJ}\cdot\text{mol}^{-1}$) and Film 2 (□, $E_a = 100 \pm 4 \text{ kJ}\cdot\text{mol}^{-1}$)..... 66
- Figure 31:** Arrhenius plots used to find the activation energy of the diffusion coefficient for A) Film 1 ($M_w = 817 \text{ kg}\cdot\text{mol}^{-1}$, $D = 1.9$, $E_a = 180 \pm 8 \text{ kJ}\cdot\text{mol}^{-1}$), B) Film 2 ($M_w = 356 \text{ kg}\cdot\text{mol}^{-1}$, $D = 1.8$, $E_a = 160 \pm$

21 $\text{kJ}\cdot\text{mol}^{-1}$), and C) a PBMA film using FRET measurements ($M_w = 420 \text{ kg}\cdot\text{mol}^{-1}$, $D = 5.0$, $E_a = 159 \text{ kJ}\cdot\text{mol}^{-1}$).⁵ The fraction of mixing was held constant for each series, as indicated in the figures..... 67

Figure 32: Diffusion coefficients and their master curves prepared using E_a for A) Film 1 and B) Film 2 using a reference temperature $T_0 = 75 \text{ }^\circ\text{C}$, and C) a PBMA film probed by FRET ($M_n = 38 \text{ kg}\cdot\text{mol}^{-1}$, $T_0 = 56 \text{ }^\circ\text{C}$).³⁰ 69

List of Tables

Table 1: Decay times (τ) and pre-exponential factors (a) for bi-exponential fits of PyLMs and their precursors in THF. The monomer lifetime was taken as the more heavily weighted decay time.	26
Table 2: Characteristics of latexes prepared by emulsion copolymerization of <i>n</i> -butyl methacrylate with PyLMs.....	31
Table 3: Composition of the films used to probe film formation and polymer diffusion.	42
Table 4: Overview of colour changes observed during film formation for Film 1.	55
Table 5: Overview of colour changes observed during film formation for Film 2.	56
Table 6: Shift factors for the reduced diffusion coefficients used to prepare the master curves.....	62

List of Schemes

Scheme 1: Reaction scheme for the synthesis of PyEG ₃ OH.	16
Scheme 2: Reaction scheme for the synthesis of PyEG ₃ MA.....	16
Scheme 3: Equilibrium between pyrene monomers and dimers in a pyrene-labelled film above the MFT.	40

Abbreviations

A	Acceptor
AOT	Sodium dioctyl sulfosuccinate
a_T	Temperature shift factor
<i>a.u.</i>	Arbitrary units
B_1	Contribution of donors that undergo FRET
B_2	Contribution of donors that emit with their natural lifetime
BMA	<i>n</i> -Butyl methacrylate
C_0	Initial concentration of labelled polymer
C_{Py}	Local pyrene concentration
D	Apparent diffusion coefficient
D'	Temperature-normalized apparent diffusion coefficient
D	Donor
\bar{D}	Molecular weight dispersity
DIW	Deionized water
DCM	Dichloromethane
DLS	Dynamic light scattering
DMF	<i>N,N</i> -Dimethylformamide
DMSO	Dimethyl sulfoxide
DRI	Differential refractive index
f_m	Corrected fraction of mixing
f'_m	Apparent fraction of mixing
FRET	Fluorescence resonance energy transfer
GPC	Gel permeation chromatography
I_E/I_M	Ratio of the fluorescence intensity of the pyrene excimer over that of the pyrene monomer
IPD	Interparticle polymer diffusion
K	Experimental scaling factor
K'	Equilibrium constant between pyrene monomer and dimer
MFT	Minimum film formation temperature
M_n	Number-average molecular weight

M_t	Mass of labelled polymer that has diffused across the boundary at time t
M_w	Weight-average molecular weight
NMR	Nuclear magnetic resonance
P	Fitted parameter proportional to the acceptor concentration
PBMA	Poly(n -butyl methacrylate)
PSD	Particle size dispersity
Py	Pyrene
PyEG _{n} MA	Pyrene-labelled monomer with an oligo(ethylene glycol) linker length having a degree of ethoxylation n
PyLM	Pyrene-labelled monomer
Py-PBMA	Pyrene-labelled poly(n -butyl methacrylate)
R	Latex particle radius
T_{an}	Annealing temperature
T_0	Reference temperature
τ_D	Donor lifetime
T_g	Glass transition temperature
THF	Tetrahydrofuran
UV	Ultraviolet
V_o	Volume of film irradiated
Φ_{ET}	Energy transfer efficiency

Chapter 1

Introduction

1.1 Background

Films formed by aqueous latex dispersions have many uses, particularly in the paint industry. The conditions under which a uniform film is formed from latex particles strongly affect the rate at which the polymer chains in the particles interdiffuse. A film in which the latex particles are not allowed to fully coalesce can lead to poor mechanical strength and a performance below expected standards.^{1,2} For example, if a film is to be used for corrosion resistance and it is not fully coalesced, small voids may be present which will allow small molecules, such as water, to permeate through and reach the substrate, thereby undermining the protective properties expected for the film. The formation of latex films is generally divided into three main stages:^{1,3,4} evaporation of water, packing of the latex particles, and coalescence of the particles into a uniform film. In the first stage, water evaporates and leaves a matrix of uniformly packed latex particles. The array of particles in Stage 1 has numerous voids. Stage 2 involves the deformation of the latex particles as they fill in the voids in the matrix. In Stage 3, the polymer chains diffuse across the latex boundaries to generate the film. In order for the latex particles to deform and coalesce, a certain minimum temperature is required, namely the minimum film formation temperature (MFT), which is generally slightly above the glass transition temperature (T_g) of the polymer constituting the latex.⁵ Above the MFT the polymer chains can interdiffuse between the latex particles, generating entanglements leading to the formation of a homogeneous film. The degree of interparticle polymer diffusion (IPD) is a measure of the extent of chain diffusion that takes place between the latex particles. Several methods have been developed to probe IPD, but to date fluorescence resonance energy transfer (FRET)⁶⁻⁸ and small angle neutron scattering (SANS)⁹ have been most commonly used.

In FRET studies two fluorophores, an energy donor like phenanthrene and an energy acceptor like anthracene, are selected to fluorescently label the latex particles. The two types of latex particles, one labelled with the donor and one with the acceptor, are mixed to form a film such that the edges between the two particles are the only locations in the film where FRET initially takes place. As the latex film is annealed ($T > MFT$) and the particles begin to coalesce the level of energy transfer increases, which can be monitored through time-resolved fluorescence. Although this method is very informative, it requires careful selection of the chromophores. The fluorescence spectrum of the donor must overlap with the absorbance spectrum of the acceptor, and the absorbance spectrum of the acceptor must offer a spectral window where the donor can be selectively excited. This procedure also requires that two separate batches of fluorescently labelled polymers be produced. Furthermore chromophores like phenanthrene and anthracene, intensively used to probe IPD in latex films by FRET, both emit in the ultraviolet (UV) region, which prevents the rapid visual inspection of the fluorescently labelled films. Small angle neutron scattering measurements use films prepared from a mixture of deuterated and non-deuterated latex particles. Diffusion of the deuterated polymer chains through the latex matrix can be monitored by neutron scattering. Although this method only requires the production of one batch of labelled latex particles, the deuterated polymer is very expensive, and the measurements necessitate the use of a neutron source and detector. Both of these methods are powerful means to probe the MFT and IPD of latex films, but we believe that the same information can be obtained in a simpler manner using the dye pyrene.

1.2 Using Pyrene to Probe IPD

We propose a new approach to probe the MFT and IPD in latex films using pyrene excimer formation. When pyrene is excited by a photon of light, it emits a blue colour. If an excited pyrene encounters a ground-state pyrene, it forms an excited dimer (excimer) which emits a turquoise colour. The amount of excimer formed can be quantified with a steady-state (SS) fluorometer, by measuring the ratio of the

fluorescence intensity of the pyrene excimer over that of the monomer, namely the I_E / I_M ratio. A diagram depicting the kinetic scheme of pyrene excimer formation and the resulting SS fluorescence spectrum is shown in Figure 1. By preparing a polymer randomly labelled with pyrene by emulsion polymerization and incorporating it into a matrix of non-fluorescent latex particles, the I_E / I_M ratio can be used to determine the MFT and monitor the degree of IPD.

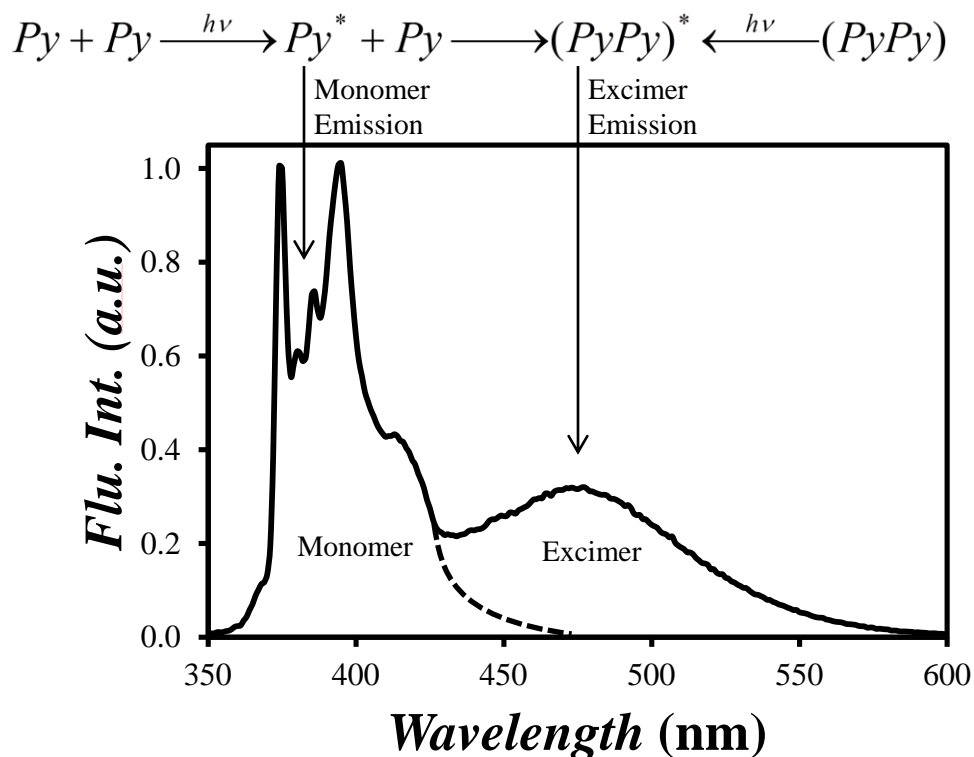


Figure 1: Reaction scheme for pyrene excimer formation (top) and resulting steady-state fluorescence spectrum (bottom). The dashed line represents the monomer emission spectrum hidden underneath the excimer spectrum. The fluorescence intensity is displayed in arbitrary units (a.u.).

The I_E / I_M ratio depends on the local concentration of pyrene (C_{Py}) in the film. When the fluorescently labelled latex particles are first mixed into a matrix of native latex the I_E / I_M ratio is

expected to be high, and the film should fluoresce with a turquoise colour. As the film is heated above its MFT and the pyrene-labelled copolymer diffuses throughout the matrix, C_{Py} decreases, lowering the I_E/I_M ratio and causing a colour change from turquoise to blue. Due to the visible fluorescence emission change of the pyrene-labelled polymer as the film anneals, the MFT and level of IPD could be qualitatively probed by mere visual inspection of the polymer film irradiated with a handheld UV lamp. This proposed method, although based on fluorescence as previous FRET studies, has several distinct advantages such as the use of a single fluorescently labelled latex, and the possibility to probe IPD either quantitatively, with an easy to operate steady-state fluorometer, or qualitatively, by visual inspection of a latex film irradiated with a handheld UV lamp.

1.3 FRET Theory

When FRET is used to probe IPD in a latex film, the film initially consists of individual latex particles containing polymers labelled with either a donor (D) or an acceptor (A). As the film anneals the polymer chains in the individual latex particles begin to diffuse into neighbouring particles, allowing the donor and acceptor labels to mix as illustrated in Figure 2.⁶ The fraction of donors and acceptors that have mixed can be determined by time-resolved fluorescence, to obtain quantitative information about the diffusion coefficients of the diffusing polymer chains.



Figure 2: Illustration of the mixing between latex particles containing polymers labelled with a donor (D) and an acceptor (A) as the particles are annealed above the MFT.

In the analysis of FRET data, two time scales play an important role. The excited fluorophore decays to the ground state within a few tens of nanoseconds, while IPD occurs over times ranging from minutes to days. In order to obtain quantitative information about IPD, time-resolved fluorescence decays must be obtained for the energy donor. When the donor is excited by a photon of light, it emits with its natural lifetime τ_D . If a ground-state acceptor is nearby, the donor can transfer its excess energy to the acceptor which becomes excited. The rate of energy transfer is inversely proportional to the sixth power of the distance (d) separating the donor from the acceptor. Because of this, distance plays a very important role in the rate of energy transfer, and since every donor-acceptor pair is separated by different distances throughout the latex, the analysis of the fluorescence decays is complicated. By assuming that donors and acceptors are evenly distributed in the regions of the film where the particles have coalesced, the fluorescence decay curve of the energy donor $I_D(t)$ can be fitted to Equation 1.¹⁰

$$I_D(t) = B_1 \exp\left[-\frac{t}{\tau_D} - P\left(\frac{t}{\tau_D}\right)^{\frac{1}{2}}\right] + B_2 \exp\left(-\frac{t}{\tau_D}\right) \quad (1)$$

In Equation 1, B_1 is the contribution to the fluorescence intensity from the donor that undergoes FRET, B_2 is the contribution from the donor that does not undergo FRET, and P is a fitting parameter that is proportional to the local acceptor concentration felt by the excited donor. The experimental apparent volume fraction of mixing $f'_m(t)$, where t is the annealing time, can then be calculated from the B_1 and B_2 terms using Equation 2.

$$f'_m(t) = \frac{B_1}{B_1 + B_2} \quad (2)$$

A correction to this term must be made since the boundaries of the latex particles at $t = 0$ are in contact and can undergo energy transfer, causing $f'_m(0)$ to be greater than zero. Similarly the film may not be

fully mixed at long annealing times, causing $f'_m(\infty)$ to be close but not equal to unity. The corrected fraction of mixing $f'_m(t)$ in Equation 3 takes these effects into account.

$$f'_m(t) = \frac{f'_m(t) - f'_m(0)}{f'_m(\infty) - f'_m(0)} \quad (3)$$

In a paper by Wang and Winnik, it was pointed out that if the P term in Equation 1 did not remain constant as a function of time (as it should), then an error was introduced into the calculation of $f'_m(t)$ and the results were skewed.⁶ By integrating the decay curve and using the area under the curve $Area(t)$ as a measure of the efficiency of energy transfer, the problem of time-dependent P values could be avoided. Based on these considerations, Equation 3 was rewritten into Equation 4. Since the area under the decay curve is proportional to the energy transfer efficiency $\Phi_{ET}(t)$, $Area(t)$ in Equation 4 can be replaced by $\Phi_{ET}(t)$ as defined in Equation 5.⁷

$$f'_m(t) = \frac{Area(t) - Area(0)}{Area(\infty) - Area(0)} = \frac{\Phi_{ET}(t) - \Phi_{ET}(0)}{\Phi_{ET}(\infty) - \Phi_{ET}(0)} \quad (4)$$

$$\Phi_{ET}(t) = 1 - \frac{Area(t)}{\tau_D} \quad (5)$$

It should be noted that Equation 1 relies on the assumption that the donors and acceptors are evenly distributed in the mixed volume at the interface between the latex particles. This assumption represents an approximation which affects the calculation of f'_m with Equation 4. This approximation can be avoided by conducting Monte Carlo simulations, whereby a film is generated by randomly placing donors and acceptors centered around a plane representing the midpoint of the interfacial volume between the two latex particles where the donor and acceptor labels mix. The donor fluorescence intensity decay from a film may then be fitted to an equation which takes into account the distribution of D-A pair distances in the interfacial region. A study by Yang and Winnik found that assuming a constant concentration of

acceptors in the mixed volume as done with Equation 4 led to an overestimation of Φ_{ET} as compared to what was obtained by this Monte Carlo method.¹¹

In order to describe quantitatively IPD, the diffusion coefficients of the polymer chains reptating across the latex boundary must be determined. This was achieved by applying Fick's law to molecules diffusing out of a spherical particle as shown in Equation 6.

$$\frac{\partial C(r,t)}{\partial t} = \frac{1}{r^2} \frac{\partial}{\partial r} \left(Dr^2 \frac{\partial C(r,t)}{\partial r} \right) \quad (6)$$

In Equation 6, $C(r,t)$ is the local acceptor concentration, r is the distance from the center of the latex particle and D is the diffusion coefficient of the polymer chains bearing the fluorophores. Integration of this differential equation yields $C(r,t)$ as given by Equation 7.

$$C(r,t) = \frac{C_0}{2} \left[\operatorname{erf} \left(\frac{R+r}{2(Dt)^{\frac{1}{2}}} \right) + \operatorname{erf} \left(\frac{R-r}{2(Dt)^{\frac{1}{2}}} \right) \right] - \frac{C_0}{r} \left(\frac{Dt}{\pi} \right)^{\frac{1}{2}} \left[\exp \left(-\frac{(R-r)^2}{4Dt} \right) - \exp \left(-\frac{(R+r)^2}{4Dt} \right) \right] \quad (7)$$

In Equation 7, $\operatorname{erf}(x)$ is the error function associated with the integration of a normal distribution, R is the radius of the latex particle, and C_0 is the initial concentration. The fraction of mixing is equated to the fractional mass of polymer $f_m(t)$ that has diffused across the particle interface at time t :

$$f_m(t) = \frac{M_t}{M_\infty} \quad (8)$$

The total mass of polymer in the latex particle M_∞ is given by Equation 9,

$$M_\infty = \frac{4}{3} \pi R^3 C_0 \quad (9)$$

whereas the mass that has diffused across the interface at time t (M_t) can be calculated with Equation 10:

$$M_t = M_\infty - \int_0^R C(r,t) \cdot 4\pi r^2 dr \quad (10)$$

Substituting Equations 9 and 10 into Equation 8 yields the calculated fraction of mixing at time t given in Equation 11.

$$f_m(t) = 1 - \frac{\int_0^R C(r,t) \cdot 4\pi r^2 dr}{\frac{4}{3}\pi R^3 C_0} \quad (11)$$

By numerical integration of Equation 7 for a given D , and equating the calculated f_m value in Equation 11 to the experimental value found from Equation 4, D can be optimized to find the value which satisfies this equality.

1.4 Thesis Outline

The primary goal of this project was to demonstrate a new and simpler method to quantitatively probe the film formation process in latex films. As discussed in Chapter 2, a pyrene-labelled monomer must be prepared and copolymerized with *n*-butyl methacrylate to prepare a pyrene-labelled latex particle. Several PyLMs were prepared and characterized by proton NMR and UV absorbance. The fluorescently labelled particles must only contain pyrene that is bound to the polymer backbone, but since pyrene is highly hydrophobic and the PyLM needs to diffuse through the water phase during the emulsion polymerization, a PyLM needed to be identified for the emulsion in order to meet this requirement. A combination of gel permeation chromatography and UV absorbance measurements were used to characterize the polymer chains and the incorporation of the PyLM. Dynamic light scattering was used to characterize the size of the latex particles. Once the pyrene-labelled latex was prepared, it was mixed with non-fluorescent latex particles to form a latex film and the I_E/I_M ratio of the film was monitored as a function of the annealing time with a steady-state fluorometer as described in Chapter 3. Using these I_E/I_M ratios, the fraction of mixing f_m between the latex particles was calculated and its behavior as a function of annealing time was compared to other examples reported in the literature. In addition, the diffusion coefficients for the

copolymer chains bearing the pyrene pendants were calculated for different annealing temperatures over time. In order to further test this new method used to probe film formation, the apparent activation energy of diffusion and the c_1 and c_2 terms from the William-Landel-Ferry (WLF) equation were calculated. This was achieved by applying two different methods. The first procedure was based on the WLF equation and the second one relied on a method developed by the Winnik group.^{2,4-6,8} A more qualitative analysis of the film formation process by visual colour change was also developed.

Chapter 2

Preparation of Pyrene-Labelled Latex Particles

2.1 Overview

The first step in this project was to find a pyrene-labelled monomer (PyLM) that was suitable for use in both emulsion polymerization and interparticle polymer diffusion (IPD) measurements. The first requirement of the PyLM was a suitable level of hydrophobicity. The water solubility of the PyLM had to be tuned such that the monomer remained hydrophobic, but could still be incorporated into a copolymer by emulsion polymerization. On the one hand, an extremely hydrophobic monomer would not be able to diffuse readily enough through the aqueous phase during emulsion polymerization and thus would not be incorporated into the polymer backbone at sufficiently high levels. On the other hand, if the monomer were too hydrophilic, it would remain in the aqueous phase and again would not be fully incorporated into the polymer particles. Another aspect of the PyLM that must be taken into account is its molecular weight. Ideally, the fluorescently-labelled copolymer should have the same physical properties, such as T_g in the case of IPD measurements, as its native counterpart being studied. This way, the results from the IPD measurements obtained using the labelled copolymer would be expected to be the same as the unlabelled latex. The T_g of a copolymer can be estimated using Equation 12 which was derived by Fox,¹²

$$\frac{1}{T_g} = \frac{w_1}{T_{g,1}} + \frac{w_2}{T_{g,2}} \quad (12)$$

where w_1 and w_2 are the weight fractions of each monomer component and $T_{g,1}$ and $T_{g,2}$ are the T_g of the homopolymers derived from each monomer. From this equation, it is easily seen that in order to minimize the change in T_g between the native and labelled polymers the weight fraction of PyLM must be minimized. Upon consideration of all the desired features for the PyLM, it became obvious that a fine balance needed to be achieved between increasing the linker length to enhance the water transportability

of the PyLM during the emulsion polymerization, while still maintaining a short enough linker length such that the final polymer would still exhibit the same properties as the native polymer (see Figure 3). To this end, a series of PyLMs were prepared with varying hydrophobicity.

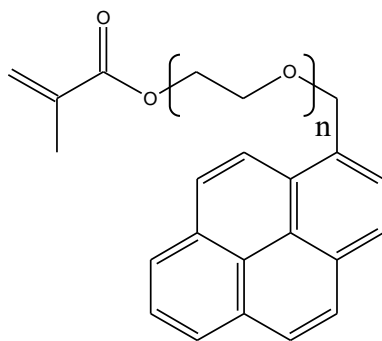


Figure 3: General structure of pyrene-labelled monomers (PyLMs) with a degree of ethoxylation n .

Two different synthetic methods were used to prepare the PyLMs with a chemical structure as shown in Figure 3. The first method was used to prepare monomers with short ($n = 1-3$) oligo(ethylene glycol) spacers, while the second was used for longer ($n \geq 9$) poly(ethylene oxide) chains. Method 1 was adapted from published procedures on the monoprotection of a diol with benzyl bromide¹³ followed by methacrylation of the alcohol.¹⁴ This procedure resulted in a PyLM with a monodisperse linker length. However, its preparation was limited to smaller scale reactions (2-3 g) due to the limited availability and high cost of the required materials. Method 2 used anionic polymerization and thus allowed for larger scale production. However, it required handling toxic ethylene oxide and resulted in a PyLM with a polydisperse linker length. In total, five PyLMs were synthesized with $n = 1, 2, 3, 9,$ and 71 . Procedures of both methods for the preparation of the PyLMs with $n = 3$ for Method 1 and $n = 9$ for Method 2 are described in the following sections.

The next step of the project was to prepare both non-fluorescent and pyrene-labelled (fluorescent) latex particles. The latex particles were prepared by emulsion polymerization using n -butyl methacrylate

(BMA) for the native particles, and a mixture of BMA and PyLM for the fluorescently-labelled latex particles. The emulsion recipe was first optimized for the native latex such that the resulting latexes were stable, had a reproducible particle size, and a low particle size dispersity (PSD). After optimization, the final recipe used a semi-batch emulsion process with a pre-emulsified monomer feed. Using this recipe, the fluorescently-labelled latex particles were prepared in a similar manner.

2.2 Materials

Acetone (Sigma-Aldrich, 99.9%), ammonium persulfate (APS, Sigma-Aldrich, 98%), *n*-butyl methacrylate (BMA, Sigma-Aldrich, 99%), calcium hydride (CaH₂, Aldrich, 98%), 4-dimethylaminopyridine (DMAP, Alfa Aesar, 99%), dioctyl sodium sulfosuccinate (AOT, Sigma-Aldrich, 98%), ethanol (Fisher Scientific, HPLC), ethyl acetate (Sigma-Aldrich, 99.7%), hexane (mixture of isomers, Sigma-Aldrich, 98.5%), methacrylic anhydride (MAAn, Sigma-Aldrich, 94%), methanol (Sigma-Aldrich, 99.9%), 1-pyrenemethyl bromide (Sigma-Aldrich, 98%), silver (I) oxide (Sigma-Aldrich, 99%), sodium bicarbonate (BDH, 99.7%), tetrahydrofuran (THF, Sigma-Aldrich, 99%), distilled in glass tetrahydrofuran (inhibitor-free, Caledon), triethylamine (Sigma-Aldrich, 99%), and triethylene glycol (Sigma-Aldrich, 99%) were used as received. Dichloromethane (DCM, Sigma-Aldrich, 99.8%) was freshly distilled prior to use. Deionized water (DIW) was used to prepare all the emulsions.

1-Pyrenemethanol (Sigma-Aldrich, 98%) was purified by recrystallization according to the following procedure. 1-Pyrenemethanol (3.5 g, 15 mmol) and ethanol (10 mL) were added to a 100 mL Erlenmeyer flask. The solution was heated on a hot plate until the ethanol began to boil, and an additional 15 mL of ethanol was then slowly added until all the 1-pyrenemethanol dissolved. The flask was removed from the heat, sealed, and cooled in a refrigerator for 1 h. The solution was then filtered through Whatman #1 filter paper on a suction flask and rinsed with cold ethanol. The collected 1-pyrenemethanol (3.0 g, 13 mmol, 86% yield) was dried under vacuum and stored in the dark.

Ethylene oxide was purified before use according to the following procedure. A glass manifold with a round bottom flask was mounted on a high vacuum line together with an ampule containing powdered CaH_2 and a magnetic stirring bar, along with an ethylene oxide supply line. The system was evacuated (ca. 0.1 mm Hg) and the glassware was flamed to remove residual moisture. Once the glassware had cooled, the ampule containing CaH_2 was sealed. The rest of the system was purged with dry nitrogen, a 2 M solution of phenylmagnesium chloride in THF (corresponding to ca. 10 % of the volume of ethylene oxide to be purified) was added to the round bottom flask, and the THF was removed under vacuum with stirring. The manifold was then isolated under vacuum, the round bottom flask containing the phenylmagnesium chloride was cooled in an ice bath, and ethylene oxide was transferred from the tank. The ethylene oxide was stirred with the phenylmagnesium chloride for 10 min and the monomer was degassed with three freeze-pump-thaw cycles, using liquid nitrogen to freeze the monomer and an ice bath to thaw it. After the final thaw, the ethylene oxide was transferred under vacuum to the ampule containing CaH_2 by cooling the ampule in liquid nitrogen. Once the ethylene oxide transfer was completed, the ampule was sealed and slowly warmed to room temperature with stirring.

2.3 Instrumentation

^1H NMR: All proton NMR samples were prepared in deuterated dimethyl sulfoxide (d_6 -DMSO, Sigma-Aldrich, 99.9 atom% D) and acquired using 16 scans on a 300 MHz Bruker instrument.

UV-Vis Absorbance: All UV-Vis absorbance measurements were carried out using a Cary 100 Bio UV-Visible spectrophotometer. Samples were prepared using inhibitor-free THF and run in a 1 cm path length quartz cell. The absorption was scanned from 400 to 250 nm in 1 nm increments at a scan rate of 10 $\text{nm}\cdot\text{s}^{-1}$.

Steady-State Fluorescence: Measurements were carried out using a Photon Technology International (PTI) steady-state fluorometer equipped with a xenon arc lamp. The samples were excited at a wavelength

of 344 nm and the emission was scanned from 350 to 600 nm in one nanometer increments at a scan rate of $10 \text{ nm}\cdot\text{s}^{-1}$. Samples were prepared in a custom-made sealable 1 cm x 1 cm quartz cell and outgassed with nitrogen for 45 minutes to remove dissolved oxygen. The solution was prepared such that the absorbance was no greater than 0.12 at 344 nm. The slit widths were set at 1 nm for excitation and 1/2 nm for emission.

Time-Resolved Fluorescence: The fluorescence decays of the samples used for the steady-state fluorescence experiments were acquired using an IBH time-correlated single photon counting (TC-SPC) fluorometer equipped with a nanoLED-340. The monomer decays were acquired by exciting the sample at 344 nm and monitoring the emission at 375 nm. A 370 nm cut-off filter was placed between the sample and the emission monochromator to minimize light scattering. The fluorescence decays were fitted with a bi-exponential function. To measure the goodness-of-fit the residuals, autocorrelation function of the residuals, and chi-squared (χ^2) were determined. The χ^2 is a measure of the sum of the errors between the data and a model, where unity would correspond to a perfect fit.

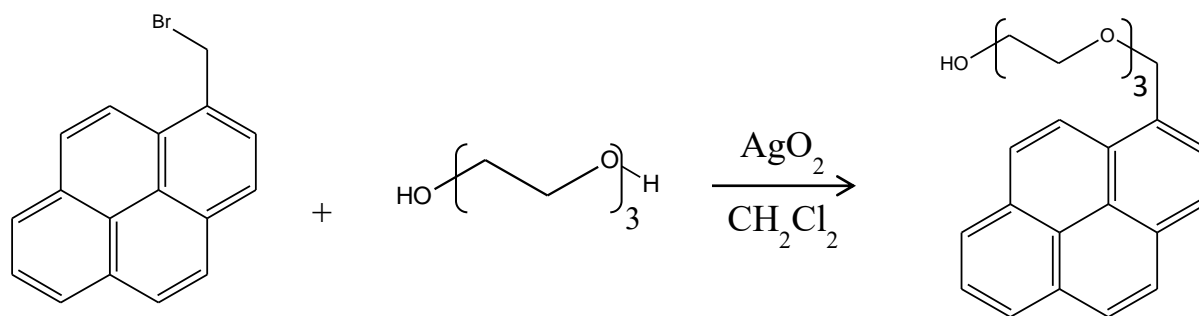
Gel Permeation Chromatography (GPC): A Viscotek VE 2001 GPC solvent/sample module was used in tandem with a TDA 305 triple detector array and a UV detector 2600 using a series of three PolyAnalytik SupeRes mixed bed columns and with THF as the mobile phase for all GPC measurements. The flow rate was set to $1 \text{ mL}\cdot\text{min}^{-1}$ with the column temperature maintained at $35 \text{ }^\circ\text{C}$. Samples were prepared at a concentration of $1 \text{ mg}\cdot\text{mL}^{-1}$ in THF and filtered through a PTFE membrane filter with a pore size of $0.22 \text{ }\mu\text{m}$ prior to injection. Differential refractive index (DRI), right-angle light scattering (RALS), low-angle light scattering (LALS) and viscosity detectors were used to calculate the absolute molecular weight and the dispersity (D) of the injected polymer samples. The UV absorbance at 344 nm was also collected in order to monitor the incorporation of pyrene in the polymer sample.

Dynamic Light Scattering (DLS): DLS measurements were carried out on a Brookhaven BI-200SM instrument equipped with a Clare Lasers Quiet-Power-660 laser light source. The light scattering was measured at a right angle to the incident beam with a sample temperature of 25 °C. The analysis was completed using a BI-9000AT digital autocorrelator. The hydrodynamic diameter of the particles was calculated by analyzing the autocorrelation function of the scattering intensity according to the method of moments that yielded the diameters d_1 and d_2 representing the first and second order moments of the autocorrelation function, respectively. The particle size was taken as the average of the two diameters and the particle size dispersity (PSD) as the ratio d_2/d_1 .

2.4 Synthesis of Pyrene-Labelled Monomers

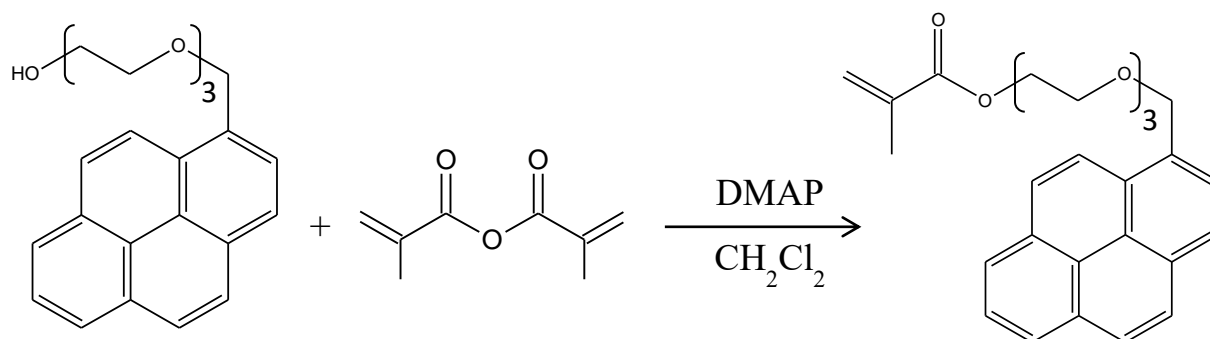
2.4.1 Method 1: Williamson Ether Synthesis Using Silver (I) Oxide

In a flame-dried 50 mL round bottom flask purged with nitrogen, triethylene glycol (1.0 g, 6.7 mmol) was dissolved in dry dichloromethane (25 mL) with stirring. Silver (I) oxide (2.3 g, 9.9 mmol) was then added to form a suspension in the solution. After 1 h of stirring, 1-pyrenemethyl bromide (Sigma-Aldrich, 2.0 g, 6.8 mmol, 1.02 eq) was added to the reaction which was stirred in the dark for two days (Scheme 1). The solution was then filtered to remove the silver oxide and concentrated on a rotary evaporator. The crude product was purified by column chromatography on silica (50 g, 2.0 cm diameter by 40 cm length) using a solvent gradient from ethyl acetate to acetone. The column was started with 150 mL of ethyl acetate. After ca. 75 mL of solvent had eluted, a 2:1 mixture of ethyl acetate and acetone (75 mL) was added to the reservoir. The addition of 75 mL of solvent was repeated once more with the 2:1 mixture after another 75 mL had eluted, and the procedure was repeated again with two 75 mL portions of 1:1 and 1:2 mixtures of ethyl acetate and acetone, and finally with two 75 mL portions of pure acetone. The product was collected as the second to last band (exhibiting green fluorescence under UV light) eluting from the column as a pale yellow oil (1.8 g, 72% yield) after solvent removal.



Scheme 1: Reaction scheme for the synthesis of PyEG₃OH.

In a flame-dried 50 mL Schlenk flask, ethoxylated pyrenemethanol (1.8 g, 4.9 mmol) and dimethylaminopyridine (DMAP, 60 mg, 0.5 mmol) were dissolved in dichloromethane (15 mL) under nitrogen. The solution was cooled in an ice bath and methacrylic anhydride (1.1 mL, 7.5 mmol, 1.5 eq) was added. The flask was sealed and stirred for 30 min in the ice bath, warmed to room temperature, and stirred further for 16 h (Scheme 2). A saturated aqueous solution of sodium bicarbonate (10 mL) was then added and stirred vigorously for 30 min. The monomer was washed once more with an aqueous solution of sodium bicarbonate (10 mL) and then with water (10 mL). Unreacted pyrene was removed by column chromatography on silica (20 g) using acetone with 0.1 vol% triethylamine (120 mL) as eluent. The product was collected as the second band that exhibited green fluorescence under UV light. Solvent removal yielded a pale yellow oil (2.0 g, 94% yield).



Scheme 2: Reaction scheme for the synthesis of PyEG₃MA.

2.4.2 Method 2: Anionic Polymerization

The purified ethylene oxide ampule and two empty ampules were mounted on a vacuum line manifold, and the glassware was flamed to remove residual moisture with the exception of the ampule containing ethylene oxide, which was cooled in an ice bath. An approximate amount (ca. 3 mL) of ethylene oxide was transferred to one of the ampules by cooling it in an ice bath, while the monomer ampule was warmed to room temperature. The manifold was then filled with dry nitrogen and the ampule containing the transferred ethylene oxide was removed for weighing, to determine the exact amount of ethylene oxide (2.51 g, 57 mmol) transferred. The amount of recrystallized 1-pyrenemethanol required for the target $n = 10$ (1.33 g, 5.7 mmol) was then loaded in the second ampule, along with 0.64 g (5.7 mmol) of potassium *tert*-butoxide. 1-Pyrenemethanol and potassium *tert*-butoxide were dissolved in dry THF (50 mL) and the solution was stirred for 30 min to deprotonate 1-pyrenemethanol. The solution was then frozen in liquid nitrogen and the purified ethylene oxide transferred under vacuum. The ampule was sealed, thawed in an ice bath, filled with nitrogen, and warmed to room temperature. After 10 min of stirring, the ampule was placed in a bath at 60 °C for ca. 60 h in the dark. The polymerization was terminated by the addition of several drops of deionized water. The solvent was removed under vacuum and purified by column chromatography over alumina (100 g) in a 3.5 cm diameter by 55 cm length column using a 2:1 mixture of ethyl acetate and hexane (1.1 L) as eluent. The product eluted as a tight cluster of bands, with the last collected fraction as the second to last band (exhibiting green fluorescence under UV light) and was recovered as a yellow oil (3 g, 78% yield) after solvent removal. The poly(ethylene oxide) chain segment had a degree of polymerization $n = 9$ based on NMR analysis.

A similar procedure as that used to prepare PyEG₃MA was applied to convert PyEG₉OH to the PyEG₉MA monomer.

2.5 Characterization of Pyrene-Labelled Monomers

In this section, the characterization of the PyLMs prepared by the two synthetic procedures above is described. More details are provided for the characterization of the PyLMs prepared by the two methods with $n = 3$ and 9. Although only these two PyLMs are discussed in full detail, each PyLM was fully characterized. An overview of the results from the time-resolved fluorescence analysis is provided at the end of the section in Table 1.

The PyLM synthesis using Method 1 ($n = 3$) was completed in two steps as depicted in Schemes 1 and 2. A common problem encountered during the synthesis was the degradation of pyrene, which resulted in a skewed steady-state fluorescence spectrum. Since the steady-state fluorescence spectrum of pyrene is pivotal to the project, it was important to ensure that all fluorescent impurities were removed after each synthetic step, so that the final PyLM was fluorescently pure. The ethoxylated 1-pyrenemethanol (PyEG₃OH) was first characterized by ¹H NMR analysis. Figure 4 shows the ¹H NMR spectrum obtained for the ethoxylated pyrenemethanol in *d*₆-DMSO with the signals for all the protons assigned.

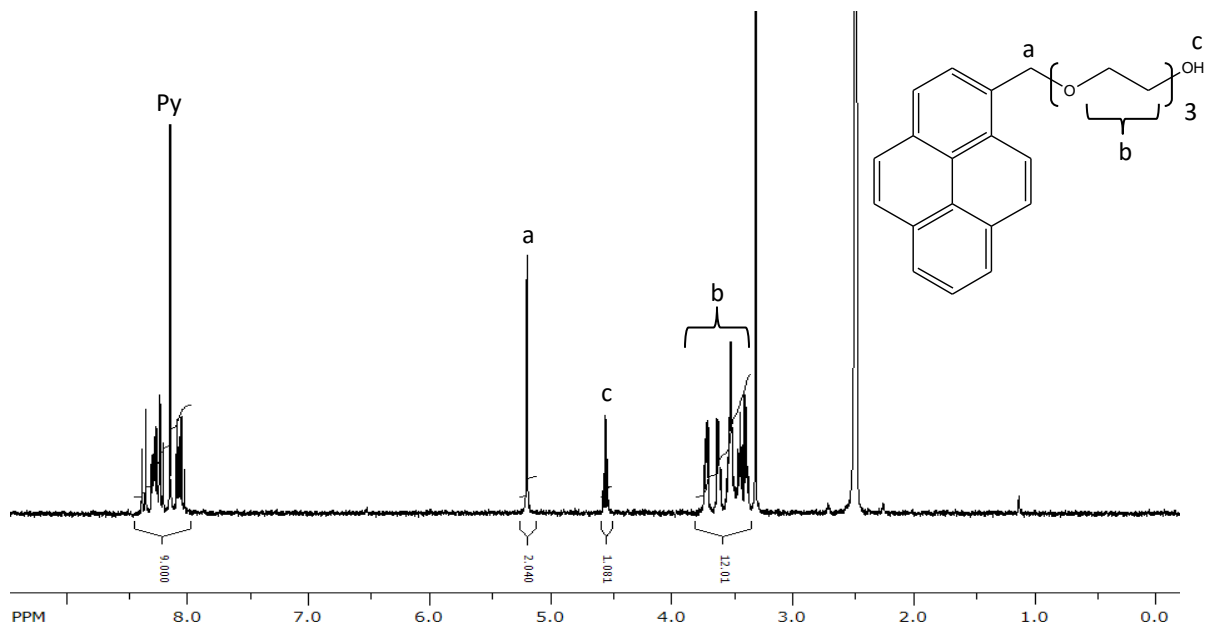


Figure 4: 300 MHz ^1H NMR spectrum for 1-pyrenylmethoxy-2-ethoxy-2-ethoxy-2-ethanol in deuterated dimethyl sulfoxide ($\text{DMSO-}d_6$): δ 8.0-8.4 (m, 9 H), 5.2 (s, 2 H), 4.6 (t, 1 H), and 3.4-3.8 ppm (m, 12 H). Residual solvent peaks are present at δ 3.3 ppm for water and 2.5 ppm for DMSO.

Since fluorescence is much more sensitive than ^1H NMR, and to insure that pyrene had not degraded during the first reaction, the fluorescence of the pyrene derivative was measured. A solution of PyEG_3OH in inhibitor-free THF was prepared with an absorbance of 0.1 at 344 nm, corresponding to a concentration of ca. 2.3×10^{-6} M. Using such a low concentration insured that there would be no intermolecular interactions between the PyEG_3OH molecules. The sample was outgassed using nitrogen for 45 minutes to remove any oxygen that would quench the pyrene fluorescence. Figure 5 shows the steady-state fluorescence spectrum and time-resolved fluorescence decay obtained for PyEG_3OH . The steady-state fluorescence spectrum, represented with a solid line, exhibits the four emission peaks characteristic for the pyrene monomer and no excimer formation. The time-resolved fluorescence decay

was fitted with a bi-exponential decay, where the lifetimes (τ_i) and corresponding pre-exponential factors (a_i) were found to be $\tau_1 = 99$ ns, $a_1 = 0.08$, $\tau_2 = 285$ ns, and $a_2 = 0.92$. The χ^2 was found to equal 1.03, where a χ^2 value of unity would represent a perfect fit. The residuals and autocorrelation function were also randomly distributed around zero, which is typical for a good fit. The lifetime of PyEG₃OH was assigned as 285 ns, i.e. the more heavily weighted decay time, while the contribution at 99 ns was attributed to a small amount of impurities. Although there were some impurities present based on the analysis of the time-resolved decays, these had no noticeable effect on the steady-state fluorescence spectrum. The spectrum represented with a dotted line in Figure 5A does not display the spectral features expected for a pyrene derivative, and indicates that the chemical modification of 1-pyrenemethanol did not proceed properly. Despite the large change in the steady-state fluorescence spectrum profile, the ¹H NMR spectrum was virtually identical to that of the fluorescently pure PyEG₃OH shown in Figure 4, as demonstrated in Figure 6. Since fluorescence is sensitive to even minute levels of impurities, it is likely that the observed change in the steady-state fluorescence spectrum was due to a small population of degraded pyrene, which remained undetected by ¹H NMR, in the otherwise pure PyEG₃OH. This fluorescently degraded sample was discarded. Figure 5A illustrates the importance of verifying the purity of the pyrene derivative after modification.

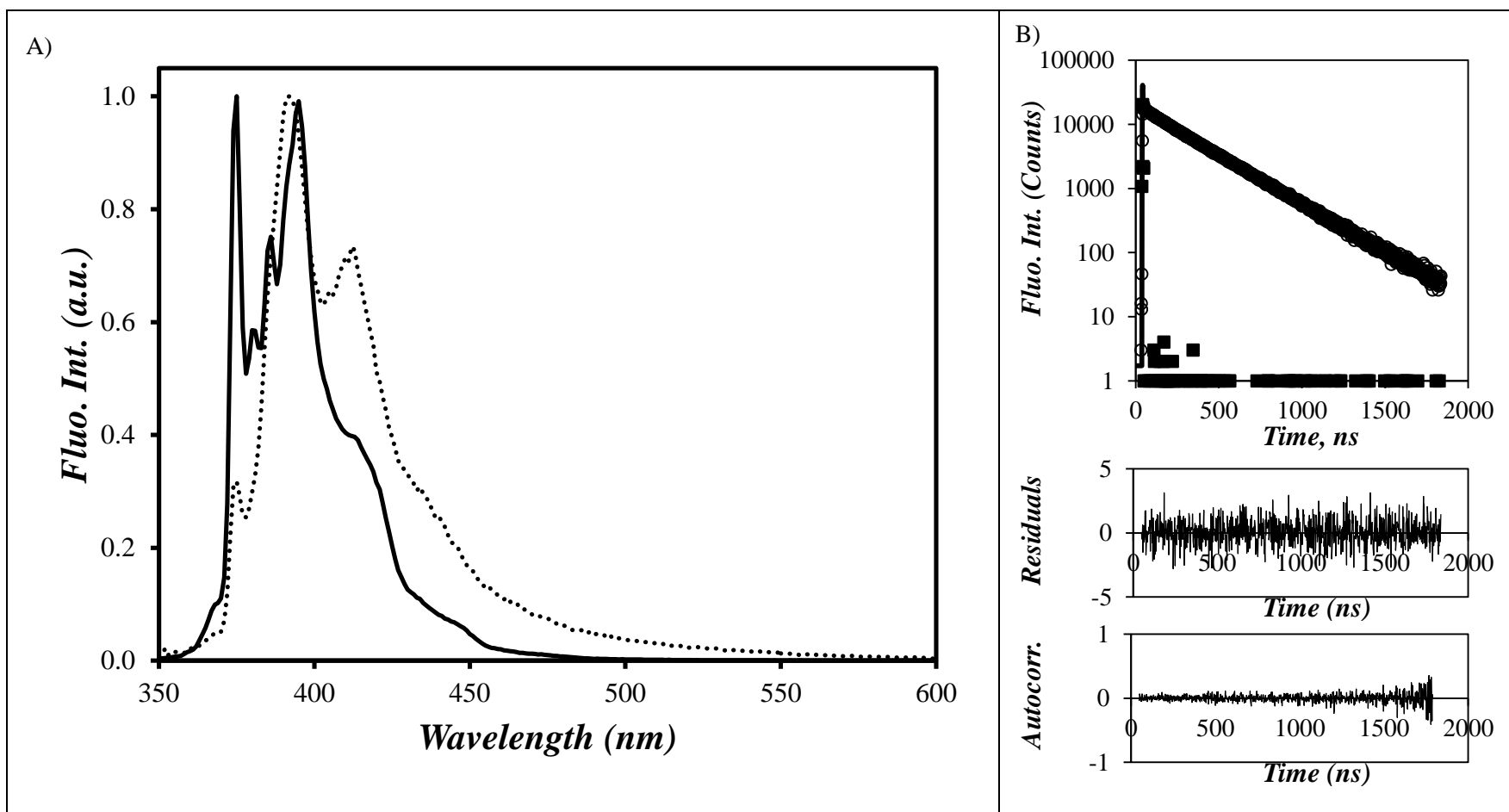


Figure 5: A) Steady-state fluorescence spectrum for PyEG₃OH (—) compared to that for a fluorescently degraded PyEG₂OH (•••) and B) time-resolved fluorescence decay of PyEG₃OH. The time-resolved fluorescence decay was acquired with a time-per-channel of 2.04 ns and fitted with a bi-exponential decay where $\tau_1 = 99$ ns, $a_1 = 0.08$, $\tau_2 = 285$ ns, and $a_2 = 0.9$. $\chi^2 = 1.03$, $\lambda_{ex} = 344$ nm. $[\text{PyEG}_3\text{OH}] = 2.3 \times 10^{-6}$ M.

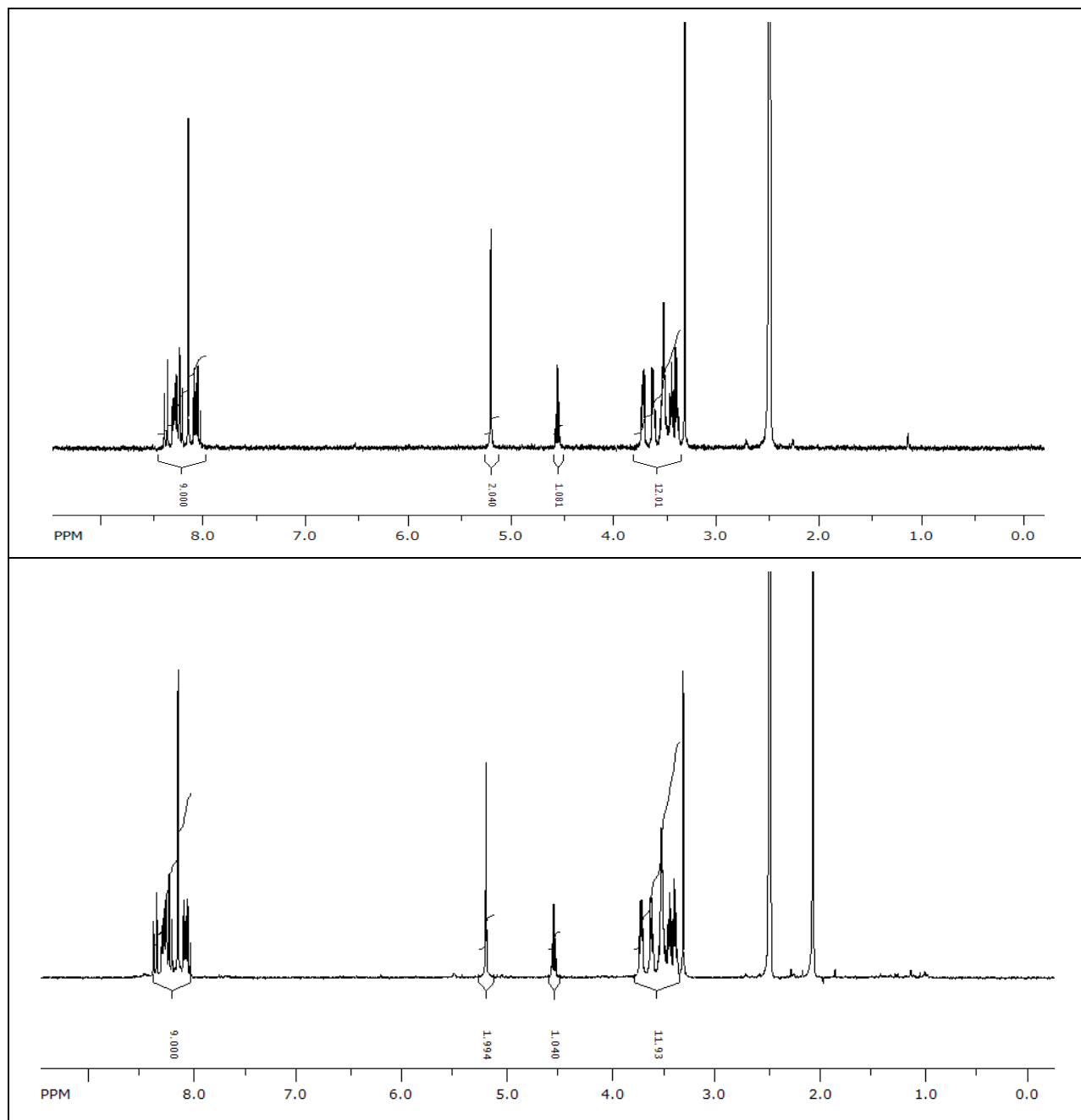


Figure 6: Comparison of the 300 MHz ¹H NMR spectra obtained for (top) fluorescently pure and (bottom) fluorescently degraded PyEG₃OH in *d*₆-DMSO: δ 8.0-8.4 (m, 9 H), 5.2 (s, 2 H), 4.6 (t, 1 H), and 3.4-3.8 ppm (m, 12 H). Residual solvent peaks are present at δ 3.3 ppm for water, 2.5 ppm for DMSO, and 2.09 ppm for acetone.

The fluorescently-pure PyEG₃OH was then reacted according to Scheme 2 to produce PyEG₃MA. Figure 7 shows the corresponding ¹H NMR spectrum with all the protons assigned. A 2.3×10⁻⁶ M solution of PyEG₃MA was prepared in inhibitor-free THF and outgassed with nitrogen for 45 minutes. The steady-state fluorescence spectrum and time-resolved fluorescence decay obtained for PyEG₃MA are given in Figure 8. Again, the steady-state fluorescence spectrum was characteristic of pyrene, and the time-resolved fluorescence decay was fitted with a bi-exponential decay with $\tau_1 = 80$ ns, $a_1 = 0.06$, $\tau_2 = 281$ ns, and $a_2 = 0.94$. The fit yielded a χ^2 value of 1.06 and the residuals and autocorrelation were randomly distributed around zero, indicating a good fit. The small amount of impurity observed by time-resolved fluorescence had an insignificant effect on the steady-state fluorescence spectrum. The PyLM was then stored in a -80 °C freezer until it was used for emulsion polymerization.

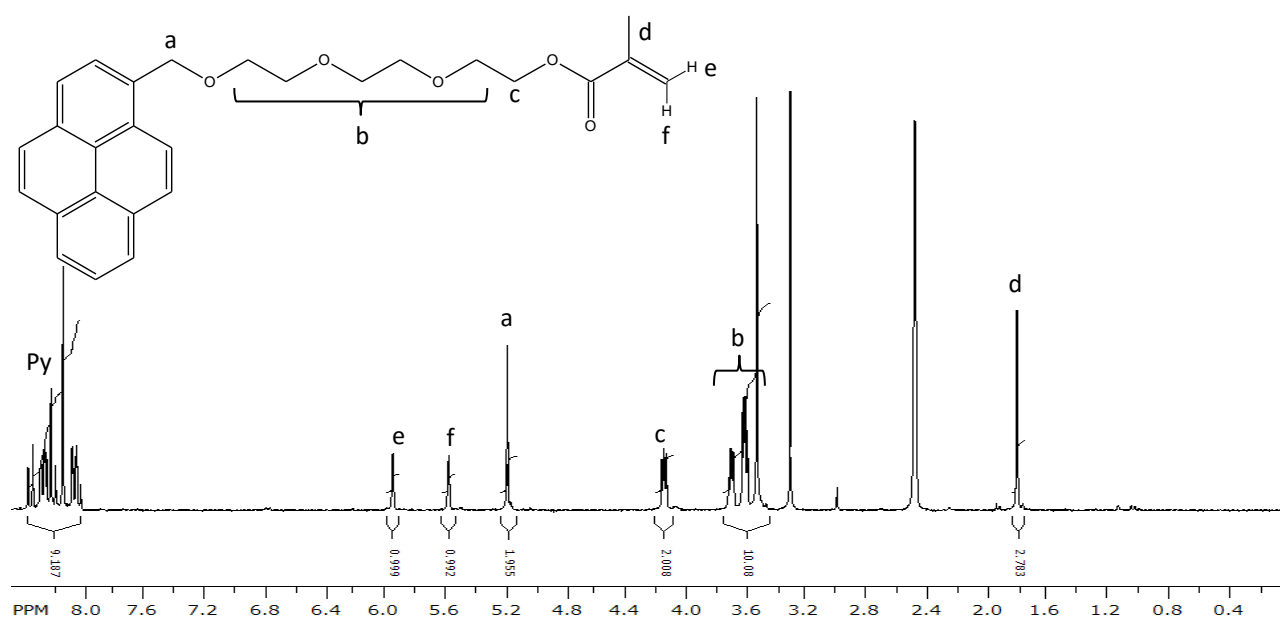


Figure 7: 300 MHz ¹H NMR spectrum for 1-pyrenylmethoxy-2-ethoxy-2-ethoxy-2-ethoxy methacrylate in deuterated dimethyl sulfoxide (DMSO-*d*₆): δ 8.0-8.4 (m, 9 H), 5.9 (s, 1 H), 5.6 (s, 1 H), 5.2 (s, 2 H), 4.1 (t, 2 H), 3.5-3.7 (m, 10 H) and 1.8 ppm (s, 3 H). Residual solvent peaks are present at δ 3.3 ppm for water and 2.5 ppm for DMSO.

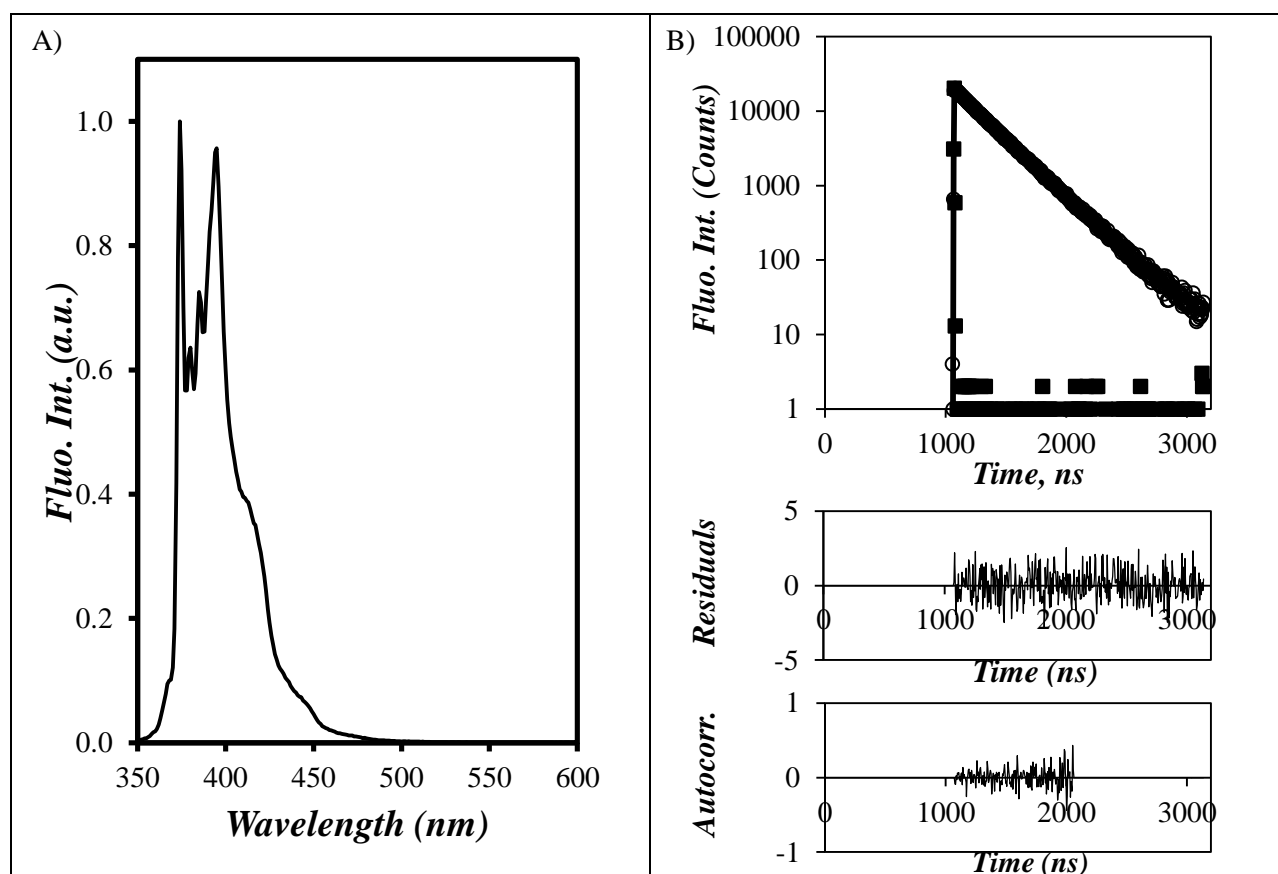


Figure 8: A) Steady-state fluorescence spectrum and B) time-resolved fluorescence decay for PyEG₃MA. The time-resolved fluorescence decay was acquired with a time-per-channel of 5.06 ns and fitted with a bi-exponential decay where $\tau_1 = 80$ ns, $a_1 = 0.06$, $\tau_2 = 281$ ns, and $a_2 = 0.94$; $\chi^2 = 1.06$, $\lambda_{ex} = 344$ nm, $[\text{PyEG}_3\text{OH}] = 2.3 \times 10^{-6}$ M.

The PyLM prepared with a longer ethylene oxide linker ($n = 9$) was synthesized according to Method 2. The ¹H NMR spectrum is shown in Figure 9 and the signal of all protons were assigned. The degree of polymerization was calculated using the integration of the ¹H NMR peaks and UV absorbance. By comparing the integration of the peaks corresponding to ethylene oxide (b and c) to that of pyrene (Py) the degree of polymerization (n) was found to equal 8.9, and when compared to the allylic hydrogens (a) $n = 9.9$, or on average $n = 9.4$.

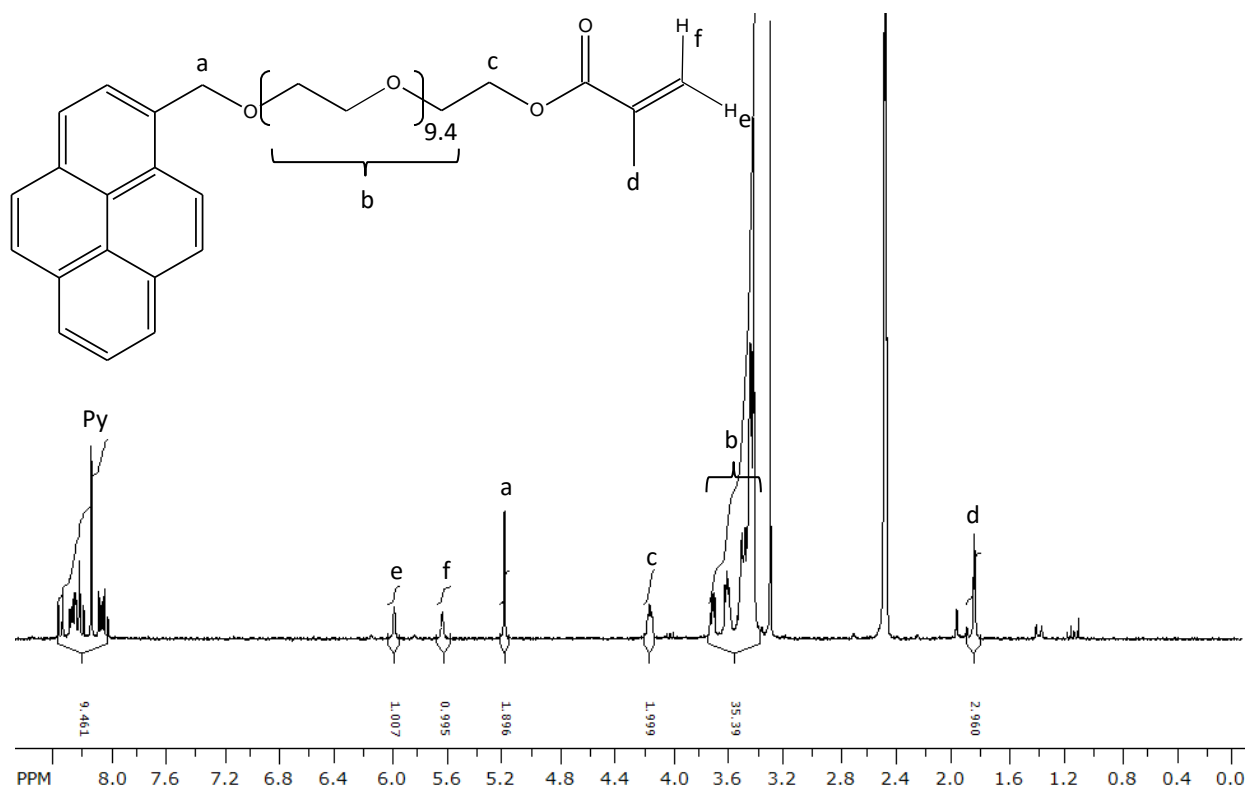


Figure 9: 300 MHz ^1H NMR spectrum for 1-pyrenylmethoxy-PEO_{9.4}-methacrylate in deuterated dimethyl sulfoxide (DMSO- d_6): δ 8.0-8.4 (m, 9 H), 6.0 (s, 1 H), 5.6 (s, 1 H), 5.2 (s, 2 H), 4.2 (t, 2 H), 3.4-3.7 (m, 35 H) and 1.8 ppm (s, 3 H). A residual solvent peak is present at δ 3.3 ppm for water. The small peaks at δ 2.0, 1.4 and 1.1 ppm are impurities from the methacrylic anhydride used.

In order to obtain a more precise value for n , UV-Vis absorption was used. A sample of PyLM was dissolved in inhibitor-free THF and diluted until the absorbance was ca. 0.5 at 344 nm. Using the molar absorption coefficient (ϵ) at 344 nm of the model compound 1-pyrenemethanol ($42\,700\ \text{M}^{-1}\cdot\text{cm}^{-1}$)¹⁵ and rearranging the Beer-Lambert law, n was found to equal 9.5 via Equation 13:

$$n = \frac{\frac{l \cdot \varepsilon \cdot \rho}{A} - MW_{PyMA}}{MW_{EO}} \quad (13)$$

where ρ is the massic concentration of PyLM, A is the absorbance at 344 nm, MW_{PyMA} is the molecular weight of PyLM with $n = 0$, equal to $300 \text{ g} \cdot \text{mol}^{-1}$, and MW_{EO} is the molecular weight of ethylene oxide, equal to $44 \text{ g} \cdot \text{mol}^{-1}$. Excellent agreement was thus observed for the degrees of ethoxylation determined by ^1H NMR and UV-Vis absorption analysis. To confirm the fluorescence purity of the sample, both steady-state and time-resolved fluorescence were applied. The steady-state fluorescence spectrum was similar to that of the previously prepared PyLMs and consistent with that of 1-pyrenemethanol in THF. The time-resolved fluorescence decay was fitted with a bi-exponential decay with $\tau_1 = 116 \text{ ns}$, $a_1 = 0.05$, $\tau_2 = 280 \text{ ns}$, and $a_2 = 0.95$. The residuals were randomly distributed around zero with $\chi^2 = 1.06$. The monomer was stored in a $-80 \text{ }^\circ\text{C}$ freezer until needed. A summary of the pre-exponential factors and decay times obtained for all the pyrene derivatives prepared for this research is provided in Table 1.

Table 1: Decay times (τ) and pre-exponential factors (a) for bi-exponential fits of PyLMs and their precursors in THF. The monomer lifetime was taken as the more heavily weighted decay time.

Monomer Unit	τ_1	a_1	τ_2	a_2	χ^2
PyEG ₁ OH	98.3	0.13	285.3	0.87	0.95
PyEG ₁ MA	74.6	0.15	280.5	0.85	1.08
PyEG ₂ OH	99.0	0.08	285.0	0.92	1.02
PyEG ₂ MA	103.1	0.09	277.3	0.91	1.15
PyEG ₃ OH	99.5	0.08	285.1	0.92	1.02
PyEG ₃ MA	79.7	0.06	281.0	0.94	1.06
PyEG ₉ OH	87.4	0.03	282.6	0.97	1.03
PyEG ₉ MA	116.4	0.05	280.2	0.95	1.06
PyEG ₇₁ OH	85.3	0.05	280.5	0.95	0.98

2.6 Emulsion Polymerization

2.6.1 Native Latex

A 125 mL straight-walled, three-necked glass reactor was equipped with a mechanical stirrer, a reflux condenser and a thermocouple probe. A diagram of the experimental setup is given in Figure 10. Deionized water (DIW, 63 mL) and sodium dioctyl sulfosuccinate (AOT, 57 mg, 0.13 mmol) were then added. While stirring at 550 rpm, the reactor was purged with nitrogen and the solution was heated to 80 °C with a heating mantle. A pre-emulsified monomer feed was prepared from *n*-butyl methacrylate (BMA, 2.0 g, 14 mmol), AOT (19 mg, 43 μmol), and DIW (1 mL). Once the reactor temperature had stabilized, ammonium persulfate (APS, 4.7 mg, 21 μmol) dissolved in DIW (1 mL) was added, followed by a rinse with DIW (1 mL). After five minutes, the monomer mixture was fed in over a three-hour period using a syringe pump. The temperature remained constant within ± 1 °C throughout the reaction. The resulting white latex was filtered through Whatman #4 filter paper to remove any coagulum formed to yield a poly(*n*-butyl methacrylate) latex (PBMA-latex-1).

2.6.2 Pyrene-Labelled Latex

A similar procedure was applied to prepare the pyrene-labelled latex. The main difference with the previous procedure was the composition of the pre-emulsified monomer feed which contained *n*-butyl methacrylate (BMA, 2.1 g, 15 mmol), 4.6 mol% of pyrene-labelled monomer (PyEG₃MA, 0.31 g, 0.72 mmol), AOT (20 mg, 45 μmol), and DIW (1 mL). Immediately following the completion of the monomer feed, the reaction was stopped. The resulting pale yellow latex was filtered through Whatman #4 filter paper to yield a pyrene-labelled poly(*n*-butyl methacrylate) latex (Py-PBMA-latex-1).

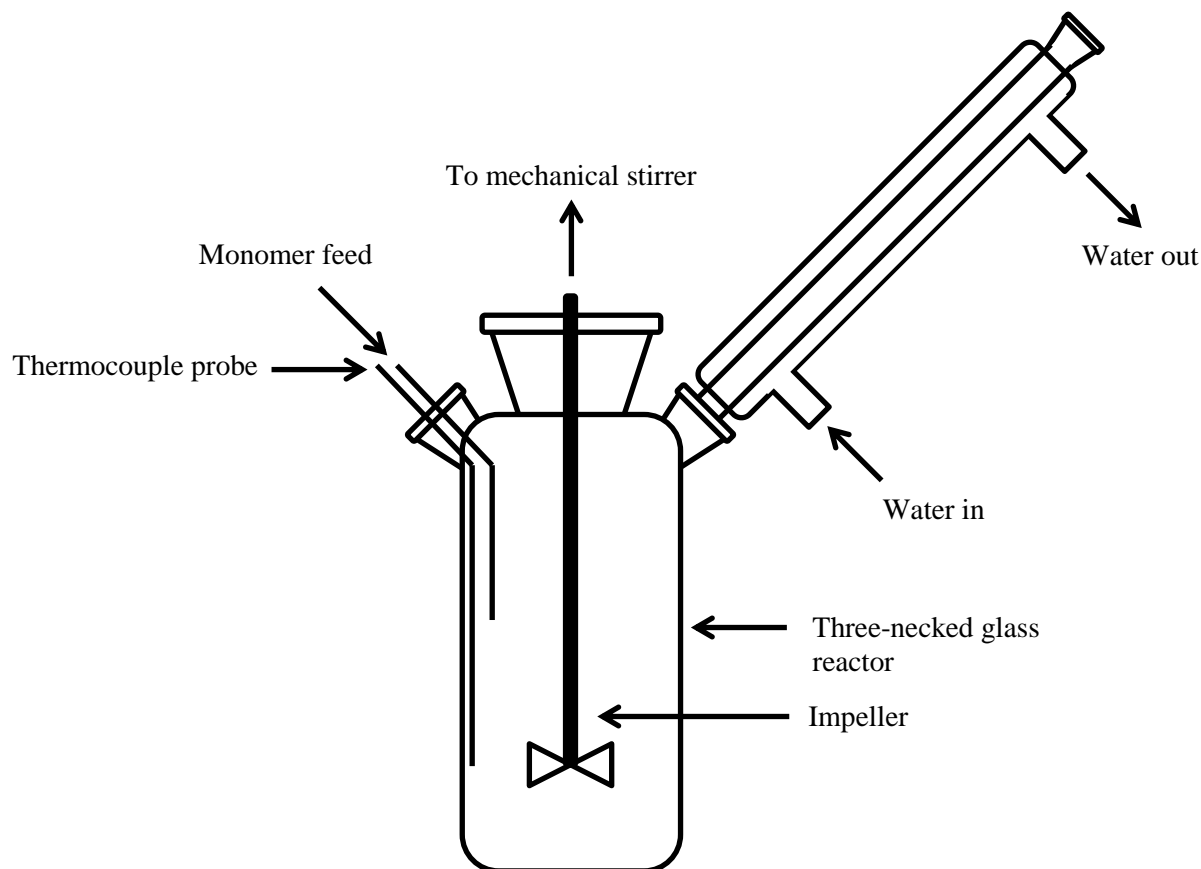


Figure 10: Diagram of the experimental setup used for emulsion polymerization.

2.6.3 Polymer Isolation

Dialysis: After the emulsion polymerization, dialysis was used to remove small unbound molecules, such as unreacted initiator and monomer, while maintaining a stable emulsion. The dialysis was performed using $2.5 \text{ mL}\cdot\text{cm}^{-1}$ Spectra/Por 7 dialysis tubing with a $50 \text{ kg}\cdot\text{mol}^{-1}$ molecular weight cutoff. The latex dispersion (30 mL) was added to the tubing which was then capped at both ends with tubing clips. A 2 cm section of tubing was left unfilled to allow room for swelling during dialysis. The tube was then placed in a 2 L beaker filled with 80 vol% DIW, 20 vol% ethanol, and 2.3 g (5.2 mmol) AOT. The beaker was then covered with aluminum foil to minimize solvent evaporation and left to stir overnight. The removal of unbound pyrene was monitored by steady-state fluorescence. The fluorescence intensity of pyrene in the dialysate was compared to that of a standard to account for day-to-day fluorescence intensity fluctuations

in the fluorometer. The dialysate was then removed, and the beaker refilled with the solution of DIW, ethanol, and AOT to continue dialysis. This process was repeated until the fluorescence intensity of pyrene in the dialysate approached zero.

Precipitation: A more rapid method used to isolate the polymer directly from the emulsion (before or after dialysis) was by repeated precipitations. A 2 mL aliquot of latex was freeze-dried to remove all the water. In a 7 mL vial, 50 mg of the dried latex powder was dissolved in a minimal amount of distilled in glass THF (~10 drops). Once the polymer had fully dissolved, 4 mL of methanol was quickly added to precipitate the polymer. The vial was then agitated on a vortex mixer for 30 seconds. The polymer formed a single aggregated mass, which was removed. Dissolution and precipitation of the polymer was repeated three more times to ensure the removal of all small molecules. The purified polymer was then dried in a vacuum oven overnight. GPC analysis was performed on the dried polymer to ensure that all the small molecules had been removed.

2.7 Characterization of Latexes

The latex particles were characterized by determining their particle size distribution and the molecular weight of the polymer by DLS and GPC, respectively. The first emulsion prepared was the native latex based on the above synthesis (PBMA-latex-1). The emulsion proceeded with no complications and no coagulum was formed. The DLS measurements yielded a particle size of 95 nm and a PSD of 1.04. A sample of the latex (ca. 2 g) was freeze dried overnight to remove all the water. The dried latex powder was used to prepare a 1 mg·mL⁻¹ solution in THF, which was then filtered through a 0.2 μm filter and injected into the GPC. The GPC analysis yielded a M_n of 510 kg·mol⁻¹ and a \mathcal{D} of 2.0 for the polymer.

Following a synthetic procedure similar to the Py-PBMA-latex-1 sample, latex samples were obtained for all the PyLMs. Table 2 summarizes the results for the emulsion polymerizations containing the PyLMs. In most cases, complications during the polymerization led to a latex that was unsuitable for the final application in the IPD measurements. The pyrene content of the copolymer chains was calculated using UV-Vis absorbance. To ensure accuracy in the absorbance measurements, the polymer was isolated from the emulsion by precipitation. The polymer was precipitated a total of four times to ensure that all of the small molecules were removed, and that only the polymer remained. The sample was dried under vacuum to remove all solvent traces. The dry polymer was then dissolved in THF and the absorbance was measured. The molar fraction of pyrene (f_{Py}) incorporated into the polymer backbone was found using Equation 14,

$$f_{Py} = \frac{MW_{BMA}}{\frac{\rho_{Poly}}{C} + MW_{BMA} - MW_{PyLM}} \quad (14)$$

where ρ_{Poly} is the massic concentration of the polymer, C is the molar concentration of pyrene found by UV absorption measurements (using $\epsilon(344 \text{ nm}) = 42,700 \text{ M}^{-1} \cdot \text{cm}^{-1}$), MW_{BMA} is the molecular weight of butyl methacrylate, and MW_{PyLM} is the molecular weight of the PyLM.

The emulsions prepared with PyLMs having a spacer length $n = 1$ and 2 had very similar outcomes. In both cases, when a feed composition of 5 mol% PyLM was used, a significant amount of coagulum formed during the reaction. In addition, when analyzed, less than 1 mol% of PyLM had been incorporated into the copolymer, which was too low to observe excimer formation. These extremely low pyrene-labelling levels suggest that both PyLMs were too hydrophobic to be incorporated into the latexes. The emulsions carried out with the PyLMs prepared by anionic polymerization also led to some difficulties. The first PyLM with $n = 71$ was not expected to incorporate well, due to the extremely high molecular weight of the PEO linker resulting in a water-soluble monomer. In addition, the very high

molecular weight of the PEO linker was expected to impart properties to the pyrene-labelled latex that would be drastically different from those of the native PBMA latex. When PyEG₉MA was used for emulsion polymerization the formation of coagulum was not observed, suggesting that the PyLM was fully incorporated into the polymer. However the resulting polymer was crosslinked, meaning that it would have limited usefulness in IPD measurements. The crosslinking was likely the result of a small amount of impurities left from the synthesis. All the characterization methods were applied to the most successful latex, using the PyEG₃MA monomer.

Table 2: Characteristics of latexes prepared by emulsion copolymerization of BMA with PyLMs.

Latex	PyLM	PyLM Feed (mol%)	PyLM Incorporated (mol%)	Particle Size (nm)	PSD **	M_n (kg/mol)	\mathcal{D} ***	Coagulum (Y/N)	Cross-Linked (Y/N)
E14	Py-EG ₁ -MA	6.5	0.9	147	1.02	78	> 3	Y	Y
E27	Py-EG ₂ -MA	5.0	1.3	109	1.04	109	> 3	Y	N
E35	Py-EG ₃ -MA	4.5	1.9	118	1.04	430	1.9	Y	N
E36*	Py-EG ₇₁ -MA	4.9	-	121	1.04	-	-	N	Y
E38*	Py-EG ₉ -MA	4.9	-	106	1.04	-	-	N	Y
E39†	Py-EG ₃ -MA	1.9	1.8	120	1.04	198	1.8	N	N

* PyLM was prepared by anionic polymerization. **Particle size dispersity. ***Molecular weight dispersity. † No dialysis performed before sample analysis.

The first successful fluorescently-labelled emulsion to be carried out was the pyrene-labelled latex identified as Py-PBMA-Latex-1, corresponding to entry E35 in Table 2. No complications were observed throughout the polymerization, but during the filtration of the latex, it was discovered that a fairly large amount (ca. 0.15 g) of coagulum had formed at the bottom of the reactor. The resulting Py-PBMA-Latex-1 had a particle size of 118 nm and PSD of 1.04.

Figure 11 shows the DRI and UV absorbance traces from the GPC analysis of a sample of the freeze-dried Py-PBMA-latex-1. The DRI signal is proportional to the concentration of species present in the elution volume, while the absorbance is proportional to the concentration of pyrene. The overlapping and unimodal peaks present in both the UV and DRI traces indicate that the PyLM was evenly incorporated throughout the polymer backbone. The slight shift between the maxima of the DRI and absorbance signals is a result of the detectors being setup in series. The sharp peaks in the DRI trace after a retention volume of ca. 33 mL is due to the elution of solvent and other small molecules such as surfactant. The absorbance trace reveals a peak at a retention volume of 34 mL corresponding to pyrene-containing low molecular weight species, such as unincorporated PyLM present in the latex solution.

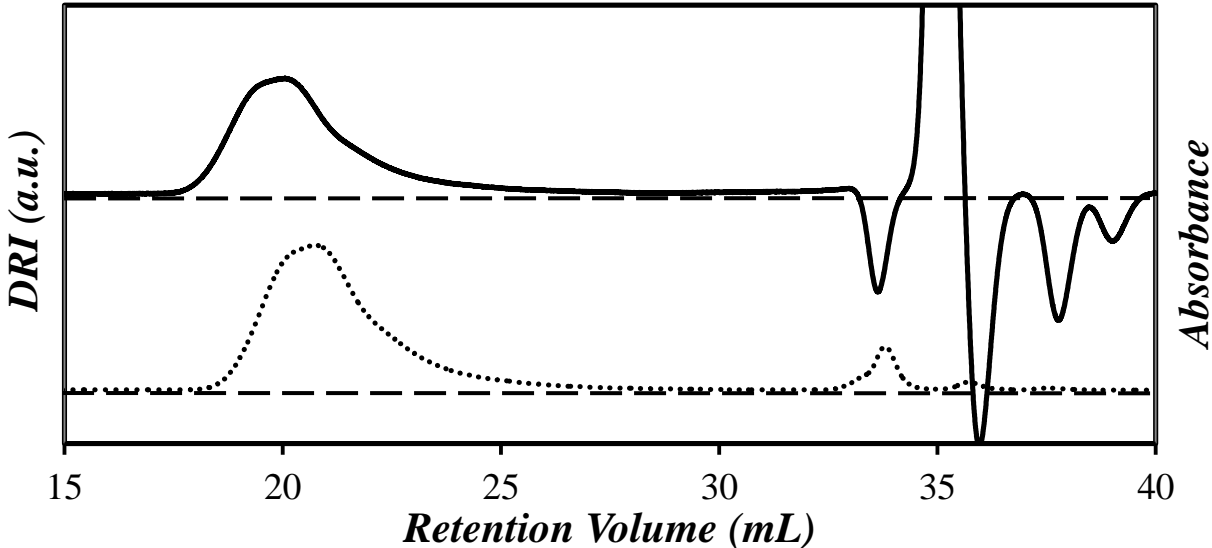


Figure 11: GPC traces for crude Py-PBMA-latex-1 obtained with differential refractive index (DRI, —) and UV absorbance (•••) detectors. The dashed lines were added to help guide the eyes.

Since the goal of the project is to use the latex samples to probe the diffusion of polymer chains by observing pyrene fluorescence, it is important to remove all the pyrene that was not bound to the polymer chains. If any unbound pyrene-containing species were to remain while polymer chain diffusion was measured, these small and faster diffusing species would most likely swamp the signal from the larger, slower diffusing polymer chains, resulting in the IPD measurements probing the free pyrene rather than the polymer chains. To remove unbound pyrene without affecting the latex particles, dialysis was performed.

The dialysis was carried out using $50 \text{ kg}\cdot\text{mol}^{-1}$ molecular weight cut-off dialysis tubing in a solution containing deionized water, ethanol, and dioctyl sodium sulfosuccinate (AOT). The ethanol and AOT were added to enhance the rate at which the hydrophobic unbound PyLM would be removed from the emulsion, without affecting the particle size distribution. The amount of PyLM removed was

monitored by steady-state fluorescence. A plot of the fluorescence intensity of pyrene in the dialysate over time is shown in Figure 12. After 19 days of dialysis the fluorescence intensity of pyrene derivatives in the dialysate approached zero, meaning that most unbound PyLM had been removed. The particle size distribution of the latex remained unchanged throughout this process, as confirmed by DLS measurements.

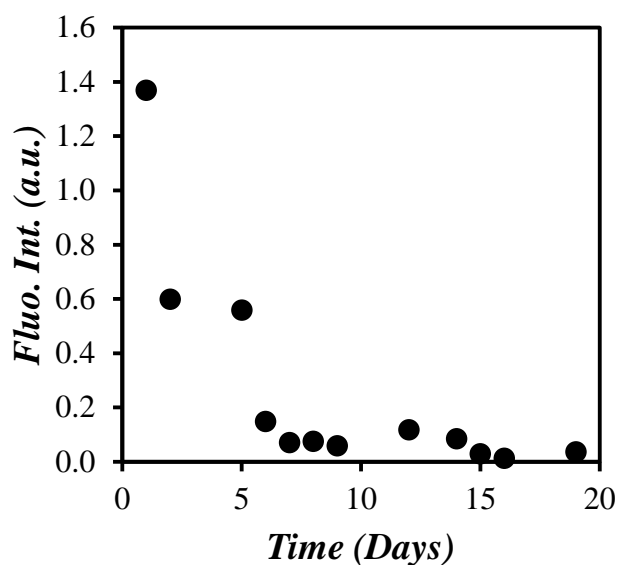


Figure 12: Fluorescence intensity of the I_1 peak for pyrene derivatives in the dialysate. The I_1 peak was normalized to a pyrene standard in ethanol.

To confirm that unbound pyrene impurities had been removed, GPC analysis was conducted on the dialyzed sample as shown in Figure 13. The overlapping peaks present in the absorption and DRI traces show that the polymer composition in terms of the pyrene incorporated into the backbone remained unchanged throughout the dialysis. The nearly complete disappearance of the small peak at a retention volume of 34 mL demonstrates that unbound PyLM was indeed removed. By comparing the areas underneath the UV absorbance trace for the polymer-bound and unbound pyrene species, it was found

that over 98% of the PyLM was bound to the copolymer. The GPC analysis gave a M_n of 430 kg·mol⁻¹ and a D of 1.9 for this pyrene-labelled PBMA sample.

Using Equation 14, the pyrene content of the copolymer was found to be 0.019, or 1.9 mol%. The lower than expected pyrene content of 1.9 mol% suggests that the PyLM was too hydrophobic to be fully incorporated into the copolymer, since the targeted pyrene content value was 4.6 mol%.

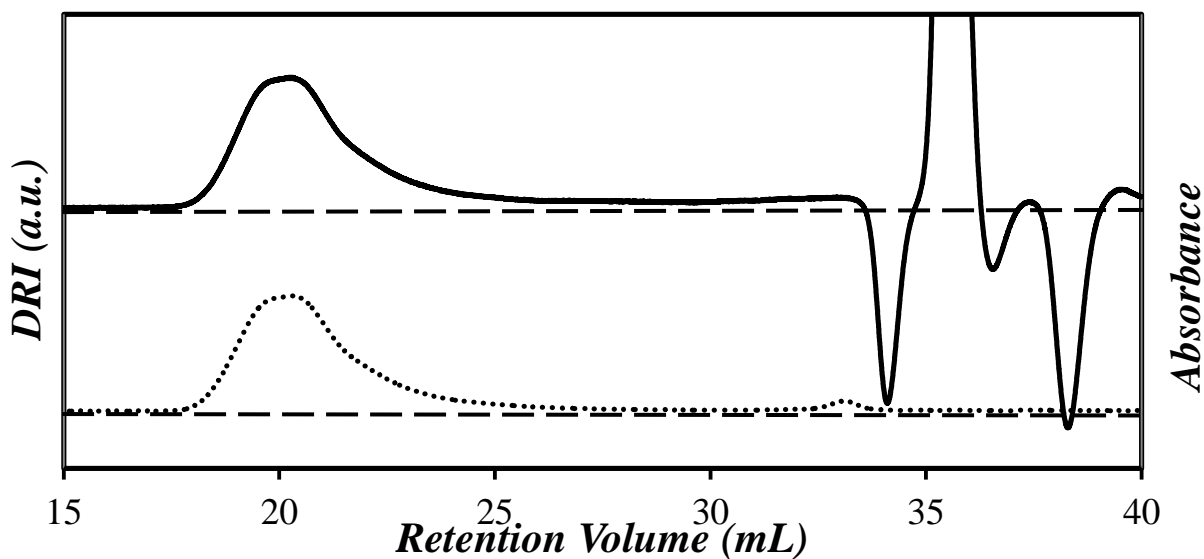


Figure 13: GPC traces for Py-PBMA-latex-1 after dialysis obtained using the DRI (—) and UV absorbance (•••) detectors. The dashed lines were added to help guide the eyes.

A second pyrene-labelled latex, Py-PBMA-latex-2 (entry E39 in Table 2) was prepared in a similar manner. However this time the monomer feed was composed of 1.9 mol% of PyEG₃MA and 98.1 mol% of BMA, i.e. a lower PyLM content that matched the amount of PyLM incorporated into the pyrene-labelled PBMA sample just described. This second emulsion was even more successful than the first one. The emulsion polymerization reached completion without the formation of any coagulum. The

latex had a particle size of 119 nm and a PSD of 1.04 by DLS. The DRI and UV absorbance traces from GPC analysis of the unpurified latex are shown in Figure 14. The GPC analysis gave a M_n of 190 kg·mol⁻¹ and a \bar{D} of 1.7. Both the DRI and UV absorbance traces overlapped, demonstrating that the PyLM was evenly incorporated into the copolymer. In contrast to the previous latex sample, there was almost no unbound pyrene remaining after the emulsion, meaning that dialysis was not required. A sample of the latex was precipitated four times in methanol and dried under vacuum for UV absorption measurements. Using Equation 14, the pyrene content of the purified copolymer was found to equal 1.8 mol%, much closer to the initial feed composition of 1.9 mol%, thus supporting the conclusion that essentially all the pyrene was incorporated into the copolymer. Moreover, by comparing the UV absorbance peaks for the bound and unbound pyrene, it was found that nearly 99% of all the PyLM was incorporated into the pyrene-labelled PBMA copolymer.

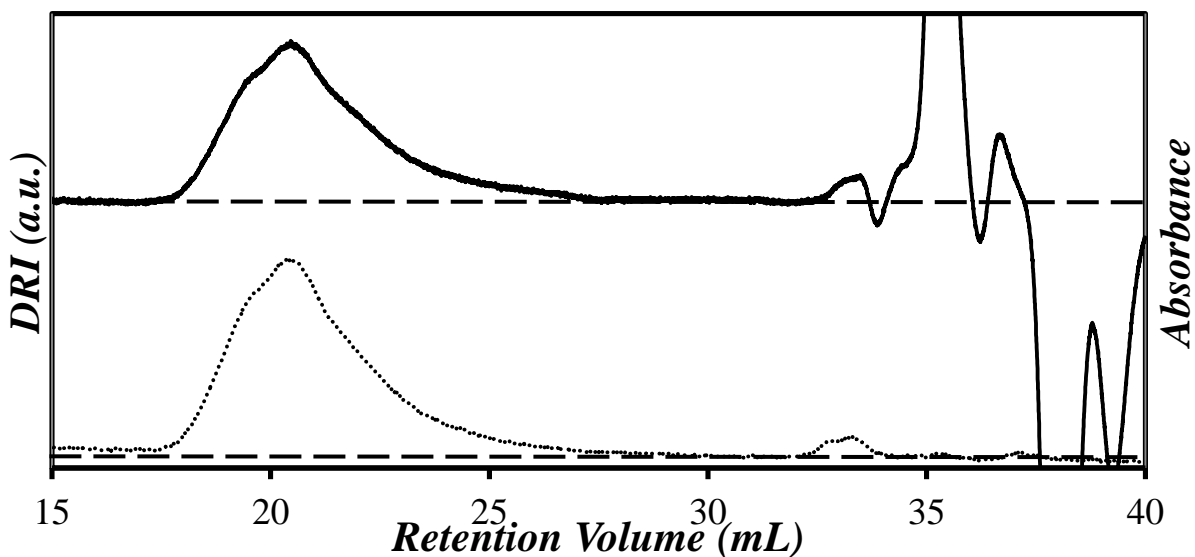


Figure 14: GPC traces for crude Py-PBMA-latex-2 obtained with DRI (—) and UV absorbance (•••). The dashed lines were added to help guide the eyes.

2.8 Summary

Several PyLMs were prepared with linkers made of 1, 2, 3, 9, and 71 ethylene glycol monomers. Both NMR and the more sensitive steady-state and time-resolved fluorescence techniques were used to determine their purity. All the PyLMs exhibited the same lifetime in THF of 280 ± 1 ns, and a fluorescence purity greater than 90%. The PyLMs were copolymerized with BMA to prepare fluorescently-labelled latexes. The PyLMs with less than three units of ethylene oxide were too hydrophobic to be incorporated into a latex at high enough levels to observe sufficient excimer formation for this project. The PyLM with a linker length of 71 units was too hydrophilic and had a molecular weight too large for our application, as it would likely affect the T_g of the corresponding copolymer (Equation 12). The PyLMs with $n = 3$ and 9 could both be used to prepare fluorescently-labelled latex samples. Although PyEG₉MA could be incorporated into the particles at a higher concentration, the resulting copolymers were cross-linked. In addition, even though a chain transfer agent could have been used to lower the molecular weight of the copolymers, it was decided that PyEG₃MA was a better-suited PyLM due to its lower molecular weight. Every 1 mol% of PyEG₉MA incorporated into the copolymer corresponds to nearly 5 wt% incorporation, whereas 1 mol% of PyEG₃MA corresponds to less than 3 wt%. Since at least 2 mol% of PyLM were required to observe sufficient excimer formation, PyEG₃MA was preferred so that the resulting copolymer still contained over 94 wt% BMA, and thus a lesser impact on the properties of the polymer would be expected. Two latex samples were prepared using PyEG₃MA. For the first latex, 5 mol% PyLM was added to the emulsion but only 1.9 mol% was incorporated. To remove the unbound PyLM, a lengthy dialysis procedure had to be performed. The second latex was prepared using 1.9 mol% PyLM in the feed. Over 99% of all the PyLM in the feed was incorporated, meaning that dialysis was not required and the latex sample could be directly used for the IPD

measurements. In addition, this second latex contained polymer chains with a M_n less than half that of the first latex prepared with 5 mol% PyLM in the feed, allowing the diffusion of two polymer samples with different molecular weights to be studied. Two native latex samples were also prepared with comparable M_n and PSD as the pyrene-labelled latexes.

Chapter 3

Film Formation

3.1 Overview

A film was prepared by depositing a mixture of native latex with a small amount of Py-PBMA latex on a substrate and allowing it to dry. The dry film consisted of a few fluorescently labelled PBMA latex particles surrounded by a matrix of non-fluorescent PBMA latex. As the film was annealed, the polymer chains diffused out of the latex particle into the surrounding regions as depicted in Figure 15. The extent of IPD was quantified by acquiring the steady-state fluorescence spectrum of the film with front face geometry and determining the ratio of the fluorescence intensity of the pyrene excimer (I_E) to that for the pyrene monomer (I_M).

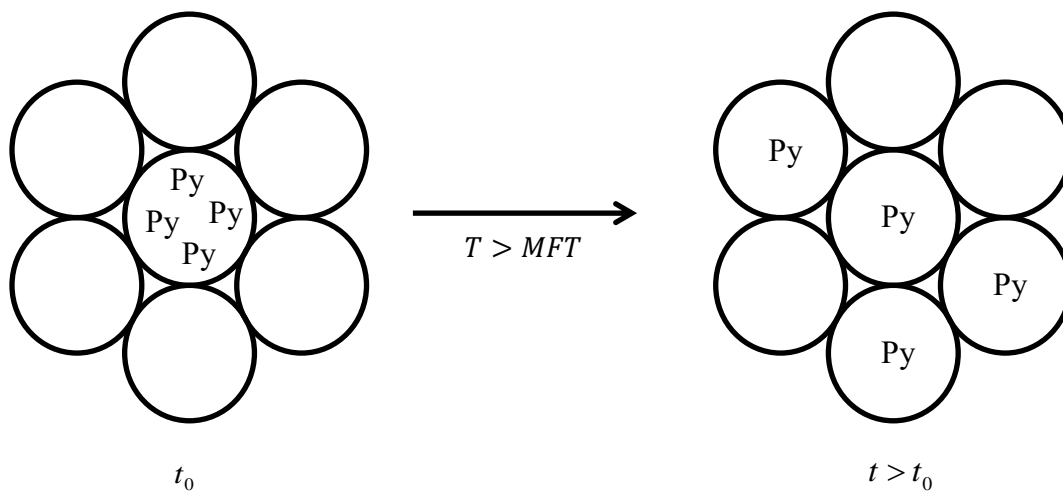
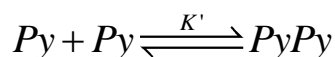


Figure 15: Illustration of the diffusion of pyrene-labelled copolymer across the latex particle boundaries from the initial time (t_0) to time $t > t_0$ as the film is annealed above its minimum film formation temperature.

When a film is heated above its MFT the pyrene pendants are able to diffuse in the bulk, resulting in the formation and dissociation of pyrene dimers as depicted in Scheme 3 with the equilibrium constant K' expressed in Equation 15.



Scheme 3: Equilibrium between pyrene monomers and dimers in a pyrene-labelled film above the MFT.

$$K' = \frac{[PyPy]}{[Py]^2} \quad (15)$$

In Equation 15, $[PyPy]$ and $[Py]$ are the local pyrene dimer and monomer concentrations, respectively. When the film was cooled below the MFT this equilibrium was frozen, and the concentration of monomer and dimer species no longer changed. Knowing that the I_E/I_M ratio is proportional to the concentration of excited dimers over that of monomers and rearranging Equation 15 into Equation 16, it can be shown that the I_E/I_M ratio is directly proportional to the local pyrene concentration, even in solid-state conditions.

$$\frac{I_E}{I_M} \propto \frac{[PyPy]}{[Py]} = K'[Py] \quad (16)$$

Consequently, the $(I_E / I_M) (t)$ ratio determined from the steady-state fluorescence spectrum at annealing time t is directly proportional to the average local pyrene concentration in the film $\langle C_{Py} \rangle (t)$ experienced by an excited pyrene. In turn, $\langle C_{Py} \rangle (t)$ is obtained by integrating the local pyrene concentration $C_{Py}(r,t)$ as a function of the distance r from the center of the pyrene-labelled latex particles. Equation 17 shows this proportionality, where K is a scaling factor depending on the experimental setup and V_o represents the volume of the film being irradiated. As illustrated in Figure 15, the local pyrene concentration in the film is expected to decrease as the polymers interdiffuse. However, $\langle C_{Py} \rangle$ is always expected to be greater than zero, even at long annealing times (t_∞), since there are multiple pyrene

pendants on a single copolymer chain that can form excimer intramolecularly. As a result, the I_E/I_M ratio was always expected to be greater than zero.

$$\frac{I_E}{I_M}(t) = \frac{K}{V_0} \int_0^\infty C_{Py}(r, t) \cdot 4\pi r^2 dr \quad (17)$$

The fraction of mixing at an annealing time t can be calculated from the experimental $(I_E/I_M)(t)$ ratios via Equation 18. This equation accounts for the fact that the I_E/I_M ratio at infinite annealing time is greater than zero.

$$f_m(t) = \frac{\left(\frac{I_E}{I_M}\right)_t - \left(\frac{I_E}{I_M}\right)_{t=0}}{\left(\frac{I_E}{I_M}\right)_{t_\infty} - \left(\frac{I_E}{I_M}\right)_{t=0}} \quad (18)$$

The diffusion coefficient can be calculated in a manner similar to the FRET studies^{2,4-6} by assuming Fickian diffusion out of a spherical particle resulting in Equation 19, with C_0 representing the initial pyrene concentration in a latex particle of radius R .

$$f_m(t) = 1 - \frac{\int_0^R C_{Py}(r, t) \cdot 4\pi r^2 dr}{\frac{4}{3}\pi R^3 C_0} \quad (19)$$

The expression of $C_{Py}(r, t)$ used in Equation 19 was defined in Equation 7. The diffusion coefficient of the copolymer chains can be found by optimizing D in Equation 7 such that the fraction $f_m(t)$ obtained mathematically in Equation 19 matches the experimentally determined $f_m(t)$ calculated from Equation 18. This procedure for the analysis of IPD using steady-state fluorescence has the distinct advantage that since pyrene excimer formation occurs only on contact between two pyrene molecules, the I_E/I_M ratio does not depend on the distance separating the pyrene groups, in contrast to FRET measurements.

3.2 Experimental

Film Preparation: The film formation process was probed for two different films. Each film consisted of 95 wt% native latex and 5 wt% pyrene-labelled latex. As shown in Table 3, the properties of the native and labelled latex particles used to prepare each film were similar. The films were prepared by depositing a small amount (ca. 0.5 mL) of the latex mixture on a $1 \times 3 \text{ cm}^2$ quartz plate. One side of the plate was raised by 1 to 2 ° to help keep the aqueous latex at one end. The film was then dried in the dark overnight.

Table 3: Composition of the films used to probe film formation and polymer diffusion.

Film	Latex	Latex Pyrene Content (mol%)	Particle Size (nm)	PSD	M_n ($\text{kg} \cdot \text{mol}^{-1}$)	\bar{D}	Weight Fraction
1	Py-PBMA-Latex-1	1.9	118	1.04	430	1.9	0.05
	PBMA-Latex-1	0	95	1.04	510	2.0	0.95
2	Py-PBMA-Latex-2	1.8	120	1.04	198	1.8	0.05
	PBMA-Latex-2	0	119	1.04	190	1.7	0.95

Film Annealing: The dry films were annealed in a glass tube submerged in a constant-temperature oil bath. The oil bath was set to the desired annealing temperature and then allowed to stabilize overnight to insure that the temperature would not change during the annealing process. The glass tube was equipped with a thermocouple probe and sealed with a rubber septum. A slight positive nitrogen atmosphere was maintained inside the glass tube using a check-valve bubbler connected to a needle inserted in the rubber septum used to seal the tube opening. The annealing time measurement was started once the film was placed into the tube, and the film was removed once the desired time was reached. The film was then quickly ($< 5 \text{ s}$) cooled to room temperature by placing it on an aluminum block (25 x 14 x 1 cm). Once cooled, the film was analyzed by steady-state fluorescence. The annealing and cooling processes were

repeated several times for each film to obtain a series of fluorescence measurements over a wide range of annealing times.

After the final annealing step, a film equivalent to an infinite annealing time also had to be prepared. To achieve this, the annealed film was dissolved in THF and then redeposited on a quartz plate, producing a homogeneous film. The film was dried in the dark for 15 minutes and then placed back into the heated oil bath at the annealing temperature for an hour, to ensure all the THF was removed and that the film was completely homogeneous.

Steady-State Fluorescence: The measurements were carried out using a Photon Technology International (PTI) steady-state fluorometer equipped with a xenon arc lamp. The samples were excited at a wavelength of 344 nm and the emission was scanned from 350 to 600 nm in 1 nm increments at a scan rate of 10 nm·s⁻¹. The films were analyzed in the fluorometer using a front-face geometry setup. The sample holder was set to an angle of 160 ° relatively to the excitation beam in order to minimize the intensity of scattered light. The slit widths were set at 1/2 nm for excitation and 1/2 nm for emission. The I_E/I_M ratio was calculated by integrating the fluorescence intensity of excimer (I_E) from 500 to 530 nm over the intensity of the monomer (I_M) from 492 to 498 nm. The spectrum for the film was acquired in three different positions of the film for each annealing time.

3.3 Steady-State Fluorescence

3.3.1 Monomer Reabsorption and the I_E/I_M Ratio

One of the well-known properties of pyrene is that the $S_1^0 \leftarrow S_0^0$ transition is symmetry-forbidden,¹⁶ meaning that the overlap between the absorption and emission spectra is minimal (See Figure 16). This also holds true for pyrene derivatives with a heteroatom in the β -position to pyrene.^{17,18} Because of this, there is typically no energy transfer between excited and ground-state pyrene monomers. However, if the pyrene concentration is sufficiently high or the monomer emission passes through a sufficiently long path length (such as a thick film), the intensity of the $S_1^0 \leftarrow S_0^0$ absorption band may increase to the point where it is no longer negligible and the first peak (I_1) of pyrene emission is reabsorbed by another ground-state pyrene. This reabsorption results in a decrease in the I_1 peak intensity and leads to a distortion of the steady-state fluorescence spectrum. Each film prepared had a slightly different thickness and thus varying degrees of reabsorption, with thicker films resulting in larger suppression of the I_1 peak. In addition, to measure the fluorescence of a fully annealed film, the film had to be dissolved and redeposited, resulting in a change in film thickness. Since this redeposited film was typically thinner the intensity of the I_1 peak tended to increase, as seen in Figure 17.

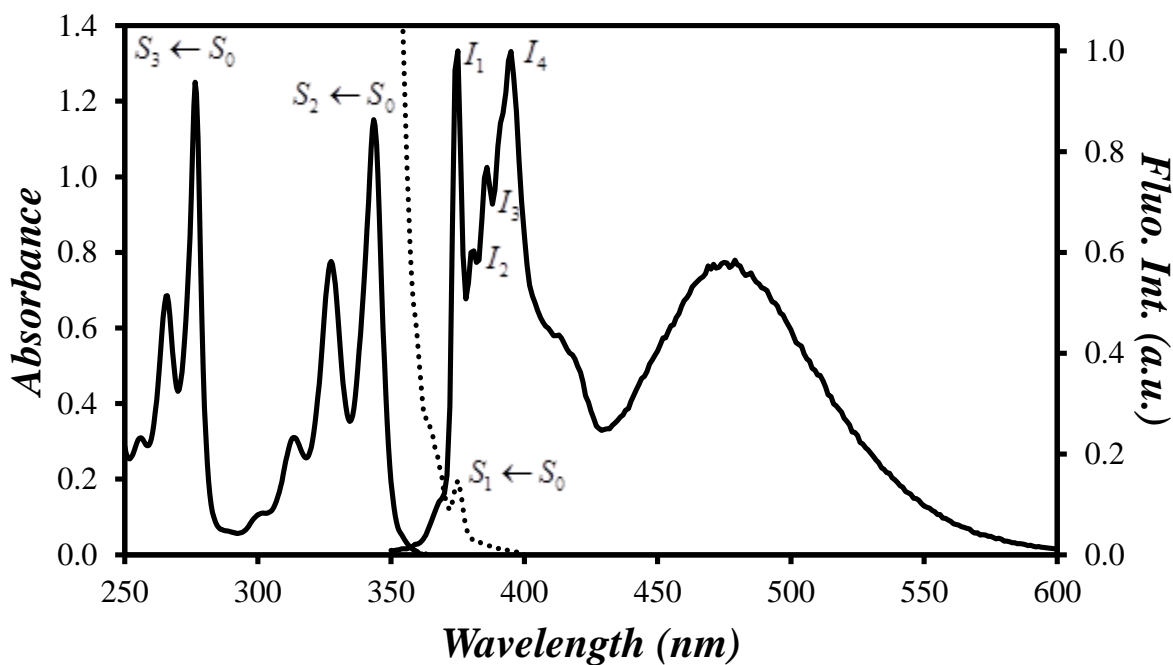


Figure 16: Comparison of the UV absorbance spectra (left) for the Py-PBMA-latex-1 copolymer in THF at relatively low (—) and high (•••) concentrations, and the steady-state fluorescence spectrum (right) for a pyrene concentration of 0.1 OD at 344 nm. $\lambda_{\text{ex}} = 344$ nm.

In our laboratory, the I_E/I_M ratio is typically calculated by integrating the emission intensity of the monomer underneath the I_1 peak at 375 nm, and the excimer from 500 to 530 nm. These ranges are selected to ensure that the emission intensity at these wavelengths arises solely from the emission of the monomer or excimer, and not from overlapping emission by both fluorescent species (see Figure 1). However, since the intensity of the I_1 peak varies from one film to the next, we chose to integrate the monomer intensity underneath the I_4 peak instead. Although the I_4 peak is much closer to the excimer emission, the overall excimer emission intensity was sufficiently low, even before annealing, to minimize overlap between the monomer and excimer emission, thus resulting in a much more reliable I_E/I_M ratio.

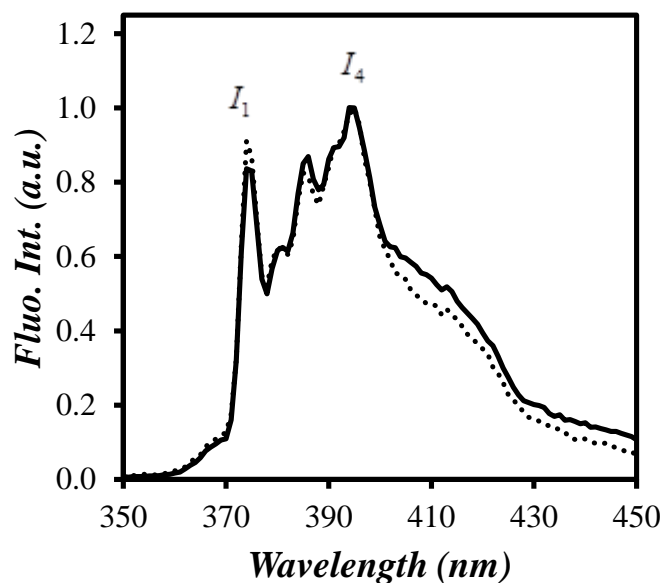


Figure 17: Steady-state spectra for Py-PBMA-latex-1 in a thick film before annealing (—) and a thin homogeneous (cast) film (•••). $\lambda_{ex} = 344$ nm.

3.3.2 Fraction of Mixing Between Latex Particles

Before steady-state fluorescence measurements on films were conducted, the films were dried overnight according to the procedure described earlier. Leaving the films to dry for this long period of time ensures the complete removal of water before annealing. This precaution is important because any remaining water may act as a plasticizer, lowering the T_g of the polymers and possibly resulting in a change in the measured diffusion coefficient for the polymer in the film.^{19,20} However since the films were dried for such a long period of time, fluorescence measurements were also conducted to ensure that no significant diffusion occurred during the drying period. To this end, a film was deposited on a quartz slide and left to dry for three hours, at which point no visible water remained. The fluorescence spectrum for the film was collected and the I_E/I_M ratio was calculated to be 0.138. The film was then left to dry further overnight. In

the morning, the fluorescence spectrum was again acquired and the I_E/I_M ratio was calculated. As seen in Figure 18, the steady-state fluorescence spectra overlap and the I_E/I_M ratio remained unchanged within experimental error at 0.134. The unchanged spectra demonstrate that no noticeable diffusion occurred at room temperature. The longer overnight drying was therefore used to ensure higher reproducibility in relation to film dryness, as compared to a film dried for only three hours.

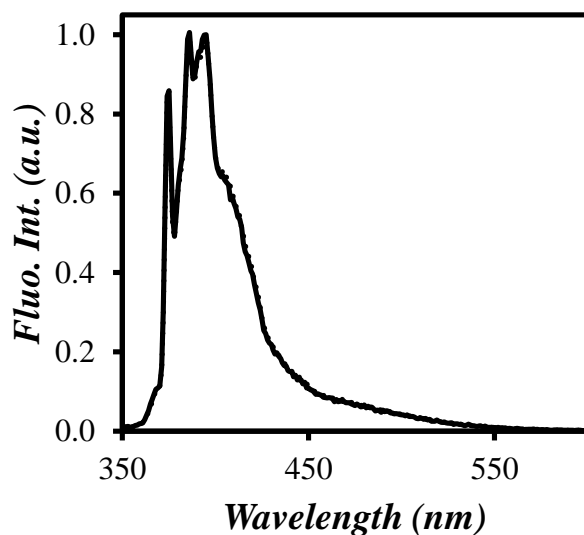


Figure 18: Steady-state fluorescence spectra for a film after drying at room temperature for 3 hours (—) and overnight (•••). $\lambda_{ex}=344$ nm.

Two films were studied in this project as outlined in Table 3. Film 1 consisted of a latex composed of a high (> 400 kg·mol⁻¹) molecular weight polymer, while the polymer in Film 2 had a molecular weight of less than half of that in Film 1. To measure the fraction of mixing (f_m) between latex particles in a film, the steady-state fluorescence spectrum of the film was acquired as a function of annealing time for a given annealing temperature. At each annealing time, three steady-state fluorescence measurements were made at different locations on the film. Figure 19A displays the changes observed in the steady-state fluorescence spectrum for Film 1, containing the higher molecular weight polymers,

annealed at 102 °C. The film exhibited the highest level of excimer formation before any annealing occurred, with an I_E / I_M ratio of 0.134. Even though the amount of excimer formed was low, it was sufficiently high to observe a noticeable change as film formation occurred, as shown in Figure 19B. As the film annealed, the amount of excimer decreased and after it had fully annealed (homogeneous film) the I_E / I_M ratio decreased to a value of 0.037.

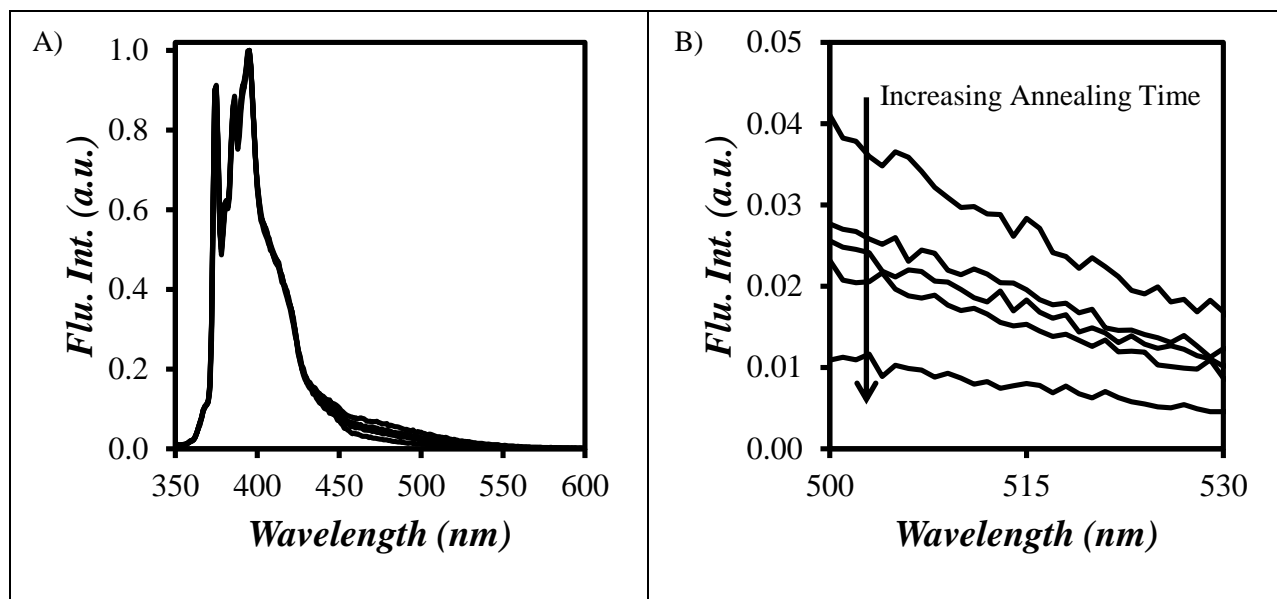


Figure 19: Steady-state fluorescence spectra obtained for A) Film 1 containing Py-PBMA-Latex-1 annealed at 102 °C and B) expanded area corresponding to the excimer fluorescence. The curves from top to bottom are for $t_{an} = 0, 25, 110, 560$ min., and a homogeneous film ($t_{an} = \infty$). $\lambda_{ex}=344$ nm.

Using the I_E / I_M ratios, the fraction of mixing (f_m) was calculated via Equation 18. A plot of f_m over time is given in Figure 20 for Film 1 annealed at 102 °C. At this high annealing temperature ($T_g(\text{PBMA}) = 27$ °C),⁵ f_m quickly rose to 0.32 after only ten minutes of annealing. As the film was annealed further f_m continued to increase, but much more slowly as time elapsed, such that after nine

hours f_m increased to only 0.59. In contrast, Film 2, containing the lower molecular weight polymers, reached a much greater f_m over the same annealing time period: After ten minutes of annealing f_m was calculated to equal 0.50, and after nine hours it reached a value of 0.82. While f_m was higher at all times for the lower molecular weight film, as would be expected, the profile was similar for both the high and low molecular weight films, as seen in Figure 20. This trend of a rapid increase in f_m at short annealing times, followed by a slow but continuous increase at long annealing times, is consistent with previous studies.^{4,5,21}

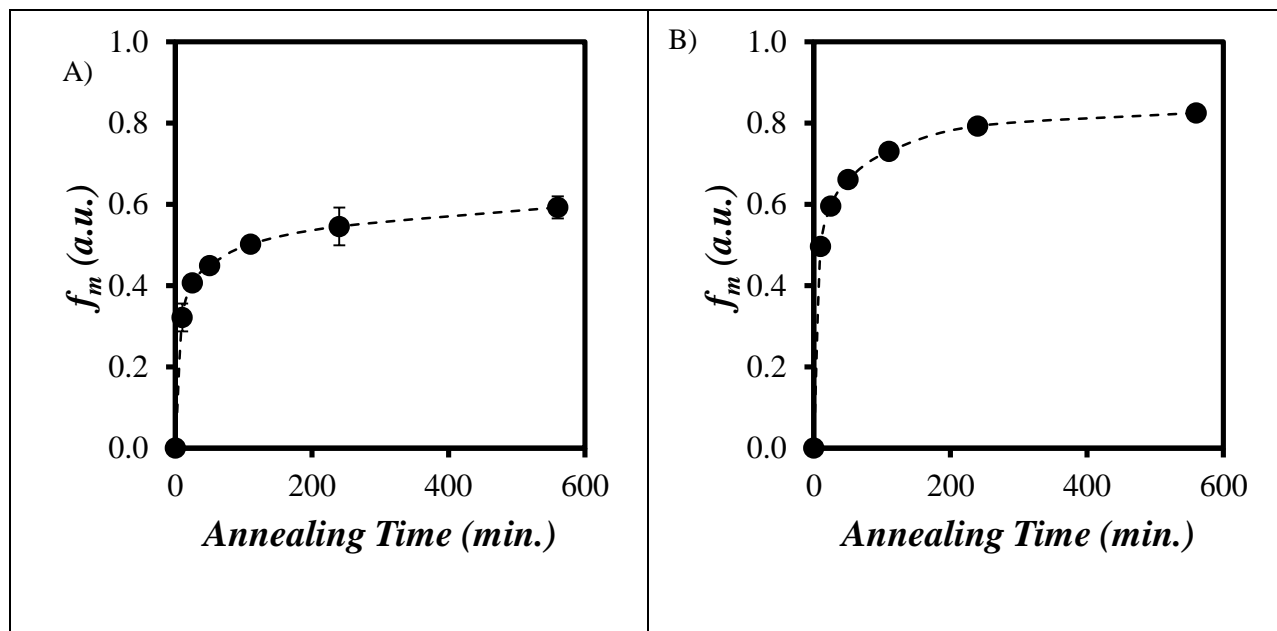


Figure 20: Fraction of mixing of A) Film 1 (Py-PBMA-Latex-1: $M_n = 430 \text{ kg}\cdot\text{mol}^{-1}$) and B) Film 2 (Py-PBMA-Latex-2: $M_n = 198 \text{ kg}\cdot\text{mol}^{-1}$) annealed at 102 °C.

This process was repeated for both Film 1 and Film 2 (Table 3) at a total of nine annealing temperatures ranging from 75 to 119 °C. At all the annealing temperatures, the I_E / I_M ratio for Film 1 decreased from 0.135 ± 0.003 before annealing to 0.031 ± 0.004 after full annealing. Similarly, annealing of Film 2 led to a significant decrease in the I_E / I_M ratio from 0.119 ± 0.006 to 0.024 ± 0.002 at all the

annealing temperatures. The slightly lower I_E / I_M ratio for Film 2 is attributed to the slightly lower pyrene content of Py-PBMA-Latex-2. The I_E / I_M ratios were then used to calculate the fraction of mixing (f_m) between the latex particles at each annealing temperature. Figures 21 and 22 display the fraction of mixing over time at all the annealing temperatures for Films 1 and 2, respectively.

The rate at which f_m increases depends on many factors such as the type of polymer, the annealing temperature,⁷ the molecular weight of the polymer,^{21,22} the presence of crosslinks,²³ and whether additives are present in the film.^{19,20,24} All the f_m -vs- t_{an} curves display similar features characterized by a rapid increase in f_m at short annealing times, and a slow gradual increase at longer annealing times. For example, when Film 1 was annealed at 102 °C, f_m increased rapidly to reach 0.40 after only 25 minutes of annealing, followed by a slower but continuous increase to 0.59 after 560 minutes of annealing. This behaviour is attributed to the dispersity D of the polymer chains.⁵ At short annealing times, the shorter chains which can diffuse more quickly dominate the f_m profile, resulting in an initial rapid increase in f_m . As annealing is continued, the short chains reach equilibrium in the film and the f_m profile starts to be dominated by the higher molecular weight chains, resulting in a slower but continuous increase in f_m .

It is also apparent that as the annealing temperature was increased, f_m reached a larger value for a set annealing time. For the sake of comparison, Film 1 was annealed for 20 minutes at 75 and 119 °C. In 20 minutes, f_m reached 0.15 and 0.55 when the film was annealed at 75 and 119 °C, respectively. Moreover, even after annealing the film at 75 °C for over 19 hours, f_m only reached a value of 0.34. This result makes it clear that the annealing temperature has a large impact on the level of mixing reached between the latex particles.

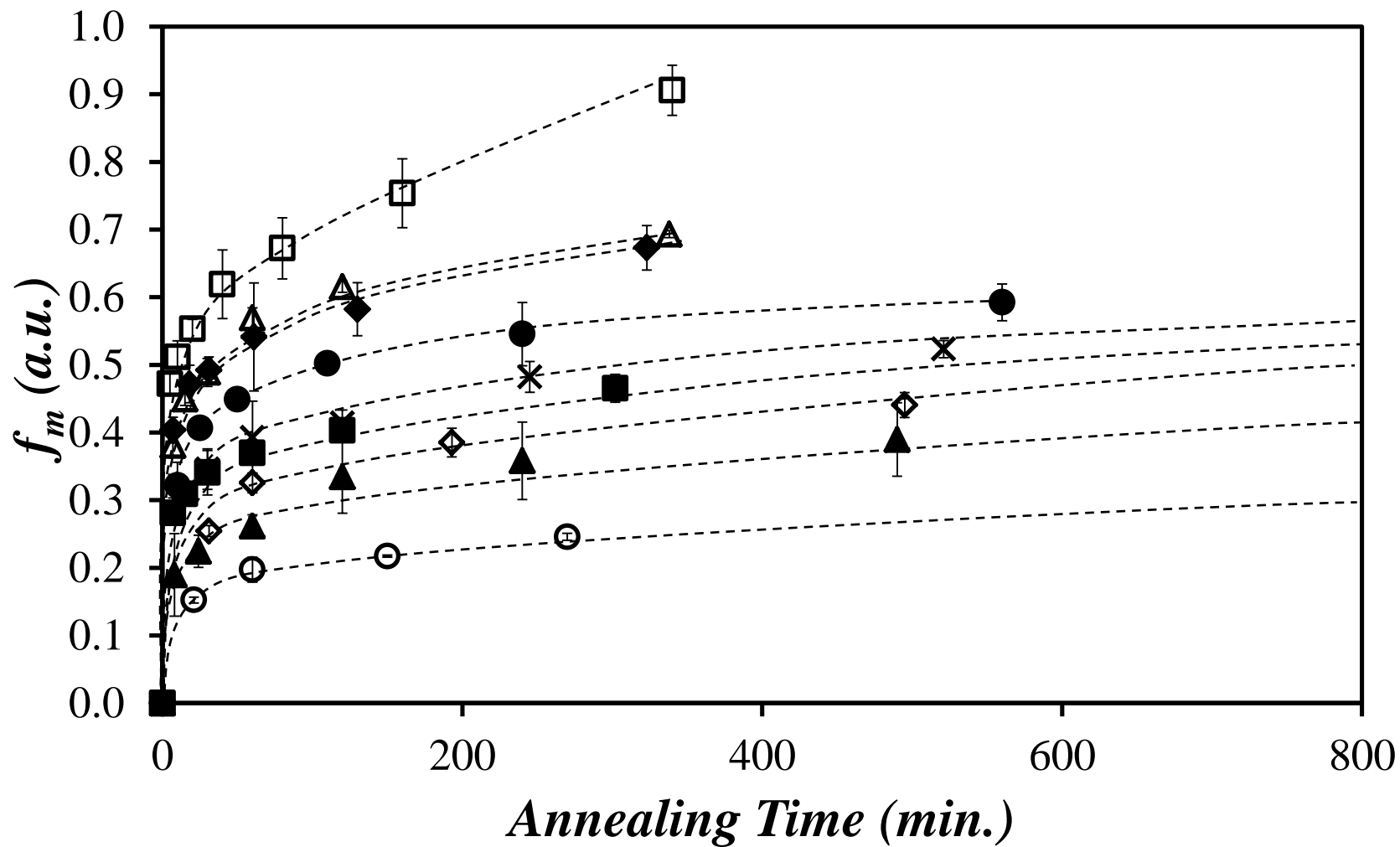


Figure 21: Fraction of mixing for Film 1, consisting of higher molecular weight copolymer. $T_{an} = 119$ (□), 112 (◆), 111 (△), 102 (●), 98 (✕), 94 (■), 88 (◇), 84 (▲), and 75 (○) °C. Py-PBMA-Latex: $M_n = 430 \text{ kg}\cdot\text{mol}^{-1}$, $D = 1.9$; PBMA-Latex: $M_n = 510 \text{ kg}\cdot\text{mol}^{-1}$, $D = 2.0$.

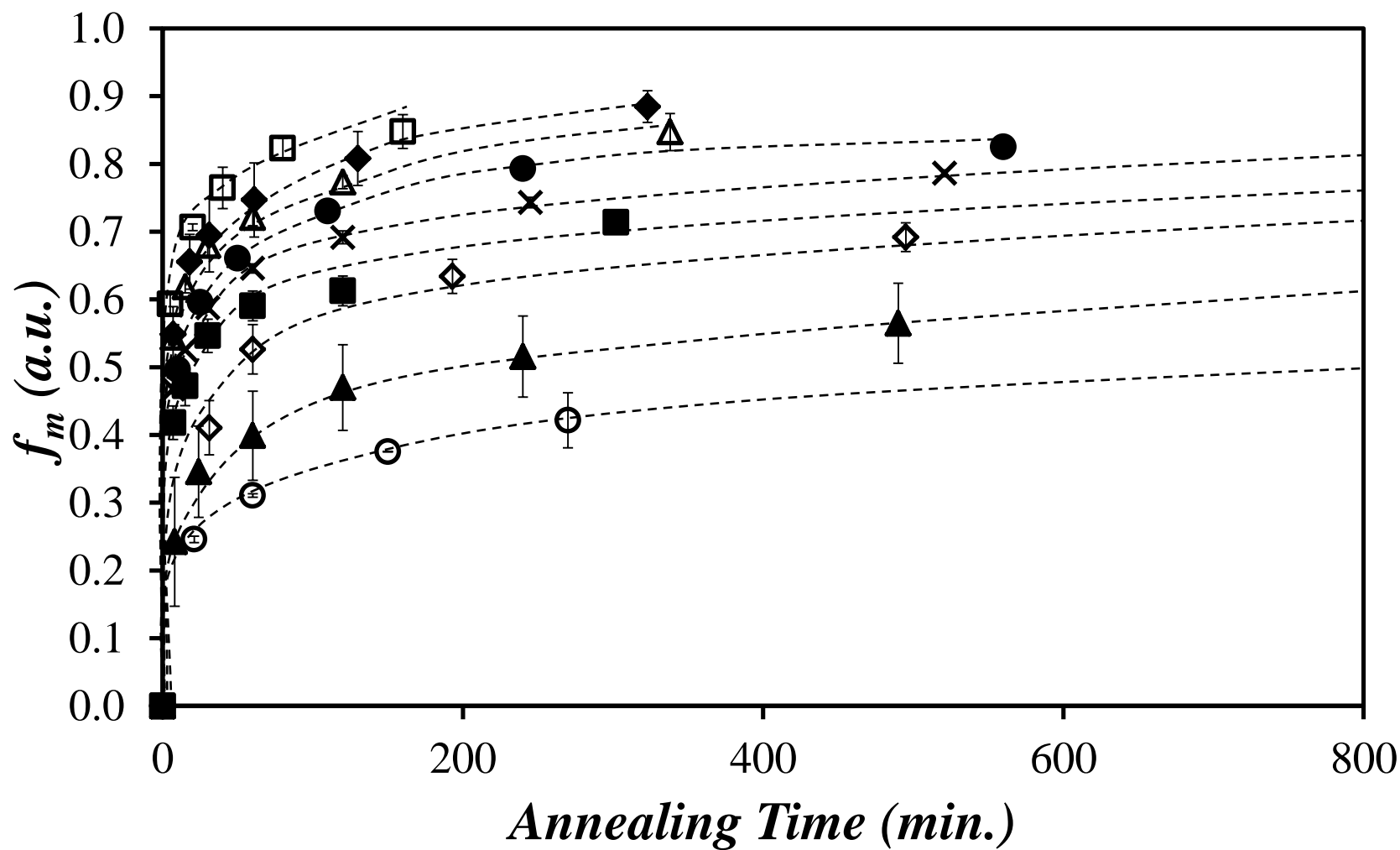


Figure 22: Fraction of mixing for Film 2, consisting of lower molecular weight copolymer. $T_{an} = 119$ (□), 112 (◆), 111 (△), 102 (●), 98 (×), 94 (■), 88 (◇), 84 (▲), and 75 (○) °C. Py-PBMA-Latex: $M_n = 198 \text{ kg}\cdot\text{mol}^{-1}$, $D = 1.8$; PBMA-Latex: $M_n = 190 \text{ kg}\cdot\text{mol}^{-1}$, $D = 1.7$.

3.3.3 Film Colour Change

A more qualitative analysis was also conducted by observing colour changes for each film during the annealing process. After each annealing time, the film was irradiated with long wavelength UV light from a hand-held UV lamp and a picture was taken. An additional photograph was also taken using a 480 nm cut-off filter, to view the pyrene excimer emission without interference from the monomer. An overview of the film colour changes observed as a function of f_m for annealing temperatures ranging from 75 to 111 °C is depicted in Table 4 and Table 5 for Films 1 and 2, respectively. Both Films 1 and 2 displayed similar trends in colour change. When a film was directly observed without cut-off filter, the film initially emitted turquoise-blue. As the film annealed the emission colour began to dull, and after complete annealing it changed to violet-blue. While the change in colour was continuous, there appeared to be a noticeable shift from turquoise to violet-blue around $f_m = 0.6-0.7$. An example of this colour change is provided in Figure 23.

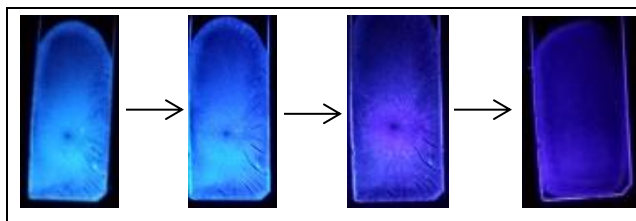


Figure 23: Emission colour change for Film 2 annealed at 84 °C, irradiated by UV light. From left to right $f_m = 0.00, 0.35, 0.69, 1.00$.

The appearance of the film changed to green when it was observed through a 480 nm cut-off filter. In contrast to observation made with the naked eye, the change observed through the cut-off filter displayed no change in colour but rather a decrease in the emitted intensity. One example of such a decrease in emission intensity is provided in Figure 24.

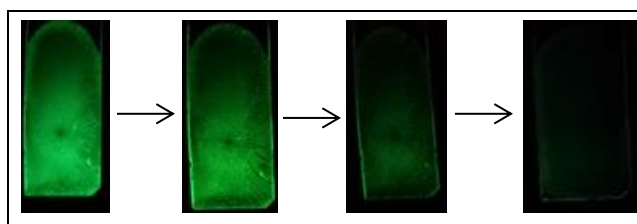






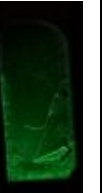
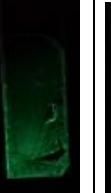






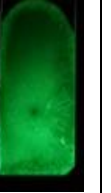
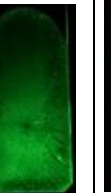







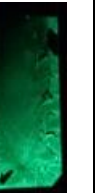





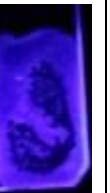
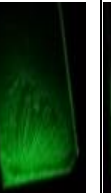






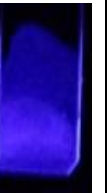
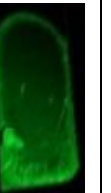

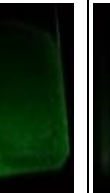






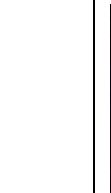

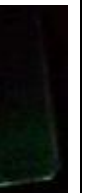



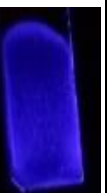


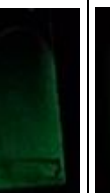
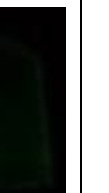
Figure 24: Decrease in the excimer emission intensity for Film 2 over the course of film formation at 84 °C. From left to right, $f_m = 0.00, 0.35, 0.69, 1.00$.

A change in emission intensity was therefore noticeable both with and without a cut-off filter. When no cut-off filter was employed, a colour change in the emission from turquoise to violet-blue was observed upon annealing, with the most noticeable change occurring for $f_m > 0.6$. Since the colour change appeared to depend on f_m , particles with a core-shell morphology could also be prepared such that the colour change would become noticeable at any selected f_m value. When the emission was observed through a cut-off filter, the green emission decreased in intensity with the annealing time. Since the colour change was continuous, the change in colour may be difficult to distinguish in Tables 4 and 5 when comparing colours for similar f_m values. When films with significantly different f_m values were compared side by side, the colour change became more apparent (e.g. Figures 23 and 24). To this end, one method to probe f_m might involve the comparison of the fluorescence of a film to that of a reference chart with colour bars corresponding to different f_m values, to allow for quick qualitative analysis.

Table 4: Overview of colour changes observed during film formation for Film 1.

T_{am} (°C)	Direct				480 nm Cut-off Filter			
	f_m				f_m			
	0.00	0.30–0.39	0.70–0.79	1.00	0.00	0.30–0.39	0.70–0.79	1.00
75								
84								
88								
94								
98								
102								
111								

Table 5: Overview of colour changes observed during film formation for Film 2.

T_m (°C)	Direct				480 nm Cut-off Filter			
	f_m				f_m			
	0.00	0.30–0.39	0.70–0.79	1.00	0.00	0.30–0.39	0.70–0.79	1.00
75								
84								
88								
94								
98								
102								
111								

3.4 Apparent Diffusion Coefficient (D)

3.4.1 The Model

To obtain more quantitative information about film formation, the apparent polymer diffusion coefficient (D) was calculated by applying a diffusive model. We selected the same model that has been used in previous FRET studies,^{2,4-6} namely a Fickian model of molecules diffusing out of a sphere (Equations 6 and 7). Typically, a Fickian model is applicable to small molecules or to polymers with less than two entanglements per chain⁴ ($M_c(\text{PBMA}) = 32 \text{ kg}\cdot\text{mol}^{-1}$),²⁵ where M_c is the critical molecular weight at which entanglements begin to form. In the case of larger polymer chains, this model is also applicable as long as the annealing time is greater than the reptation time for all the polymer chains present in the film.⁴ A reptation-based model has also been suggested for high molecular weight polymers at long annealing times. Despite the controversy over the choice of an appropriate model and suitable assumptions, there has been good agreement between the diffusion coefficients found by FRET using a Fickian model and those found by SANS based on Cook's scattering.^{4,8} In addition, some of the previously reported complications in FRET studies are a result of FRET itself. One of the most controversial assumptions in the FRET method resides in the handling of the distribution of acceptors in the film, since the FRET efficiency is extremely distance-dependent. In our case, since pyrene excimer formation only occurs upon direct contact, this additional complication does not need to be taken into account. To this end, we selected the Fickian diffusion model for its relative simplicity, and to allow for a more direct comparison of D with previous FRET studies performed by the Winnik group.

Calculations were completed by implementing an in-house optimization program using Python 2 with the NumPy and SciPy libraries. The annotated program is provided in Appendix A. Since the entire film was probed by steady-state fluorescence, the diffusion coefficient calculated is an average for all the polymer chains, large and small. Therefore, this method yields an apparent (or average) diffusion

coefficient. The diffusion coefficient was calculated by equating the experimental (Equation 18) and calculated (Equation 19) fractions of mixing using numerical integration of the concentration profile (Equation 7). A sample plot of the concentration profile derived from Equation 7 is given in Figure 25.

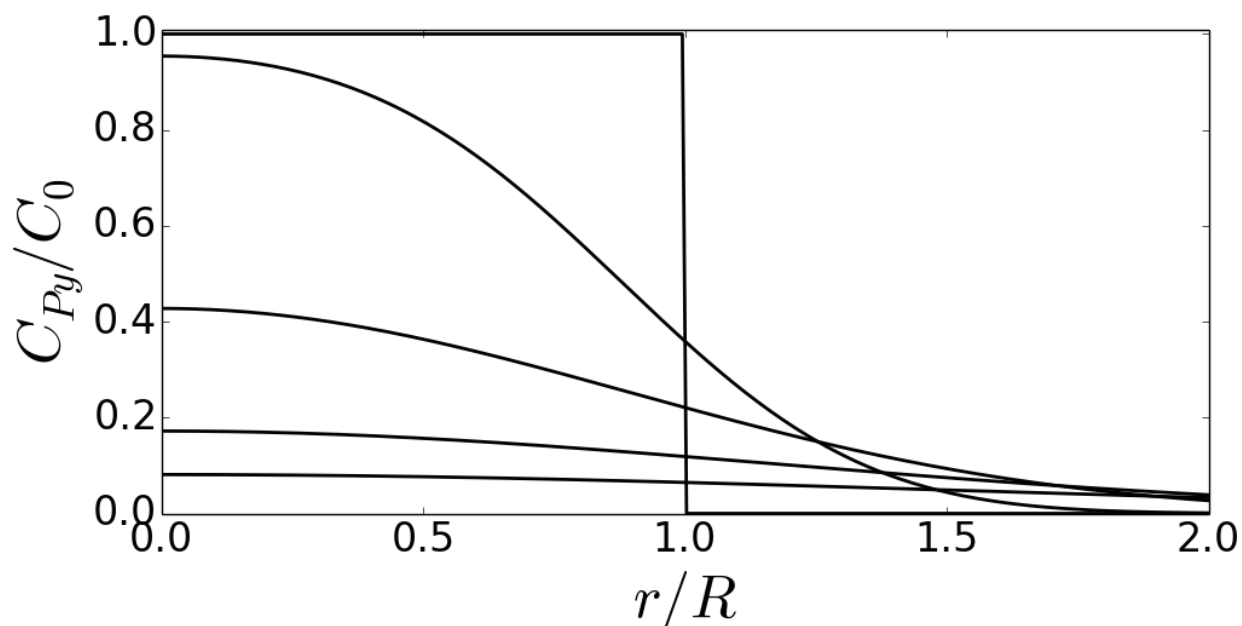


Figure 25: Concentration of pyrene diffusing out of a particle of radius R , as a function of distance r from the particle center, for different annealing times. From top to bottom: $(Dt/r^2)^{1/2}$ equals 0.00, 0.25, 0.50, 0.75, and 1.00, corresponding to $f_m = 0.00, 0.41, 0.71, 0.86,$ and 0.93 , respectively.

3.4.2 Results and Discussion

The apparent diffusion coefficients were calculated for each temperature and time increment, other than t_0 and t_∞ , since these are used as references in the I_E/I_M ratio calculations. A summary of the $I_E/I_M, f_m,$ and D values obtained at each annealing time and temperature is provided in Appendix A in Tables A1 to A9. The calculated apparent diffusion coefficient was plotted against the annealing time (Figure 26) and f_m

(Figure 27) for both films. Similarly to f_m , higher annealing temperatures resulted in larger D values. As the annealing temperature increases, the increased thermal energy results in more rapid Brownian motion of the polymer chains, leading to a larger diffusion coefficient. In addition, as expected from the results of f_m over time, Film 1 containing the higher molecular weight polymer yielded lower diffusion coefficients than for the lower molecular weight polymer constituting Film 2. Since the polymer chains were larger in Film 1 they diffused more slowly, resulting in lower D values. One of the most obvious trends was the rapid decrease in D over time (or f_m). Over the course of annealing, D decreased by up to two orders of magnitude. As discussed earlier, this decrease can be attributed to the dispersity of the polymer chains: Initially the diffusion of the shorter polymer chains dominates, resulting in a high apparent diffusion coefficient. As the film continues to anneal, these short chains reach equilibrium in the film and no longer contribute to the apparent diffusion coefficient. As this occurs, the diffusion begins to be dominated by the longer chains, resulting in a decrease in D . The decrease in D may also be the result of an additional driving force at early times: The polymer chains located close to the particle surface are under strain, as their configurational space is restricted by the particle boundary. As a result, the polymer chains close to the particle boundary are expected to diffuse more quickly at early times to reduce their strain.

To push our analysis one step further, we used these diffusion coefficients to calculate the apparent activation energy of diffusion along with the c_1 and c_2 terms in the Williams-Landel-Ferry (WLF) equation by two different methods. The first method followed the original procedure set forth by Williams, Landel, and Ferry.²⁷ The second method utilized a procedure developed by the Winnik group for the analysis of film formation by FRET.⁴

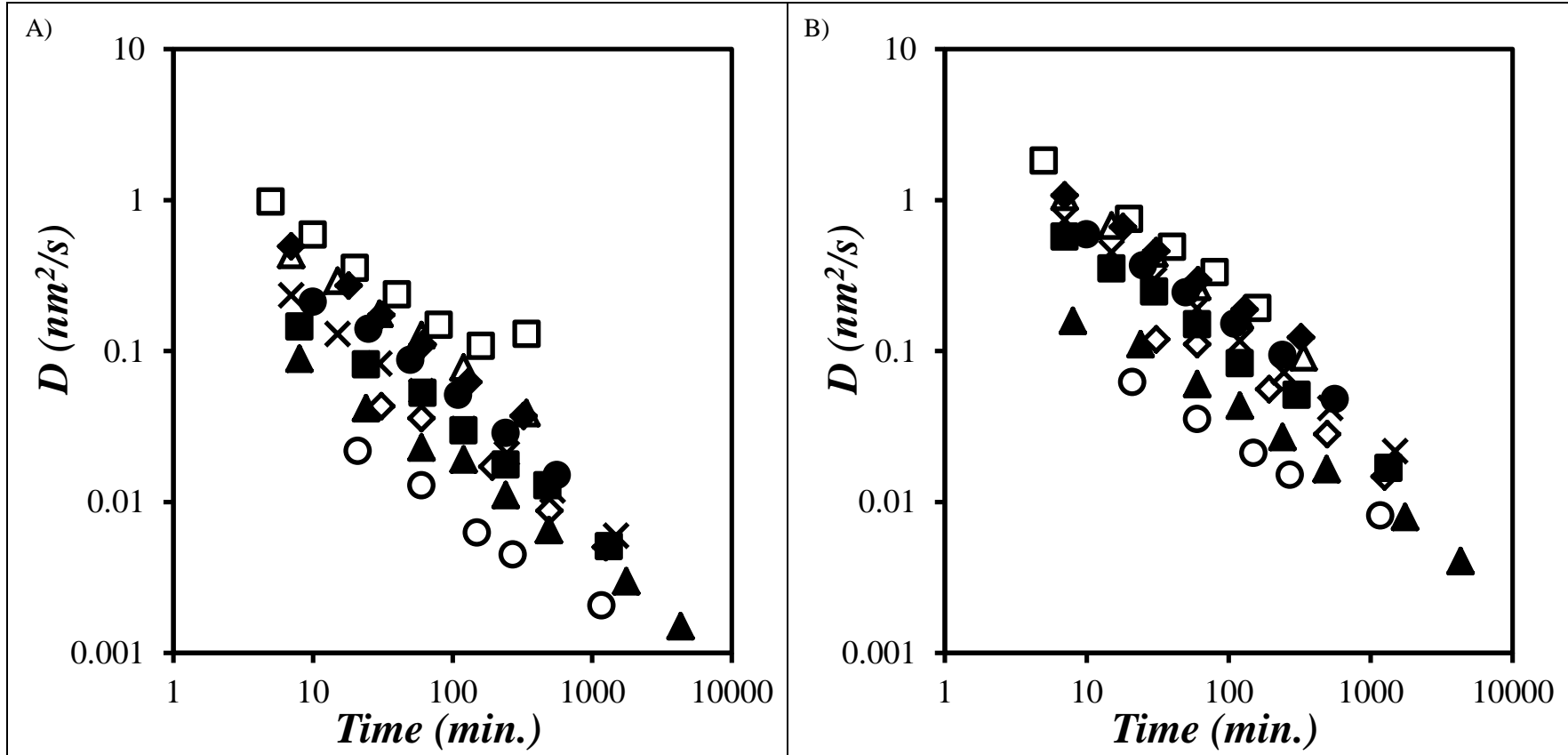


Figure 26: Plot of the apparent diffusion coefficients as a function of annealing time for A) Film 1, containing high molecular weight polymer chains (Py-PBMA-Latex: $M_n = 430 \text{ kg}\cdot\text{mol}^{-1}$, $D = 1.9$; PBMA-Latex: $M_n = 510 \text{ kg}\cdot\text{mol}^{-1}$, $D = 2.0$) and B) Film 2, containing a lower molecular weight polymer (Py-PBMA-Latex: $M_n = 198 \text{ kg}\cdot\text{mol}^{-1}$, $D = 1.8$; PBMA-Latex: $M_n = 190 \text{ kg}\cdot\text{mol}^{-1}$, $D = 1.7$). From top to bottom $T_{an} = 119, 112, 111, 102, 98, 94, 88, 84,$ and $75 \text{ }^\circ\text{C}$.

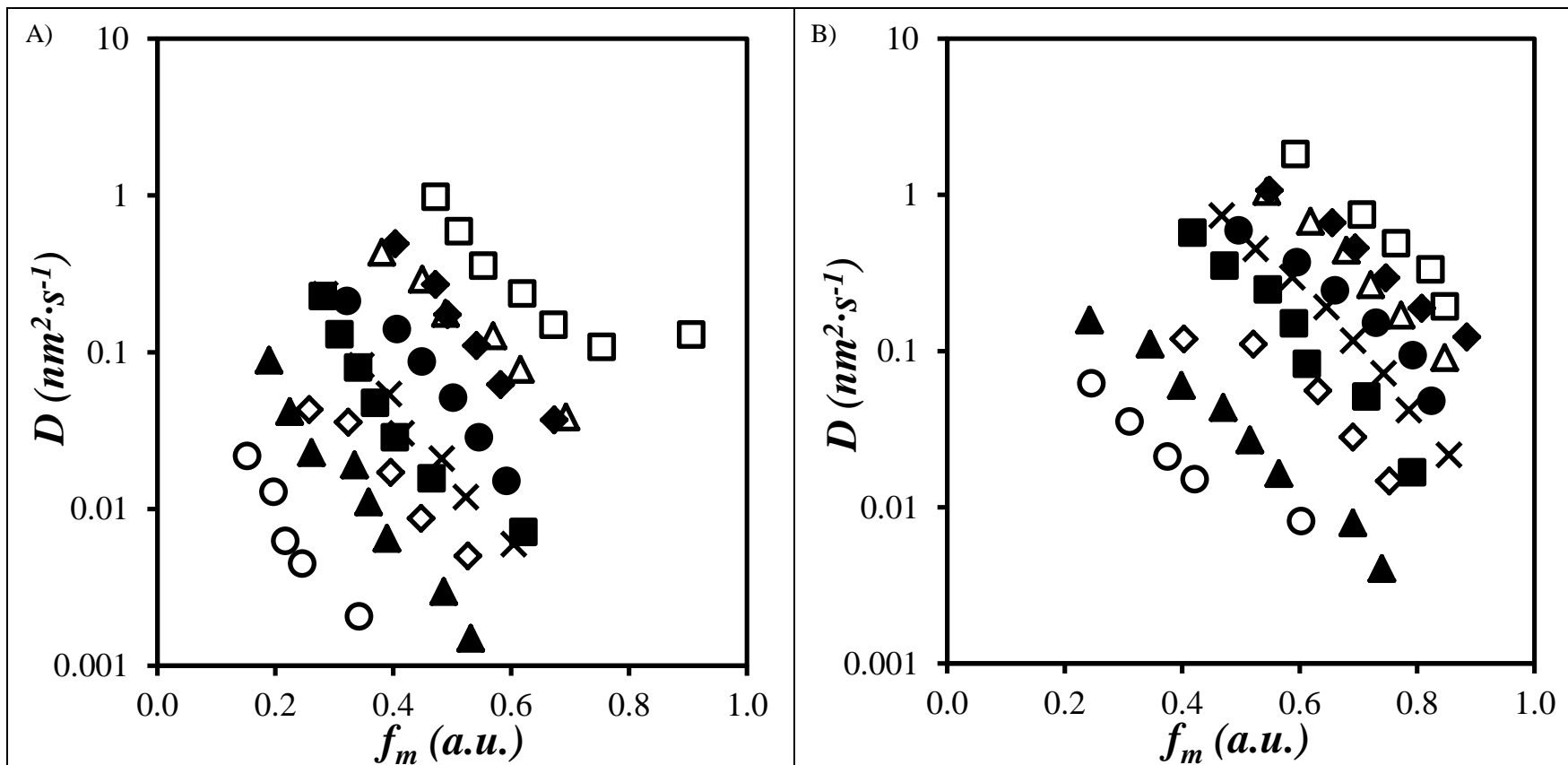


Figure 27: Plot of the apparent diffusion coefficients as a function of fraction of mixing f_m for A) Film 1, containing high molecular weight polymer chains (Py-PBMA-Latex: $M_n = 430 \text{ kg}\cdot\text{mol}^{-1}$, $D = 1.9$; PBMA-Latex: $M_n = 510 \text{ kg}\cdot\text{mol}^{-1}$, $D = 2.0$) and B) Film 2, containing lower molecular weight polymers (Py-PBMA-Latex: $M_n = 198 \text{ kg}\cdot\text{mol}^{-1}$, $D = 1.8$; PBMA-Latex: $M_n = 190 \text{ kg}\cdot\text{mol}^{-1}$, $D = 1.7$). From top to bottom $T_{an} = 119, 112, 111, 102, 98, 94, 88, 84,$ and $75 \text{ }^\circ\text{C}$.

3.4.3 Further Analysis: WLF Method

To apply the WLF method, the diffusion coefficients needed to first be normalized to a reference temperature.²⁸ The temperature selected is arbitrary and can be easily changed. We decided to use a reference temperature of 102 °C since it is close to 100 °C, at which the properties of PBMA have been investigated. Typically the measured quantity, in our case D , is reduced to yield D' in Equation 20, where the temperature is in Kelvin. The density $\rho(T)$ was not expected to change much with temperature, so it was treated as a constant in our derivation. Another possibility is to use the diffusion coefficients as is, and not to take into account changes in temperature and density. As T increases $\rho(T)$ decreases, which results in the product $T\rho(T)$ remaining more or less constant. Both approaches were examined, and no discernible difference was noted in the results. The analysis reported herein is based on the assumption that $\rho(T)$ did not change much with temperature.

$$D'(t, T_0) = \frac{D(t/a_T, T) \cdot T_0 \rho(T_0)}{T \rho(T)} \quad (20)$$

The reduced diffusion coefficients (D') were then shifted along the annealing time axis by a factor a_T . Least squares analysis was used to ensure that the shift factor was optimal. Plots of the resulting master curves are given in Figure 28. This method resulted in a very smooth line with minimal scattering for each annealing temperature. Table 6 lists the shift factors and the corresponding R^2 values thus obtained. The R^2 values were generally very close to unity, in most cases above 0.96, indicating good fits.

Table 6: Shift factors for the reduced diffusion coefficients used to prepare the master curves.

T_{an} (°C)	<i>Film 1</i>		<i>Film 2</i>	
	a_T	R^2	a_T	R^2
119	0.25	0.99	0.35	0.98
112	0.44	0.99	0.50	0.95
111	0.49	0.98	0.55	0.97
102	1.00	0.98	1.00	0.99
98	1.45	0.99	1.40	0.97
94	2.00	0.97	2.00	0.96
88	3.50	0.95	3.50	0.94
84	5.90	0.97	7.00	0.90
75	15.50	0.98	15.00	0.96

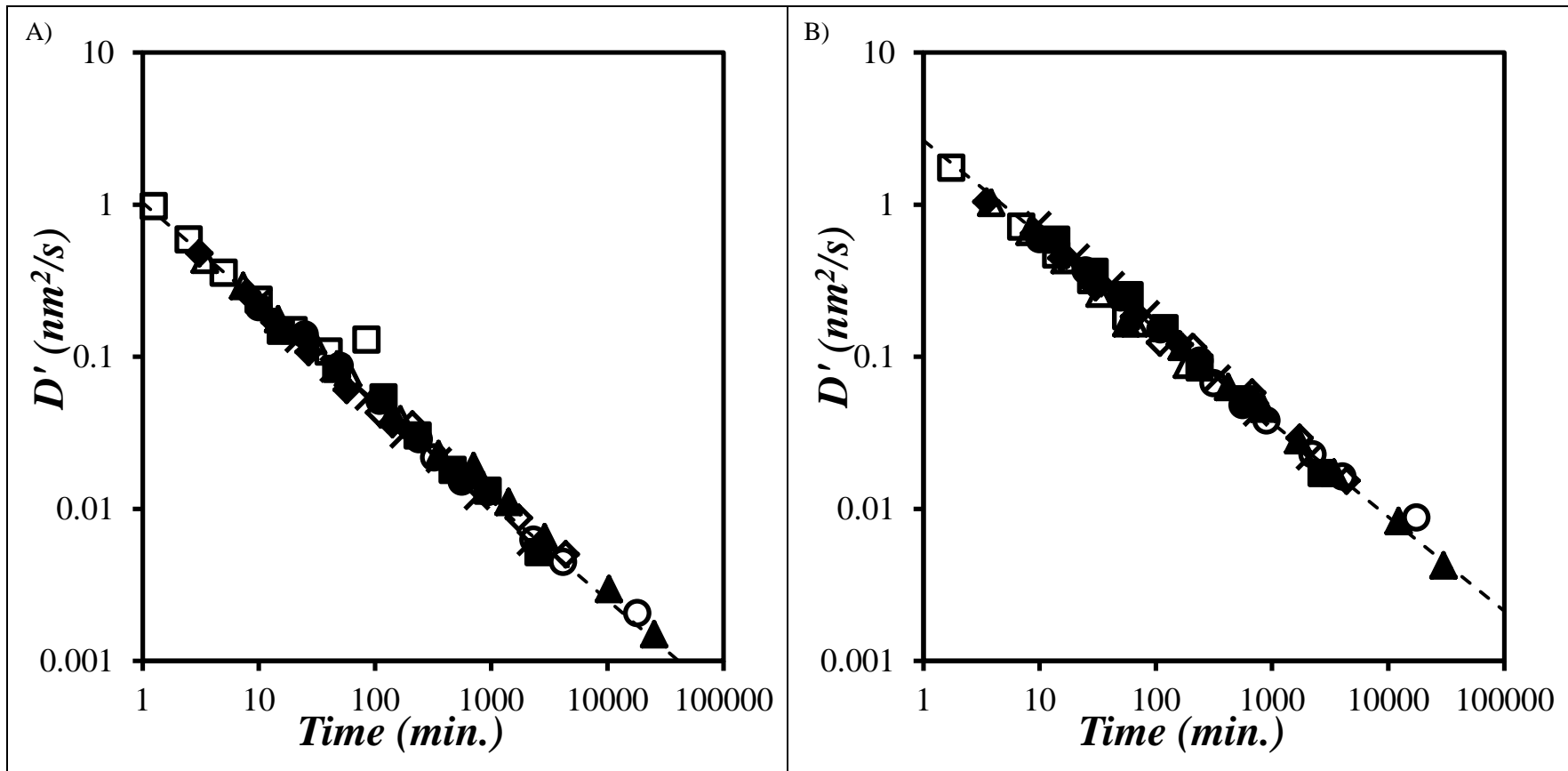


Figure 28: Master curves for the reduced diffusion coefficient plotted as a function of annealing time using a reference temperature of 102 °C for A) Film 1, containing high molecular weight polymer chains (Py-PBMA-Latex: $M_n = 430 \text{ kg}\cdot\text{mol}^{-1}$, $D = 1.9$; PBMA-Latex: $M_n = 510 \text{ kg}\cdot\text{mol}^{-1}$, $D = 2.0$), and B) Film 2, containing lower molecular weight polymer (Py-PBMA-Latex: $M_n = 198 \text{ kg}\cdot\text{mol}^{-1}$, $D = 1.8$; PBMA-Latex: $M_n = 190 \text{ kg}\cdot\text{mol}^{-1}$, $D = 1.7$). $T_{an} = 119$ (\square), 112 (\blacklozenge), 111 (\triangle), 102 (\bullet), 98 (\times), 94 (\blacksquare), 88 (\diamond), 84 (\blacktriangle), and 75 (\circ) °C.

The WLF equation, given in Equation 21, was linearized as shown in Equation 22. Using a plot of $(T-T_0)/\log(a_T)$ against $T-T_0$, the c_1 and c_2 terms could be extracted. From Equation 22, the slope and intercept of the straight line are equal to $-1/c_1$ and $-c_2/c_1$, respectively.

$$\log(a_T) = \frac{-c_1 \cdot (T - T_0)}{c_2 + T - T_0} \quad (21)$$

$$\frac{T - T_0}{\log(a_T)} = \frac{-(T - T_0)}{c_1} - \frac{c_2}{c_1} \quad (22)$$

A plot of $(T-T_0)/\log(a_T)$ versus $T-T_0$ in Figure 29 yielded a straight line for Film 1, which was constituted of the higher molecular weight polymers. The values of c_1 and c_2 were found to be 7 ± 1 and 190 ± 30 K, respectively. These values are similar to those found by dynamic mechanical analysis (DMA) of PBMA in the bulk at 100 °C, with $c_1 = 9.7$ and $c_2 = 169.6$ K.²⁶ Film 2, containing the lower molecular weight polymers, followed the same trend as Film 1 up to the reference temperature of 102 °C. Above this temperature there was a significant deviation from the linear trend however.

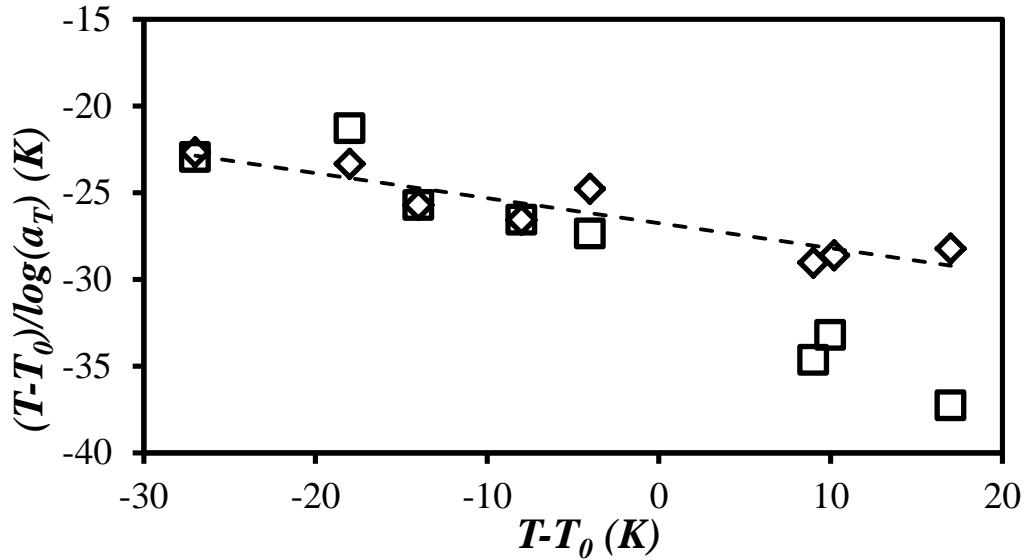


Figure 29: Plot of the linearized WLF equation used to extract the c_1 and c_2 parameters for Film 1 (◇) and Film 2 (□). The slope and intercept for the dashed line equal $\square 0.14$ and $\square 26.8$, respectively. $R^2 = 0.84$, $T_0 = 102$ °C.

One possible explanation of this deviation at the high annealing temperatures may lie in the molecular weight difference of the two films. The WLF equation is typically valid in a temperature range from T_g to $T_g + \Delta T$, where ΔT varies between 50 and 100 K depending on the polymer.^{27,29} This temperature range corresponds to the rubbery plateau of the polymers being probed. However if the temperature is increased enough to enter the liquid flow region, the WLF equation no longer applies and a deviation is expected. Higher molecular weight polymers exhibit an extended plateau. In our case it may be that Film 1, which contains a higher molecular weight polymer, still follows WLF behaviour at temperatures up to 119 °C, whereas the lower molecular weight polymer in Film 2 only obeys this behaviour up to the reference temperature.

At higher temperatures, an Arrhenius equation for the apparent activation energy of diffusion (E_a) becomes more effective at describing the behaviour of the shift factors. E_a is defined in Equation 23.²⁷ Based on earlier work, a plot of $\ln(a_T)$ against $1/T$ is expected to yield a straight line over a sufficiently narrow temperature range, with a slope equal to E_a/R . Indeed, both plots of $\ln(a_T)$ versus $1/T$ shown in Figure 30 yielded straight lines with similar slopes for both films, leading to E_a values of 105 ± 2 and 100 ± 4 kJ·mol⁻¹ for Films 1 and 2, respectively. Since this Arrhenius behaviour is better suited to higher annealing temperatures, it was expected that the activation energy for diffusion should remain constant for the two films, since they both contained high molecular weight polymers ($M_n \gg M_c$), where M_c is the critical molecular weight required for chain entanglement formation. Although the two films yielded similar E_a values, these are significantly lower than the reported E_a value of 151 kJ·mol⁻¹ found by DMA for bulk PBMA at 100 °C.²⁷ However the E_a value of ~105 kJ·mol⁻¹ matches more closely the activation energy for β -relaxation of 100 kJ·mol⁻¹.²⁶ The difference in E_a values may also be explained by the difference in morphology between polymer in the bulk, as observed in DMA, and the polymer in latex particles. As discussed earlier, the polymer chains in latex particles have their configurational space constrained to a rigid sphere, resulting in a restricted number of polymer configurations near the particle boundary. In the bulk, in contrast, this constraint is not present and the polymer is able to adopt less

strained configurations. The strained polymer chains in the latex may provide an extra driving force for diffusion to occur, thereby lowering the measured E_a values.

$$E_a = R \frac{d \ln(a_T)}{d(1/T)} \quad (23)$$

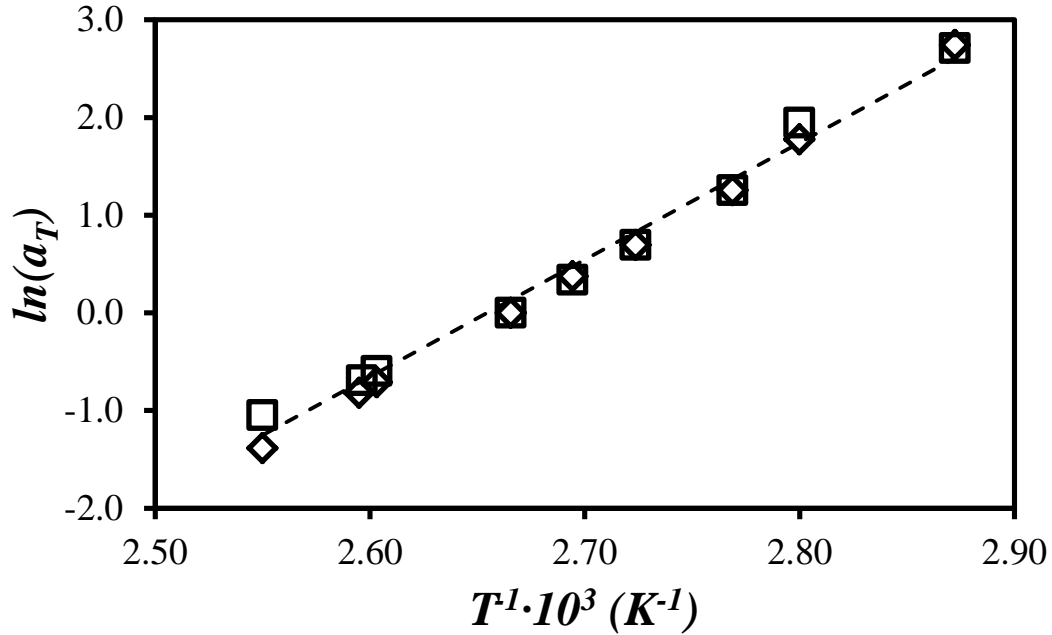


Figure 30: Arrhenius behaviour of the apparent activation energy of diffusion for Film 1 (\diamond , $E_a = 105 \pm 2 \text{ kJ}\cdot\text{mol}^{-1}$) and Film 2 (\square , $E_a = 100 \pm 4 \text{ kJ}\cdot\text{mol}^{-1}$).

3.4.4 Further Analysis: Winnik's FRET Method

The last analysis of the D values plotted in Figure 26 and 27 was based on a method developed by the Winnik group to characterize film formation using FRET.^{2,4-6,8} The apparent activation energy for diffusion was first determined. This procedure assumed that D could be described by an Arrhenius equation, whereby $\log(D)$ was plotted as a function of $1/T$. One of the critical differences in this approach is that all the diffusion coefficients used over the temperature range must be from the exact same fraction of mixing. The closer f_m remains over the temperature range, the more accurate the results. In our case this happened to be a significant limitation, since there were very few cases where f_m was identical at several

annealing temperatures despite the fact that our plots were built with no less than 56 experimental points per film, as compared to the much fewer 22 – 33 experimental points used to build similar plots in earlier studies.^{4,7} Figure 31 compares the plots generated by applying this method to the D values obtained from pyrene excimer formation for both films, to that obtained with a PBMA film probed by FRET. Both Films 1 and 2 yielded linear plots. The slopes of the lines were then used to find E_a , with corresponding values of 180 ± 8 and 160 ± 21 $\text{kJ}\cdot\text{mol}^{-1}$ for Films 1 and 2, respectively. These values are slightly higher than those found by DMA, but are very close to the values found by FRET of 151 and 159 $\text{kJ}\cdot\text{mol}^{-1}$ for PBMA.^{4,5}

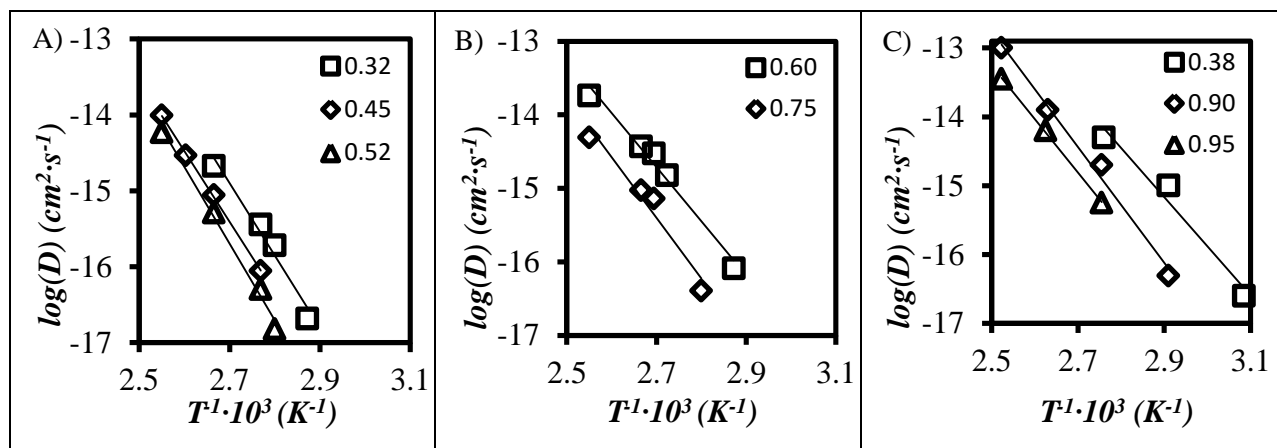


Figure 31: Arrhenius plots used to find the activation energy of the diffusion coefficient for A) Film 1 ($M_w = 817$ $\text{kg}\cdot\text{mol}^{-1}$, $D = 1.9$, $E_a = 180 \pm 8$ $\text{kJ}\cdot\text{mol}^{-1}$), B) Film 2 ($M_w = 356$ $\text{kg}\cdot\text{mol}^{-1}$, $D = 1.8$, $E_a = 160 \pm 21$ $\text{kJ}\cdot\text{mol}^{-1}$), and C) a PBMA film using FRET measurements ($M_w = 420$ $\text{kg}\cdot\text{mol}^{-1}$, $D = 5.0$, $E_a = 159$ $\text{kJ}\cdot\text{mol}^{-1}$).⁵ The fraction of mixing was held constant for each series, as indicated in the figures.

As a way to validate this approach, the calculated E_a value was then used to construct a master curve of D over f_m . Figure 32 compares the master curves generated in the present work to a trend obtained by the Winnik group for a PBMA film with a M_n of 36 $\text{kg}\cdot\text{mol}^{-1}$. Even though the molecular weights of the polymers in the two studies were very different the trend should still hold, and the only difference should reside in the magnitude of D . Overall, the master curves were indeed quite similar. The

calculated E_a value shifted the diffusion coefficients down to the selected reference temperature. The master curve obtained for Film 1 showed very little scattering of the shifted D values. Film 2 appeared to have D values shifted to slightly higher than expected values at temperatures of 94 and 98 °C. Nevertheless, the trends appeared to hold overall and were consistent with the previous FRET measurements.

Typically, the next step in the analysis would be to find the c_1 and c_2 values in the WLF equation. This is achieved by plotting $(T-T_0)/\log(a_T)$ against $T-T_0$, where a_T is equal to D_{T_0}/D_T . Again, the requirement remained that the same f_m values be maintained at each annealing temperature. Unfortunately, not enough measurements were performed that resulted in similar enough f_m values to produce any reliable plots for this type of analysis.

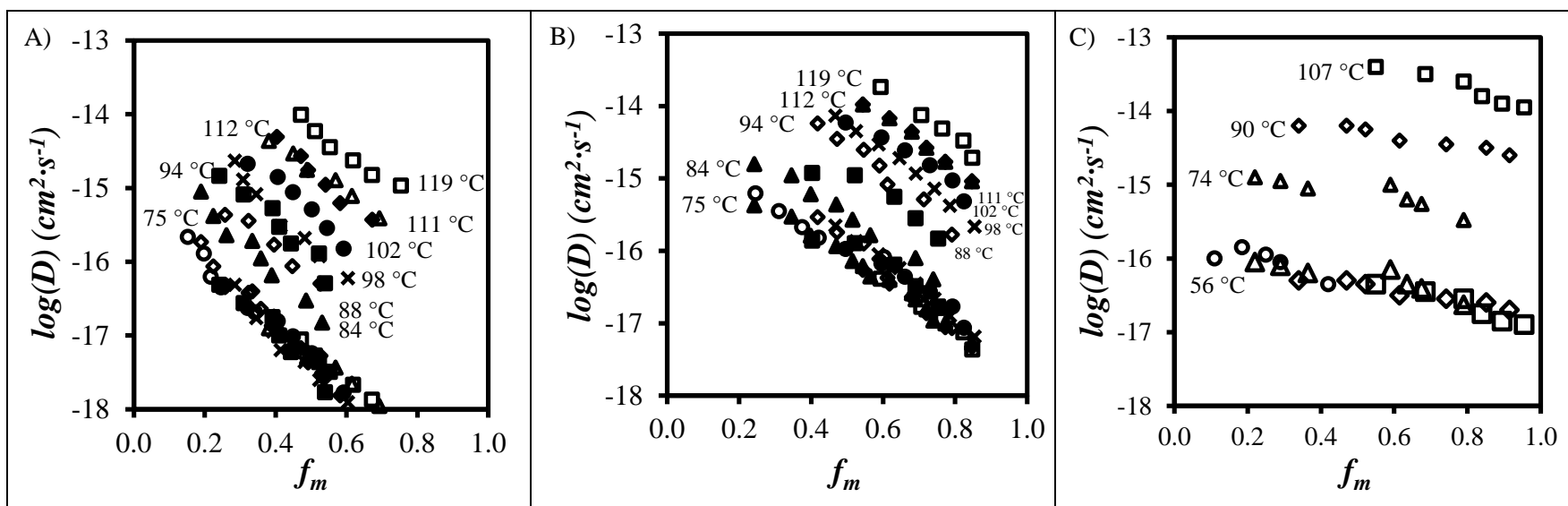


Figure 32: Diffusion coefficients and their master curves prepared using E_a for A) Film 1 and B) Film 2 using a reference temperature $T_0 = 75$ °C, and C) a PBMA film probed by FRET ($M_n = 38 \text{ kg} \cdot \text{mol}^{-1}$, $T_0 = 56$ °C).³⁰

3.5 Conclusions

Two different films were studied using our new methodology: one with a relatively high M_n of over 400 kg·mol⁻¹, and one with a lower M_n of 200 kg·mol⁻¹. First, the fraction of mixing was determined for both films. f_m increased more rapidly at higher annealing temperatures and for the film containing a lower molecular weight polymer, which is consistent with previous results obtained by other methods.^{5,30} Next, f_m was used to calculate the apparent diffusion coefficients using a Fickian diffusion model. The results were internally consistent. Higher diffusion coefficients were obtained for higher annealing temperatures and the lower molecular weight polymer. D decreased significantly for longer annealing times, a trend that was attributed to the dispersity of the polymer chains and to strain relaxation for the polymer chains constrained near the particle boundary, which could only adopt a reduced number of conformations.

A more qualitative analysis of f_m was conducted by monitoring the colour change for the films. Initially, before any annealing occurred, the films exhibited a light turquoise-blue colour. As the film was annealed and f_m increased, the colour began to fade. For f_m values around 0.6 to 0.7, the films exhibited a noticeable change to a darker blue colour. Upon further annealing, the colour darkened to violet-blue. When the film emission was observed through a cut-off filter, the colour changed to green. As the film was further annealed, the green colour faded until it nearly disappeared.

Lastly, our results were analyzed by two methods. In the first method, the D values were aligned along a master curve by determining appropriate shift factors a_T . A plot of $(T-T_0)/\log(a_T)$ as a function of $T-T_0$ yielded a straight line whose slope and intercept were used to extract the c_1 and c_2 values in the WLF equation. The c_1 and c_2 values retrieved from the analysis were close to those found by dynamic mechanical analysis of bulk PBMA. The shift factors were also used to prepare an Arrhenius plot to extract the apparent activation energy of diffusion. The resulting activation energy was found to be lower than a previously reported value, and much closer to the E_a value reported for the β -relaxation of the polymer. The second method was based on a procedure set forth by the Winnik group. The E_a was

calculated first, and was found to be much closer to the results found by DMA and nearly identical to the values found in previous FRET studies. Unfortunately, we were unable to calculate the c_1 and c_2 terms by this method due to its restrictive requirements. Overall, we believe that we have demonstrated that this new and simpler analytical tool based on pyrene excimer formation is a very useful and simple method to probe film formation.

Chapter 4

Summary and Future Work

Over the course of this project, pyrene-labelled latex particles were successfully prepared and employed to probe film formation using pyrene excimer fluorescence. The pyrene-labelled monomer with a triethylene glycol linker was optimal to label the latex particles. The PyEG₃MA monomer was fully incorporated into latex particles up to 1.9 mol% without the formation of coagulum. The particles also maintained a narrow PSD. Even at 1.9 mol% PyLM incorporation, excimer was formed in sufficiently large amount to utilize the I_E/I_M ratio to probe film formation.

Two pyrene-labelled latex particles were prepared; one with a high M_n of over 400 kg·mol⁻¹, and the other with a lower M_n of just under 200 kg·mol⁻¹. Two films were then cast using a mixture of 5 wt% pyrene-labelled particles with 95 wt% of a non-fluorescent PBMA latex. Each film contained particles with similar size and PSD, and polymers with similar M_n and \bar{D} . The films were annealed at nine temperatures ranging from 75 to 119 °C. Steady-state fluorescence was used to measure the fluorescence intensity of the films at set time intervals during the annealing process. The fluorescence spectra were used to calculate the I_E/I_M ratio at each annealing time. In all cases the I_E/I_M ratio decreased for longer annealing times.

Using the I_E/I_M ratio, the fraction of mixing (f_m) between the latex particles was measured next. f_m increased rapidly from zero at early times, followed by a gradual increase at long annealing times. The film containing the lower molecular weight polymer experienced a quicker increase in f_m as compared to the film containing the higher molecular weight polymer. Similarly, films annealed at higher temperatures also experienced larger f_m values than those annealed at lower temperatures.

The colour of the film was also monitored during the annealing process by irradiating the film with a hand-held UV lamp. When the emission colour was compared as a function of f_m , both films exhibited similar trends. Before annealing occurred, the films emitted a characteristic turquoise colour. As annealing proceeded and f_m increased, the colour began to fade and eventually turned into violet-blue. In addition, the colour was also observed through a 480 nm cut-off filter. Through the filter, the film exhibited a green fluorescence. As the film annealed, the initial bright green began to fade, and after fully annealing the colour disappeared altogether. This colour change provides a rapid qualitative tool to estimate the extent of IPD by visual inspection.

A more quantitative analysis was conducted next, by calculating the diffusion coefficients for the pyrene-labelled copolymer chains. Similarly to f_m , the diffusion coefficients were higher for lower molecular weight polymers and at higher annealing temperatures. One interesting trend was the large decrease in D observed with annealing time. This decrease was attributed to a combination of the large dispersity of the polymer chains as well as additional strain in the polymer chains close to the particle boundary.

Lastly, the calculated diffusion coefficients were used to calculate the activation energy, and the c_1 and c_2 terms in the WLF equation by two different analysis methods. The first method used was adapted directly from the WLF procedure. The diffusion coefficients were normalized to a reference temperature and then shifted by an a_T factor along the time axis to produce a master curve. By linearizing the WLF equation, a plot was constructed and the c_1 and c_2 parameters were extracted, yielding values of 7 and 190 K for c_1 and c_2 , respectively. These values were similar to those previously reported for the dynamic mechanical analysis of PBMA. Plots of $\ln(a_T)$ against $1/T$ were linear, with slopes corresponding to activation energy of diffusion values of 105 and 100 $\text{kJ}\cdot\text{mol}^{-1}$ for Films 1 and 2, respectively. The calculated activation energy was lower than previously reported, and was rather closer to the activation

energy reported for β -relaxation of the polymer. The second method was developed by the Winnik group to probe film formation by FRET. The activation energy of diffusion was found from the slope of $\log(D)$ against $1/T$. The activation energy found via this method (180 and 159 $\text{kJ}\cdot\text{mol}^{-1}$ for Films 1 and 2, respectively) was slightly higher than the reported value obtained by dynamic mechanical analysis, but was very close to the values obtained by the Winnik group through FRET measurements. Unfortunately, due to the restrictions in the determination of f_m in this analysis, the c_1 and c_2 terms could not be calculated.

On the basis of the above results we believe that this new method, using pyrene excimer formation, provides a simple manner to probe film formation. The new method described in this thesis has many distinct advantages over the previous FRET measurements. Since pyrene excimer formation occurs via direct contact between pyrene molecules, time-resolved fluorescence is not required and only the steady-state I_E / I_M ratio suffices to quantitatively probe film formation. In addition pyrene also emits in the visible region, allowing for rapid qualitative analysis by mere visual inspection of the films. One of the greatest advantages of the discussed method is the requirement that only a single batch of pyrene-labelled latex needs to be prepared. Since no modification is required for the non-fluorescent latex, the pyrene-labelled latex can be directly used to probe film formation with an off-the-shelf non-fluorescent latex. Moreover, because no modification of the non-fluorescent latex is required, the study of film formation by monitoring pyrene excimer fluorescence directly reflects the behavior of the non-fluorescent latex used. In addition, a single batch of pyrene-labelled particles can be used to probe film formation for many different non-fluorescent latexes, even if the two particles do not share similar properties, as opposed to FRET measurements which require that both particles have similar properties. This leads to several interesting future studies that would have been difficult to conduct using earlier methods. Some examples of future studies include the characterization of film formation for films having asymmetric

compositions, such as films generated from particles with different sizes, polymers with different molecular weights, and even films made from a mixture of latexes with different polymers. In summary, the procedure established in this thesis to probe latex film formation by monitoring pyrene excimer fluorescence opens new and exciting research venues which were inaccessible with prior state-of-the-art technology. It is expected to become an important tool in research focusing on latex film formation.

Appendix A

Calculated Values from Film Formation

Below are the tables for the measured I_E/I_M ratios used to determine the f_m and D values for both Films 1 and 2 at all the annealing temperatures.

Table A1: Films annealed at 119 °C.

t_{an} (min.)	<i>Film 1</i>			<i>Film 2</i>		
	I_E/I_M (a.u.)	f_m	D (nm ² ·s ⁻¹)	I_E/I_M (a.u.)	f_m	D (nm ² ·s ⁻¹)
0	0.137	0.00	-	0.122	0.00	-
5	0.089	0.47	0.977	0.068	0.59	1.824
10	0.085	0.51	0.589	-	-	-
20	0.081	0.55	0.355	0.058	0.71	0.747
40	0.075	0.62	0.237	0.052	0.76	0.489
80	0.069	0.67	0.149	0.047	0.82	0.333
160	0.061	0.75	0.108	0.045	0.84	0.193
340	0.046	0.91	0.129	-	-	-
∞	0.036	1.00	-	0.029	1.00	-

Table A2: Films annealed at 112 °C.

t_{an} (min.)	<i>Film 1</i>			<i>Film 2</i>		
	I_E/I_M (a.u.)	f_m	D (nm ² ·s ⁻¹)	I_E/I_M (a.u.)	f_m	D (nm ² ·s ⁻¹)
0	0.134	0.00	-	0.108	0.00	-
7	0.093	0.40	0.492	0.062	0.55	1.071
18	0.087	0.47	0.271	0.053	0.66	0.664
31	0.084	0.49	0.174	0.050	0.69	0.457
61	0.080	0.54	0.110	0.045	0.75	0.295
130	0.075	0.58	0.062	0.040	0.81	0.188
323	0.066	0.67	0.037	0.034	0.88	0.123
∞	0.033	1.00	-	0.024	1.00	-

Table A3: Films annealed at 111 °C.

t_{an} (min.)	<i>Film 1</i>			<i>Film 2</i>		
	I_E/I_M (a.u.)	f_m	D (nm ² ·s ⁻¹)	I_E/I_M (a.u.)	f_m	D (nm ² ·s ⁻¹)
0	0.140	0.00	-	0.122	0.00	-
7	0.097	0.38	0.434	0.067	0.54	1.051
15	0.089	0.45	0.292	0.060	0.62	0.678
30	0.084	0.49	0.176	0.054	0.68	0.442
60	0.075	0.57	0.127	0.050	0.72	0.266
120	0.070	0.61	0.078	0.045	0.77	0.170
338	0.061	0.69	0.039	0.037	0.84	0.091
∞	0.026	1.00	-	0.022	1.00	-

Table A4: Films annealed at 102 °C.

t_{an} (min.)	<i>Film 1</i>			<i>Film 2</i>		
	I_E/I_M (a.u.)	f_m	D (nm ² ·s ⁻¹)	I_E/I_M (a.u.)	f_m	D (nm ² ·s ⁻¹)
0	0.134	0.00	-	0.114	0.00	-
10	0.103	0.32	0.21	0.070	0.50	0.591
25	0.094	0.40	0.14	0.061	0.60	0.369
50	0.090	0.45	0.09	0.055	0.66	0.244
110	0.085	0.50	0.05	0.049	0.73	0.151
240	0.081	0.55	0.03	0.043	0.79	0.094
560	0.076	0.59	0.02	0.041	0.82	0.048
∞	0.037	1.00	-	0.025	1.00	-

Table A5: Films annealed at 98 °C.

t_{an} (min.)	<i>Film 1</i>			<i>Film 2</i>		
	I_E/I_M (a.u.)	f_m	D (nm ² ·s ⁻¹)	I_E/I_M (a.u.)	f_m	D (nm ² ·s ⁻¹)
0	0.140	0.00	-	0.121	0.00	-
7	0.107	0.28	0.234	0.074	0.47	0.736
15	0.105	0.31	0.129	0.069	0.53	0.450
30	0.100	0.35	0.082	0.063	0.59	0.297
60	0.095	0.39	0.054	0.057	0.65	0.191
120	0.093	0.41	0.030	0.052	0.69	0.117
245	0.085	0.48	0.021	0.047	0.74	0.072
521	0.080	0.52	0.012	0.043	0.79	0.042
1487	0.070	0.60	0.006	0.036	0.85	0.022
∞	0.026	1.00	-	0.022	1.00	-

Table A6: Films annealed at 94 °C.

t_{an} (min.)	<i>Film 1</i>			<i>Film 2</i>		
	I_E/I_M (a.u.)	f_m	D (nm ² ·s ⁻¹)	I_E/I_M (a.u.)	f_m	D (nm ² ·s ⁻¹)
0	0.131	0.00	-	0.115	0.00	-
8	0.106	0.25	0.145	0.082	0.36	0.368
24	0.100	0.31	0.081	0.069	0.50	0.255
61	0.090	0.39	0.053	0.060	0.60	0.157
120	0.089	0.41	0.030	0.055	0.66	0.100
240	0.085	0.44	0.018	0.052	0.69	0.058
480	0.077	0.52	0.013	0.046	0.75	0.038
1320	0.076	0.54	0.005	0.045	0.76	0.015
∞	0.029	1.00	-	0.024	1.00	-

Table A7: Films annealed at 88 °C.

t_{an} (min.)	<i>Film 1</i>			<i>Film 2</i>		
	I_E/I_M (a.u.)	f_m	D (nm ² ·s ⁻¹)	I_E/I_M (a.u.)	f_m	D (nm ² ·s ⁻¹)
0	0.134	0.00	-	0.118	0.00	-
31	0.107	0.26	0.043	0.080	0.40	0.119
60	0.100	0.32	0.036	0.068	0.52	0.111
193	0.093	0.40	0.017	0.057	0.63	0.056
495	0.088	0.45	0.09	0.052	0.69	0.028
1255	0.079	0.53	0.005	0.046	0.75	0.015
∞	0.030	1.00	-	0.022	1.00	-

Table A8: Films annealed at 84 °C.

t_{an} (min.)	<i>Film 1</i>			<i>Film 2</i>		
	I_E/I_M (a.u.)	f_m	D (nm ² ·s ⁻¹)	I_E/I_M (a.u.)	f_m	D (nm ² ·s ⁻¹)
0	0.132	0.00	-	0.122	0.00	-
8	0.114	0.19	0.089	0.097	0.24	0.158
24	0.111	0.22	0.042	0.087	0.35	0.111
60	0.107	0.26	0.023	0.082	0.40	0.060
120	0.010	0.33	0.019	0.075	0.47	0.043
240	0.097	0.36	0.011	0.071	0.52	0.027
490	0.094	0.40	0.006	0.066	0.56	0.016
1755	0.085	0.48	0.003	0.054	0.69	0.008
4298	0.081	0.53	0.001	0.049	0.74	0.004
∞	0.036	1.00	-	0.024	1.00	-

Table A9: Films annealed at 75 °C.

t_{an} (min.)	<i>Film 1</i>			<i>Film 2</i>		
	I_E/I_M (a.u.)	f_m	D (nm ² ·s ⁻¹)	I_E/I_M (a.u.)	f_m	D (nm ² ·s ⁻¹)
0	0.137	0.00	-	0.127	0.00	-
21	0.120	0.15	0.021	0.102	0.24	0.062
60	0.115	0.20	0.012	0.100	0.31	0.035
150	0.113	0.22	0.006	0.088	0.37	0.021
270	0.110	0.25	0.004	0.083	0.42	0.015
1170	0.099	0.34	0.002	0.065	0.60	0.008
∞	0.027	1.00	-	0.024	1.00	-

Python Program used to Model Diffusion Coefficients

```
import numpy as np
import math as ma
from scipy.integrate import quad
from scipy.optimize import fsolve
#diffusion equation was broken down to smaller functions for simplicity
def erf1(r,t,D):
    return (ma.erf((R+r)/(2*(D*t)**0.5)))
def erf2(r,t,D):
    return (ma.erf((R-r)/(2*(D*t)**0.5)))
def exp1(r,t,D):
    return (np.exp(((R-r)**2)/(-4*D*t)))
def exp2(r,t,D):
    return (np.exp(((R+r)**2)/(-4*D*t)))
def coeff(r,t,D):
    return (((D*t/np.pi)**0.5)/r)
#functions put back together
def C1(r,t,D):
    return ((erf1(r,t,D)+erf2(r,t,D))/2)-coeff(r,t,D)*(exp1(r,t,D)-
exp2(r,t,D))
def C2(r,t,D):
    return 4*np.pi*(r**2)*C1(r,t,D)
#rearranged so the zero of the equation can be found
def fs(t,D):
    return 1.0-(3.0/(4.0*np.pi*(R**3)))*quad(C2,1e-8*R,R,args=(t,D))[0]
#used to solve for zero of equation (i.e. solve for D)
t, fmexp=0,0
def f0(D,args=(t, fmexp)):
    return fs(t,D)-fmexp
print 'Save a file named "dt2.txt" with the following format:\n\nLatex
particle radius, R (nm)\nt1 (min)\nt2 (min)\n...\ntn
(min)\nfm(t1)\nfm(t2)\n...\nfm(tn)\n'
raw_input("Press Enter to Continue")
#input file name
```


References

1. Gauthier, C.; Guyot, A.; Perez, J.; Sindt, O. Film Formation and Mechanical Behavior of Polymer Laticies. *Film Formation in Waterborne Coatings*, American Chemical Society: Washington, DC, **1996**, Chapter 10, pp 163 – 178.
2. Winnik, M. A. Latex Film Formation. *Current Opin. Colloid Interface Sci.* **1997**, 2, 192-199.
3. Eckersley, S. T.; Rudin, A. Film Formation of Acrylic Copolymer Laticies: A Model of Stage II Film Formation. *Film Formation in Waterborne Coatings*, American Chemical Society: Washington, DC, **1996**, Chapter 1, pp 2 – 21.
4. Wang, Y.; Winnik, M. A. Polymer Diffusion Across Interfaces in Latex Films. *J. Phys. Chem.* **1993**, 97, 2507-2515.
5. Zhao, C.; Wang, Y.; Hruska, Z.; Winnik, M. A. Molecular Aspects of Latex Film Formation: An Energy-Transfer Study. *Macromolecules* **1990**, 23, 4082-4087.
6. Wang, Y.; Winnik, M. A. Energy-Transfer Study of Polymer Diffusion in Melt-Pressed Films of Poly(methyl methacrylate). *Macromolecules* **1993**, 26, 3147-3150.
7. Oh, J. K.; Tomba, P.; Ye, X.; Eley, R.; Radekacher, J.; Farwaha, R.; Winnik, M. A. Film Formation and Polymer Diffusion in Poly(vinyl acetate-co-butyl acrylate) Latex Films. Temperature Dependence. *Macromolecules* **2003**, 36, 5804-5814.
8. Farinha, J. P. S.; Martinho, J. M. G.; Yekta, A.; Winnik, M. A. Direct Nonradiative Energy Transfer in Polymer Interphases: Fluorescence Decay Functions from Concentration Profiles Generated by Fickian Diffusion. *Macromolecules* **1995**, 28, 6084-6088.

9. Kim, K. D.; Sperling, L. H.; Klein, A.; Wignall, G. D. Characterization of Film Formation from Direct Multi-emulsified Polystyrene Latex Particles via SANS. *Macromolecules* **1993**, *26*, 4624–4631.
10. Yekta, A.; Duhamel, J.; Winnik, M. A. Dipole-Dipole Electronic Energy Transfer. Fluorescence Decay Functions for Arbitrary Distributions of Donors and Acceptors: Systems with Planar Geometry. *Chem. Phys. Lett.* **1995**, *235* 119-125.
11. Yang, J.; Winnik, M. A. The Orientation Parameter for Energy Transfer in Restricted Geometries Including Block Copolymer Interfaces: A Monte Carlo Study. *J. Phys. Chem. B* **2005**, *109*, 18408-18417.
12. Fox, T. G. Influence of Diluent of Copolymer Composition on the Glass Temperature of a Polymer System. *Bull. Am. Phys. Soc.* **1956**, *1*, 123.
13. Bouzide, A.; Sauvé, G. Highly Selective Silver(I) Oxide Mediated Monoprotection of Symmetrical Diols. *Tetrahedron Lett.* **1997**, *38*, 5945 - 5948.
14. Sadler, J. M.; Nguyen, A. T.; Toulan, F. R.; Szabo, J. P.; Palmese, G. R.; Scheck, C.; Lutgen, S.; Scala, J. J. L. Isosorbide-Methacrylate as a Bio-Based Low Viscosity Resin for High Performance Thermosetting Applications. *J. Mater. Chem. A* **2013**, *1*, 12579 - 12586.
15. Mathew, A. K.; Siu, H.; Duhamel, J. A Blob Model To Study Chain Folding by Fluorescence. *Macromolecules* **1999**, *32*, 7100-7108.
16. Kalyanasundaram, K.; Thomas, K. Environmental Effects on Vibronic Band Intensities in Pyrene Monomer Fluorescence and Their Application in Studies of Micellar Systems. *J. Am. Chem. Soc.* **1977**, *99*, 2039 – 2044.

17. Chen, S.; Duhamel, J.; Winnik, M. A. Probing End-to-End Cyclization beyond Willemski and Fixman. *J. Phys. Chem. B* **2011**, *115*, 3289 – 3302.
18. Duhamel, J. Global Analysis of Fluorescence Decays to Probe the Internal Dynamics of Fluorescently Labeled Macromolecules. *Langmuir*, **2014**, *30*, 2307 – 2324.
19. Tsavalas, J. G.; Sundberg, D. C. Hydroplasticization of Polymers: Model Predictions and Application to Emulsion Polymers. *Langmuir* **2009**, *26*, 6960 - 6966.
20. Feng, J.; Winnik, M. A. Effect of Water on Polymer Diffusion in Latex Films. *Macromolecules* **1997**, *30*, 4324-4331.
21. Oh, J. K.; Yang, J.; Tomba, J. P.; Rademacher, J.; Farwaha, R.; Winnik, M. A. Molar Mass Effect on the Rate of Polymer Diffusion in Poly(vinyl acetate-*co*-butyl acetate) Latex Films. *Macromolecules* **2003**, *36*, 8836 – 8845.
22. Odrobina, E.; Winnik, M. A. Influence of Entanglements on the Time Dependence of Mixing in Nonradiative Energy Transfer Studies of Polymer Diffusion in Latex Films. *Macromolecules* **2001**, *34*, 6029 – 6038.
23. Wu, J.; Tomba, J. P.; Winnik, M. A.; Farwaha, R.; Rademacher, J. Effect of Gel Content on Polymer Diffusion in Poly(vinyl acetate-*co*-dibutyl maleate) Latex Films. *Macromolecules* **2004**, *37*, 4247 – 4253.
24. Kobayashi, M.; Rharbi, Y.; Brauge, L.; Cao, L.; Winnik, M. A. Effect of Silica as Fillers on Polymer Interdiffusion in Poly(butyl methacrylate) Latex Films. *Macromolecules* **2002**, *35*, 7387 – 7399.
25. Wang, Y.; Zhao, C.; Winnik, M. A. Molecular Diffusion and Latex Film Formation: An Analysis of Direct Nonradiative Energy Transfer Experiments. *J. Chem. Phys.* **1991**, *95*, 2143 – 2153.

26. Child, W.; Ferry, J. Dynamic Mechanical Properties of Poly-*n*-Butyl Methacrylate. *Colloid Sci.* **1957**, *12*, 327-341.
27. Williams, M. L.; Landel, R. F.; Ferry, J. D. The Temperature Dependence of Relaxation Mechanism in Amorphous Polymers and Other Glass-Forming Liquids. *J. Am. Chem. Soc.* **1955**, *77*, 3701-3707.
28. Ferry, J. D.; Fitzgerald, E. R.; Johnson, M. F.; Grandine, L. D. Mechanical Properties of Substances of High Molecular Weight. X. The Relaxation Distribution Function in Polyisobutylene and its Solutions. *J. Appl. Phys.* **1951**, *22*, 717 – 722.
29. Schneider, H. A.; Cantow, H. J.; Brekner, M. J. Interrelations Between Shift Factors of Viscoelastic Functions and Apparent Activation Energy of Flow. *Polym. Bull.* **1984**, *11*, 383 – 1984.
30. Ye, X.; Farinha, J. P. S.; Oh, J. K.; Winnik, M. A.; Wu, C. Polymer Diffusion in PBMA Latex Films Using a Polymerizable Benzophenone Derivative as an Energy Transfer Acceptor. *Macromolecules* **2003**, *36*, 8749–8760.